The Hashemite Kingdom of Jordan
Scientific Research Support Fund
The Hashemite University

JJEES

Jordan Journal of Earth and Environmental Sciences

Volume (13) Number (1)

Cover photo © Prof. Dr. Olaf Elicki*

JJEES is an International Peer-Reviewed Research Journal

ISSN 1995-6681 jjees.hu.edu.jo March 2022

Jordan Journal of Earth and Environmental Sciences (JJEES)

JJEES is an International Peer-Reviewed Research Journal, Issued by Deanship of Scientific Research, The Hashemite University, in corporation with, the Jordanian Scientific Research Support Fund, the Ministry of Higher Education and Scientific Research.

Editorial Board:

Associate Editorial Board: (Arranged Alphabetically)

International Advisory Board: (Arranged Alphabetically)

Editorial Board Support Team:

Submission address:

Manuscripts should be submitted electronically to the following e-mail:

jjees@hu.edu.jo

For more information and previous issues:

www.jjees.hu.edu.jo

Hashemite Kingdom of Jordan

Scientific Research Support Fund

Hashemite University

Jordan Journal of Earth and Environmental Sciences

JJEES

An International Peer-Reviewed Scientific Journal

Financed by the Scientific Research Support Fund

Volume 13 Number (1)

http:// jjees.hu.edu.jo/

ISSN 1995-6681

*Layered Ediacaran Haiyala volcanoclastics on top of Proterozoic basement at Wadi Abu Barqa (Wadi Araba).
Photographed by Prof. Dr. Olaf Elicki

JJEES
Jordan Journal of Earth and Environmental Sciences

JJEES

JJEES (2022) 13 (1): 1-15
ISSN 1995-6681

Jordan Journal of Earth and Environmental Sciences

Late Santonian - Campanian Ostracodes from Northwestern Jordan: Biostratigraphic and Paleobiogeographic Implications

Mahmoud H. Al- Tamimi[1], Jamal S. Nazzal[1], and Mohammad Alqudah[1]

[1]Department of Earth and Environmental Sciences, Yarmouk University, 21163 Irbid, Jordan

Received 15 March 2021; Accepted 25 May 2021

Abstract

Nine ostracod species are described from the Late Santonian - Campanian of Wadi Al-Kharaj section, northwestern Jordan. These species provide valuable information for biostratigraphy and paleobiogeography of the southern Tethys realm. The nine species belong to the following genera: *Cytherella*, *Bythocypris*, "*Togoina*", *Brachycythere*, *Cythereis*, "*Veenia*", *Ventrocythereis*, and *Cristaeleberis*. These species confirmed that the top of the Wadi Ghudran Formation and the base of the Amman Formation span the Coniacian-Campanian boundary. *Brachycythere* provides valuable information on the palaebiogeography of the shallow marine ostracodes.

Keywords: Ostracodes, Late Cretaceous, Biostratigraphy, *Brachycythere*

1. Introduction

During most of the Late Cretaceous global transgression, Jordan was a part of an epicontinental sea where carbonate precipitation is associated with organic matter enrichment within the shallow marine setting (Bender, 1974; Powell, 1989). Ostracodes are tiny aquatic crustaceans that are common in shallow water and their shells are often abundant in fine sediments (e.g. Anadón et al., 2002; Rodriguez-Lazaro and Ruiz-Muõz, 2012). Previously published works on ostracods of the Jordanian Late Cretaceous of Jordan are scarce. The only available record for the Late Cretaceous (Senonian) ostracodes is represented by Bassiouni (1970) who worked on the Late Maastrichtian- Paleocene succession of Jordan.

The aspects of Late Cretaceous (Senonian) ostracodes and their paleogeographic distribution of the Middle East, and the North and the West African regions have been carried out by several authors. The studies in Jordan include Bassiouni (1970). In Egypt there are Bold (1964); Bassiouni & Luger (1990); Morsi (2000); Shahin & El-Nady (2001); Abdel-Shafy et al., (2002); Shahin (2005); El-Nady et al., (2008); Boukhary et al. (2013); Morsi et al., (2019, 2020) and Hewaidy et al., (2021). Reyment (1960, 1963). El-Sogher (1992) from Libya and Donze et al. (1982) from Tunisia, Bellion et al. (1973) and Damotte et al. (1987) from Algeria, Damotte (1995) from North Africa, Mali, and Congo. In Israel, Honigstein (1984); Honigstein et al. (1987), Honigstein et al (1993) and many others.

The paleogeographical distribution of the Mesozoic ostracodes has been one of the most useful tools in understanding the breakup of Gondwana land. The genus *Brachycythere* played a critical role in establishing a faunal connection among the Gondwana land continent.

To evaluate the paleogeographic and biostratigraphic significance of the ostracodes, a section between Al-Kharaj and Haufa villages (Figure 1) at the northern part of Jordan (32° 33′ 54″ N) and (35° 49′ 27″ E) was measured and sampled for the biostratigraphical study. The significance of this study comes from being the first on Senonian ostracodes record, originating from the Amman Formation of Jordan.

All specimens described in the present paper are obtained from the Amman Formation in the Wadi Al-Kharaj area. The rock samples and the ostracodes are deposited in the collection of the Department of Earth and Environmental Sciences, Yarmouk University, Irbid, Jordan, and has the number YUPOS KH where:.

Yu = Yarmouk University, POS= Palaeontology Ostracoda, KH = Wadi Kharaj.

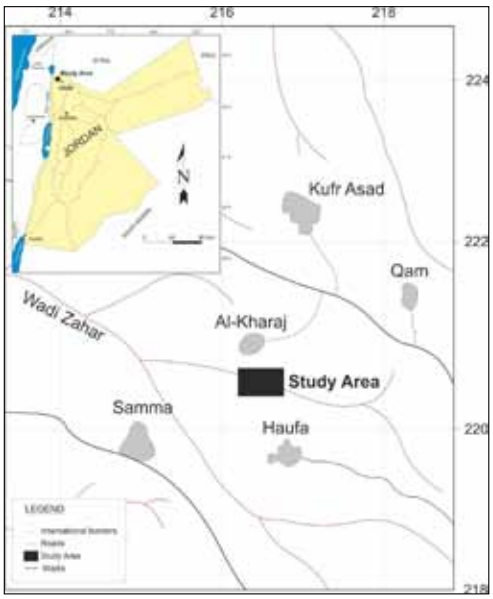

Figure 1. Detailed location map of the study area from where the Late Creatceous Ostracode section was studied between Al-Kharaj and Haufa

* Corresponding author e-mail: mohammad.alqudah@yu.edu.jo

2. Geological setting:

Sedimentation during the Mesozoic and Early Cenozoic was controlled by the configuration of Teyths Ocean in the north and northwest Jordan, which transgressed several times over parts or over the entire area of Jordan when the sea reached the southeastern part of the country. Regression of the sea in post-Eocene time was related to mountain-building events as the African-Arabian plate moved northward against the Euro-Asian plate (Bender, 1974; Powell, 1989).

During the Early and Middle Triassic, a transgression of the Tethys Ocean to the southeast was pronounced. The sea advanced from the west and northwest to the area just east of the Dead Sea, where Triassic littoral, lagoonal, and continental sedimentary rocks disconformably overlies Lower Paleozoic clastic rocks (Bandel and Khouri, 1981). After a regression during the Late Triassic and Early Jurassic, the Tethys advanced once again during Late Early Jurassic. Jurassic shorelines probably were just west of and approximately parallel to the borders of the Triassic transgression (Bandel, 1981).

Renewed epeirogenic uplift and erosion, and local volcanism, probably during the Late Jurassic, preceded Early Cretaceous sedimentation. Dominantly clastic rocks of the Early Cretaceous age, therefore, overlie the Palaeozoic, Triassic, or Jurassic formations with a regional angular unconformity. During the Early Cretaceous, a marine depositional environment dominated the northwest part of Jordan, and a transgression during the Albian reached the area east of the Jordan River. Farther east and to the south, clastic sediments of continental origin were deposited (Bender, 1974).

The shoreline lies off north Jordan during Early Cretaceous (Bandel & Mikbel, 1985). The sea advanced southwards during aseveraltransgressive episodes of short durations. In Late Albian to Early Cenomanian time, a major transgression occurred that led to the deposition of carbonate sediments in Jordan deposited on a broad platform extending to the southeastern part of the country. These facies are interfingering with fluvial siliciclastics in the south (Bender & Maedler, 1969).

The facies of Late Cretaceous in Jordan reflect a deposition on the slope and a very broad shelf, between the open Teyths Ocean to the west and northwest and the Arabian-Nubian Shield to the south, with environments controlled by the relief produced by Turonian-Coniacian incipient folding, tilt, and erosion and by Middle and Late Senonian synsedimentary folding of the Syrian Arc which led to the formation of intra-shelf and intra-slope basins and swells with differential subsidence and different rate of sedimentation, causing conspicuous variations in the thickness of the members of the Senonian sequence (Bender, 1968; Futyan, 1968; Reiss, 1988; Kolodny & Garrison, 1994). The sea-level changes, together with local tectonics, influenced bathymetry and effectiveness of basin-sills, as well as coupled with the intensity of upwelling and the resulting fertility of the photic zone, which ultimately affected the extent and degree of the oxygen minimum zone (Reiss, 1988).

A disconformity at the boundary between Ajlun and Belqa groups (Lewy, 1975; Al-Harithi, 1986) reflects non-deposition, or uplift and erosion of the platform in the Late Turonian (Bandel & Geys, 1985; Bandel & Mikbel, 1985). A renewed extensive transgression around Coniacian to Santonian reached the Saudi Arabia boundary. Sedimentation changed from platform carbonate facies to predominantly pelagic sediments deposited in the inner to mid-shelf environments. Gentle swells with phosphate, oyster beds, and chert layers and with basins of local euxinic environments led to thick accumulations of bituminous limestones and marls in the Campanian and Maastrichtian (Abed 1991 & 1994), Bandel (1981), Bandel & Mikbel (1985), Powell (1989), Nazzal & Mustafa (1993), Mustafa (2000), Bandel et al. (1999) and Mustafa (2000).

3. Material and Method:

The bulk rock samples were collected from the studied section. Six marly limestone samples were examined and prepared for ostracode content. Each sample was heated, was soaked in diluted H_2O_2, and heated till it was completely disaggregated. It was washed through 0.063 microns and dried and then stored. The ostracodes were picked under reflected stereo-microscope Specimens and then SEM-photographed using a scanning electron microscope-based in the Department of Earth and Environmental Science.

4. Lithostratigraphy:

The studied section attains a thickness of about sixty five meters and belongs to the Coniacian - Campanian stages. It can be subdivided into the Wadi Ghudran and Amman formations in stratigraphic order and discussed as follows:

4.1.1. Wadi Ghudran Formation:

The studied part of this formation attains a thickness of about 13.5 m It consists of chalky marl intercalated with marls and marly limestones Figure 2. The chalky marls are whitish, soft, laminated, thick-bedded, and fossiliferous, especially with molluscan shells (i.e. *Dentalium* and *Exogyra*) that are scattered at the bottom of this part and intense at the top. The marls are rosy, hard, and dendenselycked by shells, many bivalve shells still articulated. The marly limestones are rosy, medium-hard to hard, and laminated. At the top of the formation, hard grey dolomitic limestone is encountered.

Brownish fossiliferous chert and beige marly limestone have marked the boundary between the Wadi Ghudran and the overlying Amman formations.

4.1.2. Amman Formation:

The studied part of this formation attains a thickness of about 51.5 m. It is composed of alternations of marly limestones, chert beds and nodules, phosphatic limestones, and phosphate at the top of the formation. The marly limestones are rosy, beige, grading to yellowish or whitish, medium to hard, and laminated. The chert and limestone concretions are partially located within the marly limestone layers. The marly limestones become fossiliferous with Dentalium, molluscans, gastropods, and bivalve shells in some layers. At the top of the section, the marly limestone becomes phosphatic and hard. The chert is brownish, greyish with preserved silicified fauna such as *Baculites*, gastropods,

bivalves, scaphopods, and partially with coniqual veneer. Continuous lamination in the bottom and disturbed laminae in the top are observed in some chert layers at the top of the section. Light grey to brown, hard phosphatic layers lies at the top of the Al-Kharaj section Figure3.

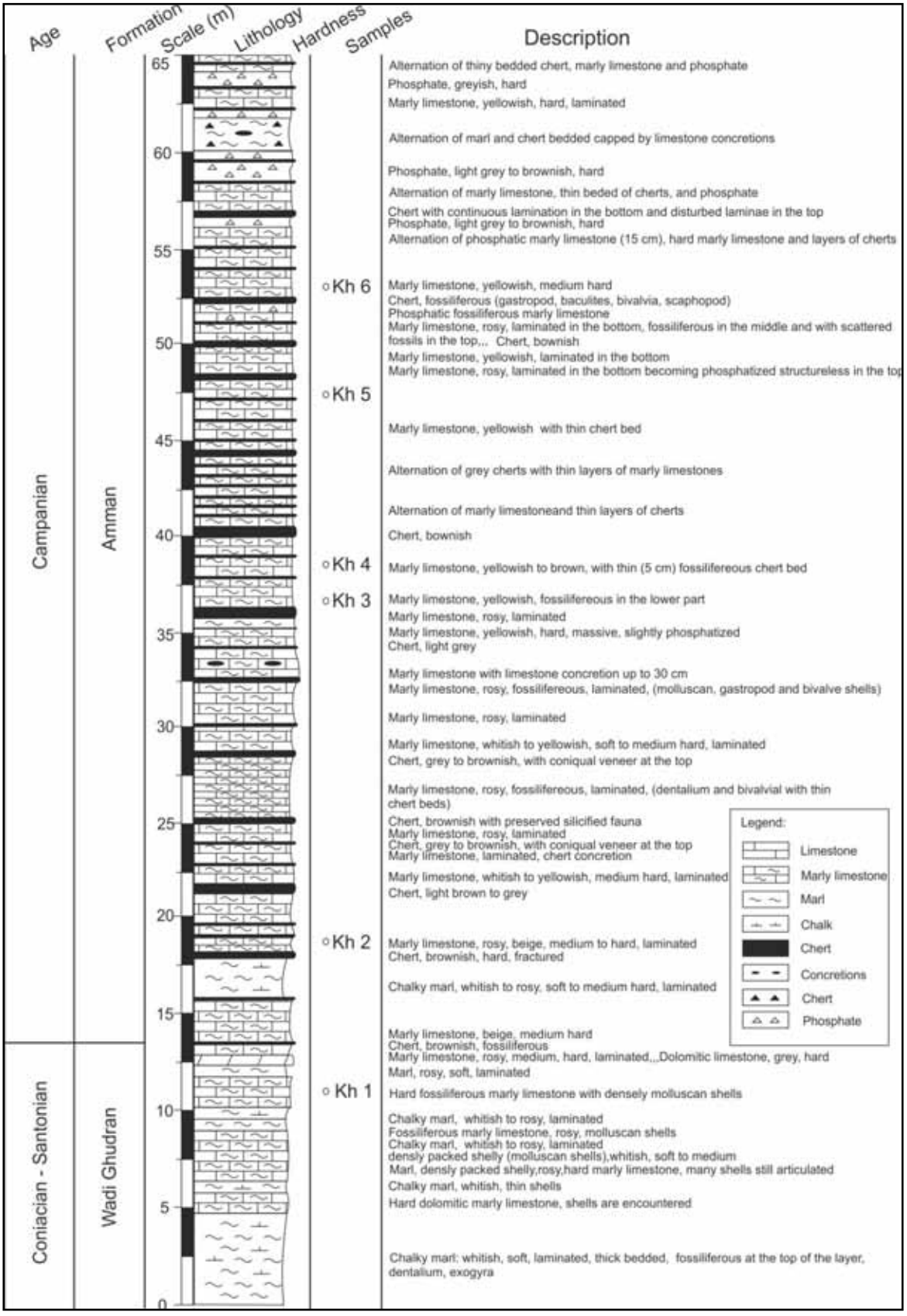

Figure 2. Studied stratigraphic columnar section logged south of AL-Kharaj town.

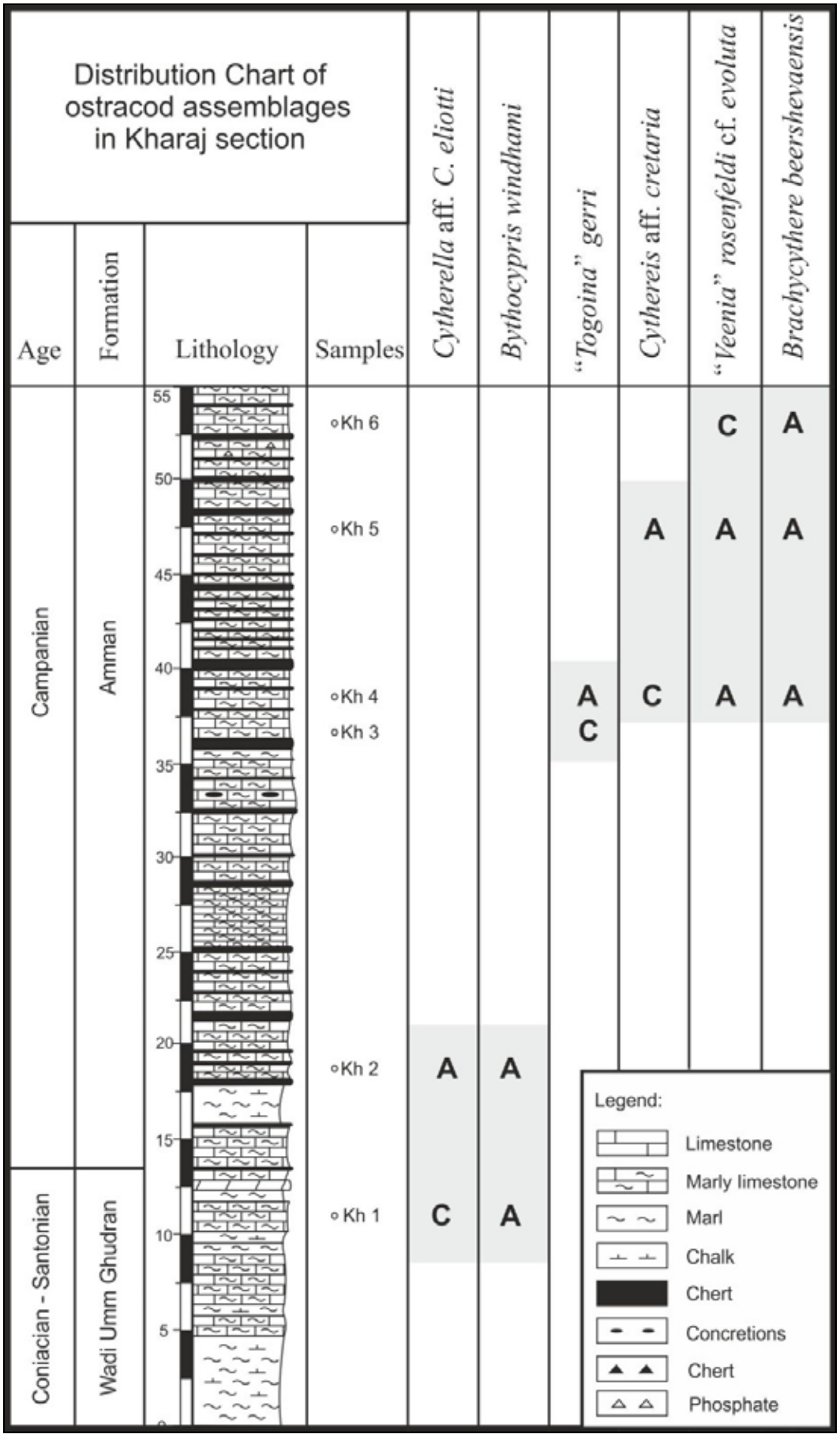

Figure 3. Distribution chart of Late Cretaceous ostracod species obtained from the top of Ghudran Formation and the lower part of the Amman Formation section in Wadi Al-Kharaj (Northwest of Jordan). A: abundant, C: common.

5. Results

5.1 Systematic Paleontology:

Nine ostracod species have been identified and described from the Late Santonian - Campanian interval of Al Kharaj section in north-western Jordan. These species belong to the following eight genera: *Cytherella*, *Bythocypris*, "*Togoina*", *Brachycythere*, *Cythereis*, "*Veenia*", *Ventrocythereis*, and *Cristaeleberis*. These genera belong to Cytherellidae Sars 1866, Bairdiidae Sars 1888, Trachyleberididae Sylvester-Bradley 1948 families. The generic assignment is based on Moore (1961) and later erected genera are treated as proposed by their authors.

Class Ostracoda Latreille 1806

Order Podocopida Mueller 1894

Suborder Platycopina Sars 1866

Family Cytherellidae Sars 1866

Genus *Cytherella* Jones 1849

Type species: *Cytherella ovata* Roemer 1840

***Cytherella* aff. *C. Elliott* Holden 1964**

Plate I, Figures 1-2

1964 *Cytherella eliotti* Holden pp.397-398, text-figs. 4a-c

1984 *Cytherella eliotti* Holden- Honigstein pp.5-7, pl.1, Figures 4-5

2002 *Cytherella eliotti* Holden- Abd-El Shafi et al. p.160, pl.1, Figures 13-14

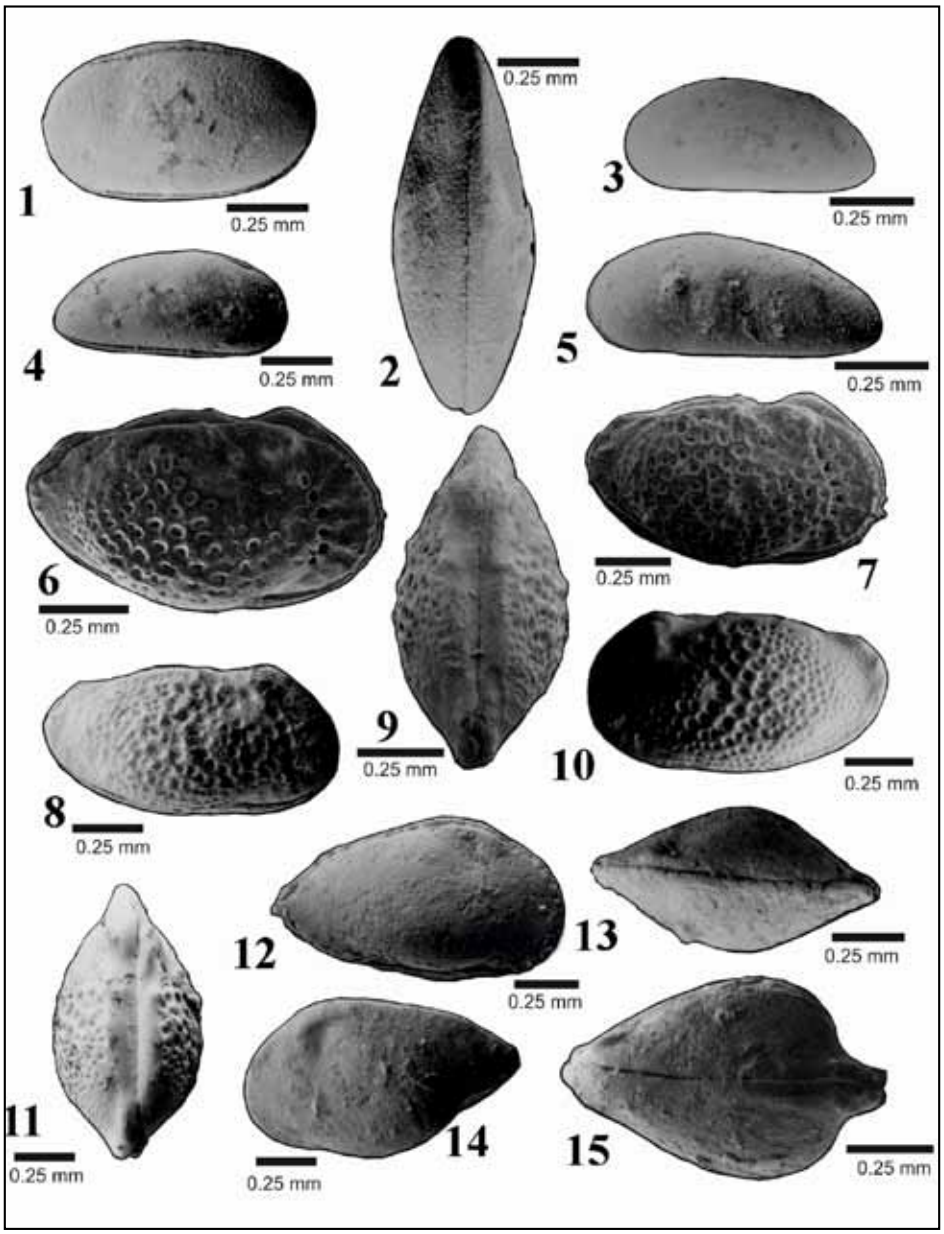

Plate I

Figs.1-2: *Cytherella* aff. *C. Elliott* Holden, 1964
Fig. LV, kh6.
Fig.2: Dorsal view.
Figs.3-5: *Bythocypris windhami* Butler and Jones, 1957
Fig.3: Male, LV, kh4
Fig.4: Female, RV.Kh 4
Fig.5: Female, RV, kh4
Fig.6-11: "*Togoina*"*gerryi* Honigstein, 1984
Fig.6: Female, RV, kh3.
Fig.7: Female, RV, kh3.
Fig.8: Male, RV, kh4.
Fig.9: Dorsal view.
Fig.10: Male, LV, kh4.
Fig.11: Dorsal view.
Figs.12-15: *Brachycythere beershevaensis* Honigstein, 1984
Fig.12: Male, RV, kh6.
Fig.13: Dorsal view.
Fig.14: Female, LV, kh6.
Fig.15: Dorsal view.

Material: Twenty-five carapaces.

Dimensions (in mm):

Females: Length: 0.69-0.7 Height: 0.39-0.42 Width: 0.29

Male: Length: 0.84 Height:0.48 Width: 0.29

Description: The medium-sized carapace is elongated oval to subrectangular in the lateral view with a dorsal margin that is moderately convex in the left valve and convex to faintly concave behind the middle in the right valve. The anterior margin is broad, well rounded, and smoothly joined to the dorsal and ventral margins. The posterior margin is broadly rounded, slightly oblique, and somewhat angled in its upper part. The ventral margin is faintly convex. The greatest length is measured at the mid-height in the males, slightly below the mid-height in the females and the greatest height is measured at the mid-length of the valves. Numerous tiny pits cover the surface; otherwise, it is almost smooth.

The carapace inside the dorsal view is lens-shaped in the males to suboval in the females. A faintly developed anterior marginal rim becomes obvious only in the dorsal view.

The assumed males are longer, relatively lower, and thinner than the assumed females.

Remarks: Although the Jordanian specimens are larger; it is similar to Cytherella aff. C. Elliott described by Honigstein (1984).

Occurrence: Honigstein (1984) recorded this species from the Santonian and Lower Campanian of Israel. Abd Elshafi et al. (2002) reported this species from the Coniacian-Santonian of Wadi El Raha and Campanian of Wadi Boudra in the eastern side of Gulf of Sues, Egypt. Specimens related to this species are found among the investigated material from the Late Campanian in Wadi Al-Kharaj section, Kh5.

Suborder Podocopina Sars 1866

Superfamily Bairdioidea Sars 1888

Family Bairdiidae Sars 1888

Genus *Bythocypris* Brady 1880

Type species: *Bythocypris reniformis* Brady 1880.

***Bythocypris windhami* Butler & Jones 1957**

Plate I, Figures 3-5

1957 *Bythocypris windhami* Butler & Jones pp. 12-13, pl.1, Figures 8a-e

1965 *Bythocypris windhami* Butler & Jones- Crane p. 197, pl.1, Figure 1

1984 *Bythocypris windhami* Butler & Jones- Honigstein p.10, pl.3, Figures 1-3.

2001 *Bythocypris windhami* Butler & Jones- Shahin & El-Nady p.158, pl.1, Figures 1

2008 *Bythocypris windhami* Butler & Jones- El Nady et al. p.545, pl.II, Figures 4-9

Material: Fifteen carapaces.

Dimensions (in mm):

Females: Length: 0.77-0.81 Height: 0.35-0.37

Males: Length: 0.75 Height: 0.32

Description: The medium-sized carapace in lateral view is elongate-subtriangular that tapers posteriorly. The dorsal margin is convex with a faint angularity in the posterior part, where it grades into acutely rounded, and only slightly oblique in its upper part. The anterior margin is well rounded, slightly oblique in its upper part. The ventral margin is straight to faintly concave. The greatest length is close to the ventral margin and the greatest height is at about one-third of the length. The carapace is the dorsal view is almost perfectly lens-shaped with sharp end margins. The greatest width is at about mid-length. The surface is smooth. The internal features are not observed. The assumed males are lower than the assumed females.

Remarks: The Jordanian and Israeli specimens of Honigstein (1984) are similar in having a smooth surface with a complete absence of fine punctae.

Occurrence: Butler & Jones (1957) had described *Bythocypris windhami* from the Late Campanian deposits of Louisiana. Later, Crane (1965) described it from the Late Campanian of the Gulf Coast. Honigstein (1984) reported *B. windhami* from the Late Coniacian-Early Campanian of Israel. This species was also described from the Early Coniacian-Early Campanian rocks of northern Sinai (Shahin & El-Nadi 2001). Specimens of this species are present among the investigated material from the Late Campanian in Wadi Al-Kharaj section, Kh5.

Family Trachyleberididae Sylvester-Bradley 1948

Subfamily Buntoniinae Apostolescu 1961

Genus *Togoina* Apostolescu 1961

Type species: *Togoina attitogoensis* Apostolescu 1961

Remarks: The genus *Togoina* was originally described to comprise large species of Paleogene age with massive, strongly swollen, subovoid carapaces with a postulate, punctuate, or reticulate surfaces and without a subcentral tubercle by Apostolescu (1961). In the present material, which is attributed to the species *Togoina Gerry* Honigstein 1984 (and probably also in *Togoina gGerry*Honigstein itself (1984, pl. 4, Figure 6)), a very shallow, rounded subcentral tubercle can be observed in well-preserved specimens. The Late Cretaceous species *T. geGerry*therefore, can not be attributed to the genus *Togoina*. However, it might represent one of the possible ancestors of the otherwise Early Tertiary true *Togoina* species.

"*Togoina*" *gerryi* Honigstein 1984

Plate I, Figures 6-11

1984 *Togoina gerryi* n. sp. – Honigstein p. 15, pl. 4, Figures 6-10.

Material: Eighteen carapaces.

Dimensions (in mm):

Females: Length: 1.02 Height: 0.56

Males: Length: 1.01-1.2 Height: 0.52-0.6 Width: 0.45-0.5

Description: The large carapace in lateral view is

suboval in the assumed females, suboval to subrectangular in the assumed males. The dorsal margin is sinusoidal (more strongly developed in the larger left valve), with a short strongly convex part anteriorly above the well-developed eye spot, followed posteriorly by a deep concavity. Behind the middle, the dorsal margin is moderately convex and ends with a weak concavity before it is angularly joined to the posterior margin. The anterior margin is broadly rounded, slightly oblique in its upper part. The ventral margin is convex. The posterior margin is angularly rounded. The greatest length is at about the mid-height. The greatest height is at about one-fourth of the length at the anterior cardinal angle. The ventral ridge is well developed, only slightly higher posteriorly. The ventral margin is convex and moderately to strongly overhanging. Coarse, deep pits cover the surface except for the end margins. At about mid-height and just in front of mid-length, a row of deep pits is arranged in a circle within a shallow depression, surrounding a small rounded, elevated, only weakly pitted shallow node, indicating the presence of a subcentral tubercle. The compressed anterior marginal area is covered by distinct, widely spaced radiating riblets and separated from the carapace inflation by a distinct row of deep rounded to almost rectangular pits. A well-developed depression is observed behind the eyespot and continues vertically down to the area of the subcentral tubercle to form a broad, shallow sulcus. Small blunt spines cover the anterior margin and posterior end in the well-preserved specimens.

In dorsal view, the carapace is oval with tapering, slightly set-off end. The greatest width is behind the mid-length. The internal feature is not observed. The sexual dimorphism is distinct; the assumed males are longer and almost subrectangular in lateral outline, lower and less tumid than females.

Occurrence: The species was originally described from the Lower Campanian of Israel (Honigstein, 1984). In the present material, it occurs in samples Kh4 and Kh5 of the Late Campanian age.

Subfamily Brachycytherinae Puri 1954

Genus *Brachycythere* Alexander 1933

Type species: *Cythere sphenoides* Reuss 1854

***Brachycythere beershevaensis* Honigstein 1984**

Plate I, Figures 12-15

1984 *Brachycythere beershevaensis* Honigstein pp. 16-17, pl.16, Figures 5-8.

1990 *Brachycythere beershevaensis* Honigstein- Bassiouni & Luger p.786, pl.9, Figures 6, 8.

2001 *Brachycythere beershevaensis* Honigstein- Shahin & El-Nady pp.161-162, pl.2, Figures 6-7

2008 *Brachycythere beershevaensis* Honigstein- El-Nady et al. pp.546, pl.II, Figure 16

Material: Thirty-two carapaces.

Dimensions (in mm):

Females: Length: 0.95-1.02 Height: 0.55-0.68 Width: 0.46-0.51

Males: Length: 0.95-1,15 Height: 0.58-0.65 Width: 0.46-0.56

Description: The large carapace in the lateral view is subtle oval. The dorsal margin is convex in the anterior part, where it is smoothly joined to the anterior margin, and almo, st sangulartraight in the strongly declining posterior part, where it is angularly joined to the posterior margin. The anterior margin is obliquely rounded in the upper part, well rounded in the lower part, and joined to the weakly convex ventral margin by a faint concavity. The posterior margin is angularly rounded. The posterior end and lower part of the anterior margin bear a few small denticles in some of the specimens. The greatest length is below the middle. The greatest height is below the well-developed eye spot in front of the middle at about one-third to one-fourth of length. The eyespot is posteriorly accompanied by a distinct short groove. The ventral ridge is posteriorly higher, distinctly overhanging the ventral margin only in the left valve. The surface of the carapace is covered by distinct round pits to be almost smooth.

The carapace is the dorsal view is oval with tapering end margins in males, suboval to pear-shaped with tapering anterior and compressed posterior margin in females. The greatest width is measured shortly behind the middle in the males, and a little more to the posterior in the females. The internal features are not observed. The sexual dimorphism is distinct in the dorsal view; the assumed females are more swollen and with a compressed posterior end rather than an oval with the tapering end in the assumed males.

Occurrence: This species was originally described from the upper part of the Early Campanian of Israel and is known from the Campanian and Maastrichtian of Sinai(Honigstein, 198the 4) and the Western Desert, Egypt (Bassiouni & Luger, 1990). It was also described from the Campanian of northeastern Sinai (Shahin & El-Nady, 2001) and eastern Sinai (El-Nady et al., 2008). The present material is from the Late Campanian sediments of Wadi Al-Kharaj section, Kh4, Kh5 & Kh6.

Subfamily Trachyleberidinae Sylvester-Bradley 1948

Genus *Cythereis* Jones 1849

Type species: *Cytherina Ciliata* Reuss 1846

Remarks: The species described here under *Cythereis* Jones (1849) are probably not true *Cythereis* species nor can they be attributed to any other known genus. Therefore, they are treated here a *˝Cythereis˝* (See also discussion in Honigstein, 1984, p.18).

"*Cythereis*" *rosenfeldi* cf. *evoluta* Honigstein 1984

Plate II, Figures 1-2

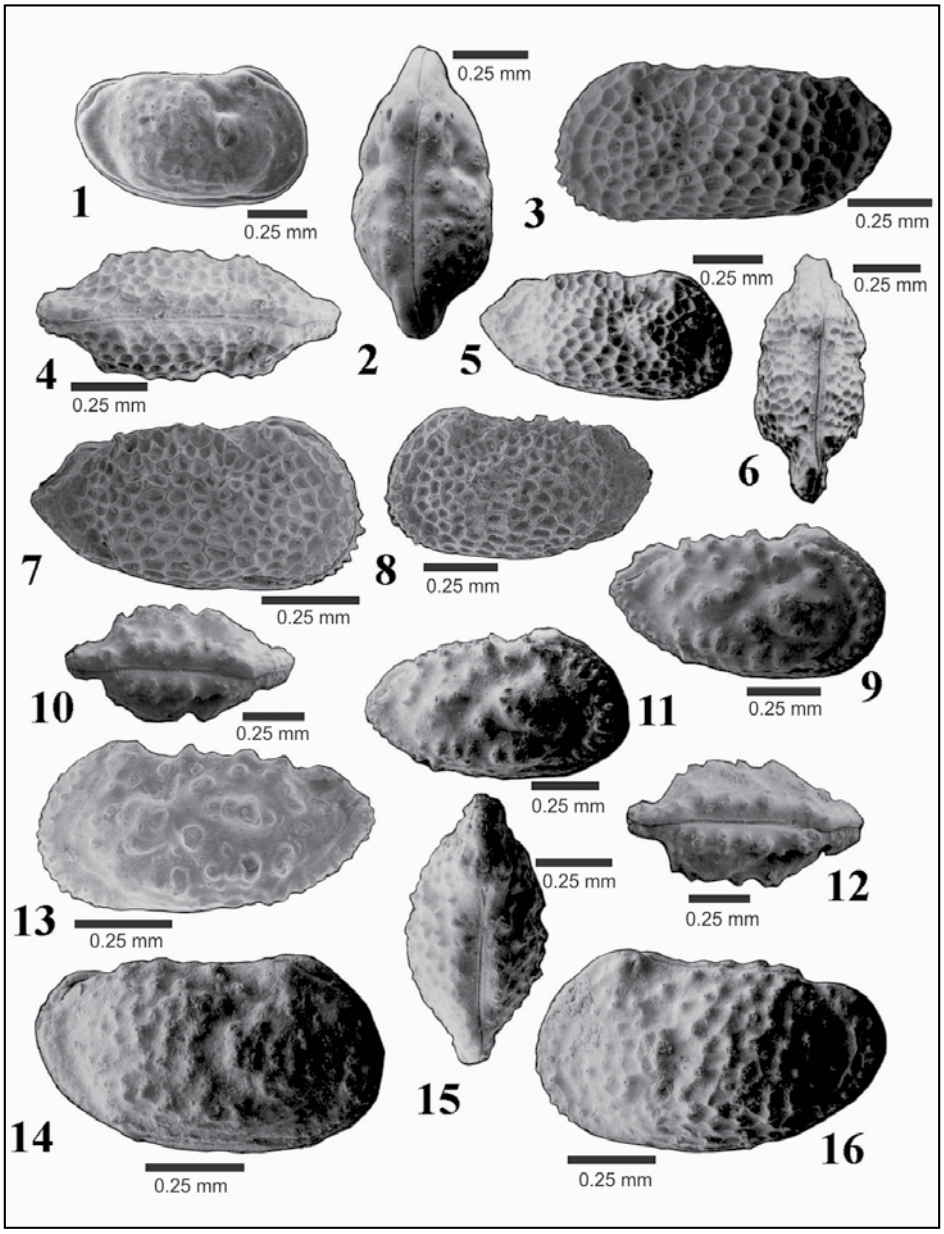

Plate II

Figs.1-2: "*Cythereis*" *rosenfeldi* cf. *evoluta* Honigstein, 1984
Fig.1: RV, kh4.
Fig.2: Dorsal view.
Figs.:3-8: *Cythereis* aff. *cretaria* Bold, 1964
Fig.3: Male, LV, kh1.
Fig.4: Dorsal view.
Fig.5: Female, RV, kh1.
Fig.6: Dorsal view.
Fig.7: Female, RV, kh2.
Fig.8: Female, LV, kh2.
Figs.9-13: "*Veenia*" *fawwarensis* cf. *dividua* Honigstein, 1984
Fig.9: Male, RV, kh3.
Fig.10: Dorsal view.
Fig.11: Female, RV, kh4.
Fig.12: Dorsal view.
Fig.13: Male, LV, kh4.
Figs.14-16: *Ventrocythereis sinaiensis* Honigstein, 1984
Fig.14: Female, RV, kh2.
Fig.15: Dorsal view.
Fig.16: Female, LV, kh2.

Cf. 1984 *Cythereis rosenfeldi evoluta* n.sp., n.ssp. Honigstein. P.25, pl9, Figures 10-11

Material: Twenty-five carapaces.

Dimensions (in mm):

Length: 0.98-1.0 Height: 0.53-0.61 Thickness: 0.50-0.55

Description: The carapace is subrectangular in lateral view. The anterior margin is broadly rounded, passing into the straight to the slightly convex ventral margin by a minor concavity. The posterior margin is broadly rounded in the left valve, angularly rounded to slightly acute in the right valve, where a small concavity is observed in the upper part. The posterior margin is smoothly joined to the gently rising ventral margin, and angularly connected to the straight dorsal margin. The dorsal margin joins the anterior margin through a well-developed convexity, which is formed by a well-developed hinge in the left valve. A similar structure can also be observed at the posterior cardinal angle. The dorsal and ventral margins are moderately converging posteriorly. The dorsal and ventral ribs are well developed; the dorsal rib is strongly overlapping the dorsal margin, while the ventral rib is only slightly overlapping the ventral margin. A third residual

rib may be indicated by an alignment of the nodes behind the well-developed subcentral tubercle, which is separated from it by a well-developed sinuous sulcus. The sulcus starts right behind the eye node, then bifurcates to surround the rounded subcentral tubercle and reunites beyond it, ending above the ventral rib. Irregularly spaced nodes cover the surface, and otherwise, it is smooth. Few small rounded nodes cover the only weakly developed anterior and posterior marginal ribs. The eyespot is small and rounded. The carapace is suboval in dorsal view, tapering anteriorly and set off at the posterior end. The maximum width is near the posterior end of the carapace inflation. The internal features were not observed. Due to the restricted number of specimens among the present material, a clear dimorphism can not be observed.

Remarks: The present material consists of mostly worn specimens, which are similar to *Cythereis Rosenfeld evoluta* Honigstein (1984). However, due to the poor preservation, the investigated material can only be compared with the subspecies of Honigstein.

Occurrence: Honigstein (1984) recorded the subspecies *C. Rosenfeld evoluta* from the Upper Santonian-Lower Campanian of northern and central Israel. The present material is from the Wadi Al-Kharaj section, Kh1, Kh2, and Kh3.

***Cythereis* aff. *critaria* Bold 1964**

Plate II, Figures 3-8

aff. 1964 *Cythereis critaria* Bold pp.126-127, pl.15, Figures 3-4.

1972 *Cytheris cf. critaria* Bold – Damote & Saint Marc .281, pl.2, Figures 13.

1984 *Cythereis cretaria* Bold- Honigstein p.19, pl.17, Figures 1-5.

2001 *Cythereis critaria* Bold- Shahin & El-Nady pp.166-167, pl.3, Figures 11-12.

2008 *Cythereis critaria* Bold- El-Nady et al. p.551, pl.V, Figures 1-2

Material: Thirty carapaces.

Dimensions (in mm):

Females: Length: 0.86-0.93 Height: 0.44-0.50 Thickness: 0.33-0.41

Males: Length: 1.0 Height: 0.50 Thickness: 0.35

Description: The carapace is subrectangular in lateral view, with subparallel ventral and dorsal margins in the males and posteriorly converging lateral margins in the females. The anterior margin is well rounded, slightly oblique in its upper part. The ventral margin is straight to faintly convex, joined to the anterior margin by a small concavity in the right valve only. The posterior margin is subtriangular, slightly pointed in the right valve, where a weak concavity can be observed. The dorsal margin is straight unless a convexity in its anteriormost part, where it joins to the anterior margin. The hinged ear is well developed in the left valve. A small rounded eyespot is present and easily detectable. The dorsal ridge is well developed, overreaching the dorsal margin, and separated from the eyespot by a small groove. The dorsal ridge starts a little below behind the eye-spot, rises rapidly above the dorsal margin, continues almost straight towards the posterior, and ends abruptly, truncated at the end of posterior carapace inflation. The ventral ridge is slightly convex and overreaches the ventral margin in its posterior two-thirds. A median ridge is only faintly developed. The anterior margin carries a strong rib on which numerous small denticles are present on its lower two-third. The subcentral tubercle is well developed, rounded, reticulated, surrounded by a small groove, and covered by small radiating reticules. In between the subcentral tubercle and the anterior margin, the otherwise irregular reticulation covering the entire carapace is arranged in concentric rows.

The carapace is the dorsal view is subrectangular, tapering anteriorly and abruptly set off at the posterior end. A small sulcus can be observed, formed by a narrow incision behind the subcentral tubercle. The maximum width is parallel to the carapace inflation. The internal features are not observed. The sexual dimorphism is distinct; the assumed males are with subparallel dorsal and ventral margins, while these margins are converging in the assumed females.

Remarks: The present specimens closely resemble *Cythereis cretaria* Bold as figured by Honigstein (1984) but smaller in size. However, they deviate from the smaller species of the originally described by Bold (1964) in the subrectangular outline in dorsal view, with almost parallel sides, rather than having undulating rectangular outline as figured by Bold (1964).

Occurrence: The species was originally described by Bold (1964) from the Campanian Abu Rawash, Egypt. The material from Israel as figured by Honigstein (1984), which is close to the described material here, was attributed to the Late Coniacian-Late Santonian. Shahin & El-Nady (2001) reported *Cythereis cretaria* from the Late Coniacian-Early Campanian of northeastern Sinai. The present material is from the Wadi Al-Kharaj section, Kh1, Kh2, Kh4, which are of the Late Santonian-Late Campanian age.

Genus *Veenia* Butler & Jones 1957

Type species: *Cythereis ozanana* Israelesky 1929

Remarks: The genus *Veenia* has been erected by Butler & Jones (1957) for species with a smooth surface and well-developed longitudinal ridges. The hingement of *Veenia* species is an amphidont-heterodont type with smooth end teeth. In the present material, the outline resembles that of *Veenia*, also the hinge is amphidont/heterodont. Some of the present material resembles that of the species *fawwarensis dividua* Honigstein (1984) which has been placed in the genus *Veenia* by this author. It does not show a well-developed median ridge. Also, the shape of this species *fawwarensis* is more like in *Cythereis*. Therefore, it may be assumed that the species *fawwarensis* and the new species listed below do not represent true *Veenia* species and are only kept provisionally under this genus.

"*Veenia*" *fawwarensis* cf. *dividua* Honigstein 1984

Plate II, Figures 9-13

Cf. 1984 *Veenia fawwarensis dividua* n.sp. n.ssp. - Honigstein p.28, pl.11, Figures 1-7, pl.15, Figures 11-12

Material: Twelve carapaces.

Dimensions (in mm):

Female: Length: 0.91-0.98 Height: 0.57-0.61 Thickness: 0.49

Male: Length: 0.92-0.94 Height: 0.48-0.51 Thickness: 0.43

Description: The carapace is subrectangular in lateral view and about twice as long as high. The maximum height is about the median length of the shell. The anterior margin is broadly rounded, passing into the otherwise straight ventral margin by a minor concavity. The posterior margin is blunt to triangularly edged, bearing a clear concavity in its upper part. The straight dorsal margin is connected to the posterior margin by a sharp angular break, and by a well-developed hinge ear to the anterior margin. In the left valve, the dorsal and ventral margins are gently converging posteriorly. The ornamentation consists of well-developed dorsal and ventral ridges, overlapping the lateral margins. Remnants of a median ridge may be represented by a row of pustules. All ridges are covered by rounded to weakly spinose nodes. A nodose subcentral tubercle is developed right behind the eye-spot at about median height. The swelling of the subcentral node is divided into four to five separate tubercles. Tubercles are often subdivided into one round prominent and one or two lower round tubercles with normal pores on their tops. A well-developed sinuous sulcus is running from behind the weakly developed eye spot, bordering the subcentral tubercle posteriorly and then running back again until the ventral rib. The otherwise smooth lateral surface carries several irregularly spaced nodes. A more prominent one of these is situated behind the sulcus at the lower part of the subcentral tubercle. A short line of more or less combined nodes is developed in the upper part of the valve, shortly behind the median length. Each of the anterior and posterior margins is marked by a well-developed rounded rib, carrying one row of widely spaced denticles at the posterior end and two rows of closely spaced fine denticles at the anterior end.

The carapace is the dorsal view is subrectangular with compressed posterior and anterior ends. The carapace inflation is gently rising from the anterior marginal zone, and steeply declining towards the posterior. The greatest width is at about one-third of the length at the protruding muscle node.

The internal features are not observed. The sexual dimorphism is distinct; the dorsal and ventral margins of the assumed females are more clearly converging posteriorly. Furthermore, they are higher and thicker than the assumed males.

Remarks: The present material deviates from *Veenia fawwarensis dividua* Honigstein (1984) in dorsal outline, which is more lense-shaped rather than subtriangular as in the present material. Therefore, the species can be conferred to "*Veenia*" *fawwarensis dividua*.

Occurrence: *Veenia fawwarensis dividua* was described from the Late Santonian-Early Campanian of Israel and North Egypt (Sinai) by Honigstein (1984). The present material is of Late Campanian from the Wadi Karaj section, Kh4.

Genus *Ventrocythereis* Honigstein 1984

Type Species: *Ventrocythereis sinaiensis* Honigstein 1984 from the Santonian-Early Campanian (upper part) of Israel.

Ventrocythereis sinaiensis Honigstein 1984

Plate II, Figures 14-16, and Plate III, figs.1-9

1984 *Ventrocythereis sinaiensis* Honigstein pp.29-30, pl.8, figs.7-11

Dimensions (in mm):

Females: Length: 0.97-1.03 Height: 0.5-0.60 Thickness: 0.5-0.55.

Males Length: 1.03-1.05 Height: 0.56-0.57 Thickness: 0.53

Description: The carapace in lateral view is subrectangular with an anterior margin that is rounded, slightly oblique in its upper part. The ventral margin is straight to slightly convex, joined with the anterior margin by a minor concavity. The posterior margin is obliquely rounded in the left valve, and broadly angular in the right valve, where it bears a small concavity in its upper part. The dorsal margin is straight, connected to the anterior margin by an only faintly developed hinge ear and by a sharp angularity to the posterior margin in the left valve. The maximum length is measured at about the median height or slightly above it. The maximum height is below the tiny rounded eye spot at about one-fourth to one-fifth of the length. The ornamentation consists of a distinct dorsal ridge overreaching the dorsal margin and a more weakly developed ventral ridge which may slightly overreach the ventral margin in its posterior part. The surface otherwise is covered by pustules and/or reticulation, and a distinct subcentral tubercle. A Conspicuous sinuous sulcus runs from just behind the eye node towards the anterior in the uppermost part of the valve, then sharply bends backward to border the well-developed muscle node and ends being bent forward again in front of the ventral margin. The dorsal and ventral ridges are covered by small rounded to spiny nodes. The only slightly elevated almost rounded subcentral tubercle is covered either by small nodes or reticules. Small pustules or reticulations otherwise cover the surface, which is only faintly developed to absent on the sulcus. The anterior margin is marked by a faintly to strongly developed marginal ridge bearing two rows of closely spaced spiny nodes. The posterior margin is bearing a well-developed marginal ridge with one row of widely to closely spaced tiny nodes. A short vertical riblet supporting the eye node is developed in most of the specimens.

The carapace is the dorsal view is suboval with moderately compressed end margins. The maximum width is just behind the middle. The hinge is amphidont/heterodont. The anterior tooth is elongated rounded, followed by a deep suboval socket in the right valve. The posterior tooth is elongated suboval. Other internal features are not observed. The sexual dimorphism is present; the assumed females show more strongly converging lateral margins.

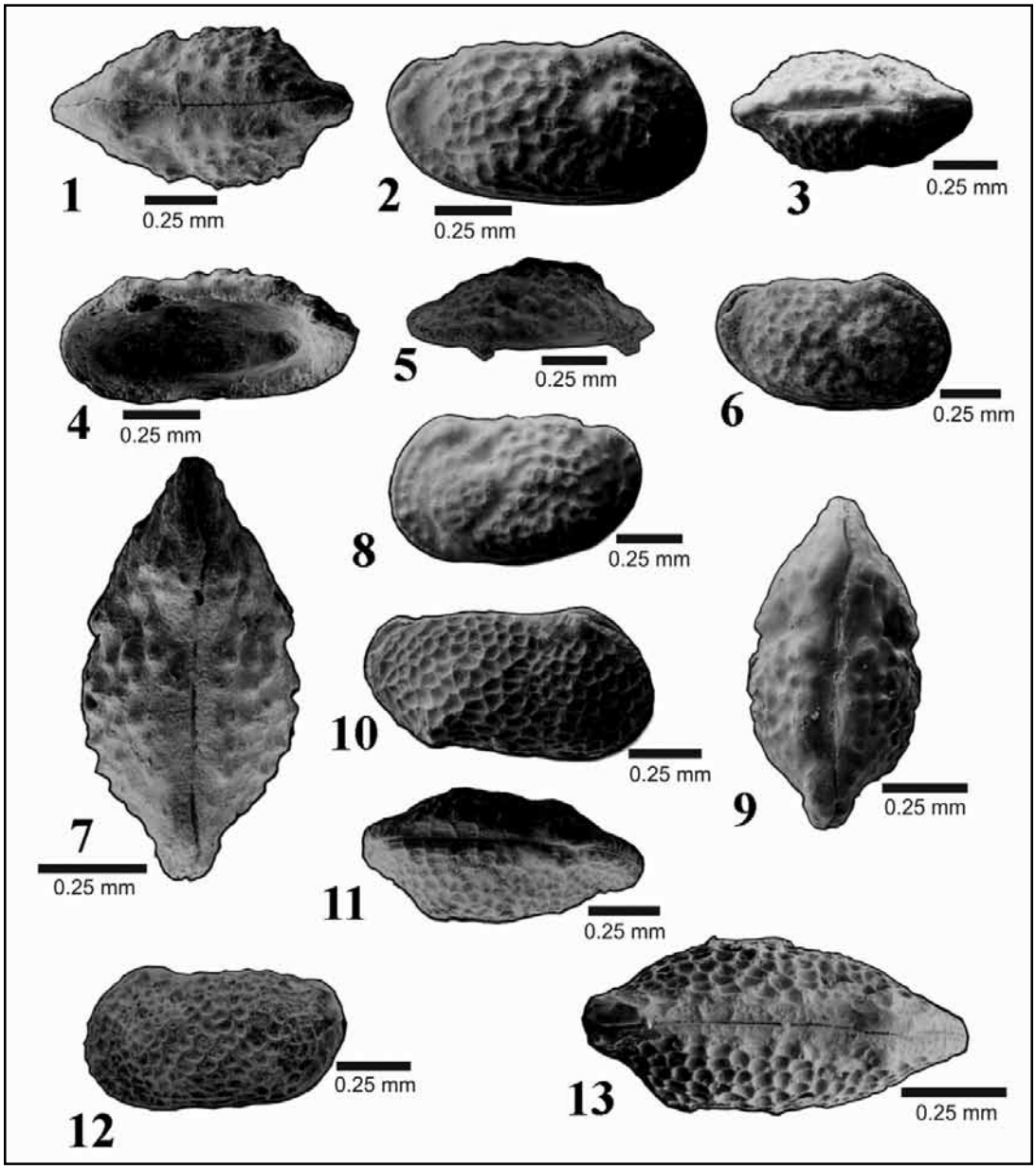

Plate III
Figs. 1-9: ***Ventrocythereis sinaiensis*** **Honigstein, 1984**
Fig.1: Dorsal view.
Fig.2: Male, RV, kh3
Fig.3: Dorsal view.
Fig.4: Female?, RV, internal features, kh3.
Fig.5: Dorsal view.
Fig.6: Female, RV, kh3.
Fig.7: Dorsal view.
Fig.8: Female, LV, kh3.
Fig.9: Dorsal view.
Figs.10-13: ***Cristaeleberis*** **cf.** ***C. fornicata*** **Bassiouni, 1970**
Fig.10: Male, RV, kh6**.**
Fig.11: Dorsal view.
Fig.12: Male, LV, kh6.
Fig.13: Dorsal view.

Occurrence: *Ventrocythereis sinaiensis* was originally described by Honigstein (1984) from the Upper Santonian-upper part of Lower Campanian of Israel. Specimens belonging to this species are found among the investigated material in the Late Campanian of North Jordan, from Wadi Al-Kharaj section, Kh3, Kh4, and Kh6.

Genus *Cristaeleberis* Bassiouni 1970

Type Species: *Cristaeleberis reticulata* Bassiouni 1970

Cristaeleberis cf. ***C. fornicata*** Bassiouni 1970

Plate III, Figures 10-13

Cf.1970 *Cristaeleberis fornicata* Bassiouni, p. 29, pl. 3, Figures 9-10

1984 *Cristaeleberis fornicata* Bassiouni- Honigstein, p. 35, pl. 10, Figures 5-8

2008 *Cristaeleberis fornicata* Bassiouni- El-Nady et al., p.550, pl. IV, Figures 11- 12

Material: Twenty-eight carapaces.

Dimensions (in mm):

Females: Length: 0.85-1.02 Height: 0.46-0.59 Width: 0.46-0.51

Males: Length: 0.88-1.14 Height: 0.47-0.56 Width: 0.380.46

Description: The large carapace is subrectangular in

lateral view. The left valve is larger than the right valve, overreaching it at the anterior and posterior cardinal angles. The dorsal margin is strong to moderately convex at the anterior cardinal angle, faintly convex to straight behind it, and ending with a weak concavity before it joins the posterior margin with a blunt edge. The anterior margin is broadly rounded and smoothly joined to the moderately convex (in assumed females) and straight (in the assumed males) ventral margin, where a weak concavity may be developed at about one-fourth of length. The posterior margin is obliquely rounded in the left valve, bluntly subtriangular with a pointed end in the right valve. The greatest length is at about the mid-height. The greatest height is at about one-fourth of the length below the anterior cardinal angle, where a small rounded eyespot is developed, which is posteriorly accompanied by a small groove. The anterior and posterior margins have numerous small denticles in the well-preserved specimens. The dorsal ridge is only weakly developed, faintly overreaching the dorsal margin behind the middle, or absent. The ventral ridge is only clearly developed in the right valve, where moderately convex and slightly overreaching the ventral margin, ending either in a blunt spine, or a node or a sharp edge, marking the posterior end of the ventral carapace inflation at about four-fifths of length. The surface of the valve is ornamented by sharp to smooth reticulation, being concentrically arranged in the anterior part of the valve, otherwise, it is irregularly spaced. The subcentral tubercle is absent.

The carapace is the dorsal view is suboval with compressed ends. The posterior end of carapace inflation is of unequal outline due to the strongly edged end of the ventral rib in the right valve. The greatest width is behind the middle. The internal features are not observed. The sexual dimorphism is present; the assumed males are relatively longer, lower, and less swollen than the assumed females.

Remarks: *Cristaeleberis fornicata* described by Bassiouni (1970) and Bassiouni & Luger (1990) and even described by Honigstein (1984) are smaller in size.

Occurrence: Bassiouni (1970) described *Cristaeleberis fornicata* from the Maastrichtian of Jordan. Honigstein (1984) reported the same species from a wider interval (Early Middle Santonian-Maastrichtian) in Israel. Records from the Maastrichtian include also Bassiouni & Luger (1990) and Shahin & El-Nady (2001) from Egypt. Specimens belonging to this species are found among the investigated material from the Late Campanian of North Jordan from the following horizons, Kh4, Kh5, and Kh6, from the Wadi Al-Kharaj section.

6. Discussion

6.1 Biostratigraphy:

The most comprehensive study on Late Cretaceous marine ostracodes from the neighbouring countries is that of Honigstein (1984), who gave a detailed description of the taxonomy and the biostratigraphic significance of species recorded in Israel. He established six ostracod assemblage zones, based on the first appearance of a diagnostic species; these zones are:

- *Phyrocythere lata* (S-1) Zone of Upper Coniacian (?Lower Santonian) age.
- *Cythereis rosenfeldi rosenfeldi* (S-2) Zone of Lower/ Middle Santonian age.
- *Limburgina miarensis* (S-3) Zone of Upper Santonian age.
- *Leguminocythereis dorsocostatus* (S-4) Zone of Lower Campanian age (lower part).
- *Brachycythere beershevaensis* (S-5) Zone of Lower Campanian (upper part)-Upper Campanian age.

The closeness of the studied area to the Israeli region makes some of the biozonations established by Honigstein (1984) are accepted here.

Comparing the recorded Jordanian association with the Israeli ones; the Jordanian association (Figure 3) can be referred to as the assemblage Zones S-3, Late S-4, and S-5. No species were observed belonging to the Lower Santonian. Although the zonal marker species *Limburgina miarensis* of the (S-3) (only Upper Santonian) Zone of Honigstein (1984) has not been observed in Kh1, the characteristic association of this zone is common. *Cythereis cretaria*, *Cythereis rosenfeldi* cf. *evoluta*, "*Veenia*" *fawwarensis* cf. *dividua* and *Ventrocythereis sinaiensis* have been recorded from these levels. Therefore, Upper Santonian can be attributed to the upper part of the Wadi Ghudran Formation and the lower part of the Amman Formation. This assignment is strongly supported by the findings of planktic foraminifera (Al-Rifay et. Al, 1993; Al- Harithi, 1986); ammonites (, Nazzal & Mustafa 1993), and shark teeth (Mustafa, 2000).

Honigstein (1984) found that *Togonia gerri* is only common to frequent in the assemblage zone (S-4) which has been attributed to the Early Campanian age. Here, abundant"*Togoina*" *gerri* has been observed in Kh4, and its presence extends to Kh5. Therefore, this interval can be compared with S-4 and belongs to the Early Campanian age.

This study shows that *Brachycythere beershevaensis* is an excellent marker fossil up to now in Jordan, Egypt, and Israel for Campanian age assignment. So, the samples Kh5 and Kh6 in the studied section correspond well to the S-5 Zone of the Late Campanian age. The associated *Baculites* and *Trachyscaphites* described from the same horizons by Nazzal & Mustafa (1993) support this assignment as well. The associated planktic foraminifera and ammonites in the studied section besides the closeness of the studied area to the Israeli region make some of the biozonations established by Honigstein (1984) are acceptable here.

A Late Santonian - Late Campanian age is assigned here to the studied material from the Al Kharaj section, which seems to be correlatable in part with the assemblage zones established by Honigstein (1984); *Cytheris rosenfeldi rosenfeldi* S-2 from the Late Santonian and *Brachcythere beershavaensis* S-5 from the Late Lower Campanian-Early Upper Campanian.

6.2: Paleobiogeographic apects:

The paleobiogeographic implication of Tethyan Cretaceous ostracodes has been enhanced by many authors (Babinot & Colin, 1988, 1992; Dingle, 1988; Puckett, 2002; Luger, 2003; see also additional references in Luger, 2003). Babinot & Colin (1992) proposed four paleobioprovinces for the Teythyan Late Cretaceous ostracodes.

The Jordanian ostracod assemblages show a strong affinity to those of Israel since all the species recorded here were also recorded in the Senonian of Israel (Honigstein 1984). A similarity to species described from Egypt (North Africa) is confined by the common occurrence of these ostracods in both sites. Nearly all the recorded Jordanian species were recorded in Egypt (Bassiouni & Luger, 1990; Morsi et al., 2000; Shahin & El-Nady, 2001and many others) ranging from the Early Coniacian-Early Campanian. Out of these ostracodes, *Bythocypris windhami* Butler & Jones 1957 was of common occurrence in the Santonian and Lower Campanian ranges in Egypt (Shahin & El-Nady, 2001) and northern, central, and southern Israel (Honigstein 1984 and Honigstein et al., 1987). Also, *Cristaeleberis fornicata* Bassiouni (1970) was originally described from the Late Maastrichtian of Jordan (Bassiouni, 1970) and was described later from the Maastrichtian of Egypt (Bassiouni & Luger, 1990; Shahin & El-Nady, 2001and many others). It ranges in Israel from the Santonian to Maastrichtian (Honigstein, 1984). This study showed that this species also occurs in a lower stratigraphic horizon in Jordan (Late Campanian). Regarding the *Cytherella eliotti* Holden 1964; it was described from the Santonian/Campanian-Lower Campanian in northern and southern Israel (Honigstein, 1984), and the Santonian-Campanian of southern Egypt (Abd-Elshafy et al., 2002). In the present work, it is reported from the Late Santonian- Late Campanian. This great similarity in the ostracod assemblage with the neighboring counties refers to a direct connection between them during that time.

The Santonian-Maastrichtian interval witnessed a great diversification of African brachycytherine ostracodes (Babinot & Colin, 1988; 1992); Puckett (2002); Luger (2003); Seeling et al. (2004). The group continued to be dominant constituents of the shallow marine deposits across Africa. Babinot and Colin (1988, 1992) recognized this provincialism and defined Tethyan and Australian paleobioprovinces, in which the studied brachycytherine ostracodes played an important role.

Brachycythere provides valuable information on the palaeoecology of shallow marine environments. The genus *Brachycythere* Alexander has been considered as one of the most important genera for understanding the routes and timing of ostracod migration through the Tethyan realm and West Africa (Figure 4). This species is taken into consideration because it has numerous records in Gondwanide localities (Reyment, 1980; Honigstein, 1984; Okosun, 1992; Shahin & El-Nady, 2001; Caus, et al. 2002; and the present work). They found that the dominance of the genus *Brachycythere* (with different species) is a common element in the Upper Cretaceous ostracods of North America, entire Africa, and northern part of southern America. Its extremely widespread distribution in these regions with its absence in the European Cretaceous provides an interesting insight into the development of the Atlantic Ocean and the role of the Tethys Ocean as an effective barrier to North-South faunal exchange (Caus, et al. 2002).

The recoded *Brachycythere beershevaensis* Honigstein 1984 was originally described from the Campanian of Israel (Honigstein, 1984) and extended to the Early Maastrichtian (Honigstein et al., 1987). It was also recorded from Egypt from the Early to Middle Maastrichtian of southern Egypt (Bassiouni & Luger (1990) and in northeast Sinai (Shahin & El-Nady, 2001) and from the Late Campanian of Jordan (present study). This great similarity with the neighboring countries refers to and confirms a direct connection between them during that time.

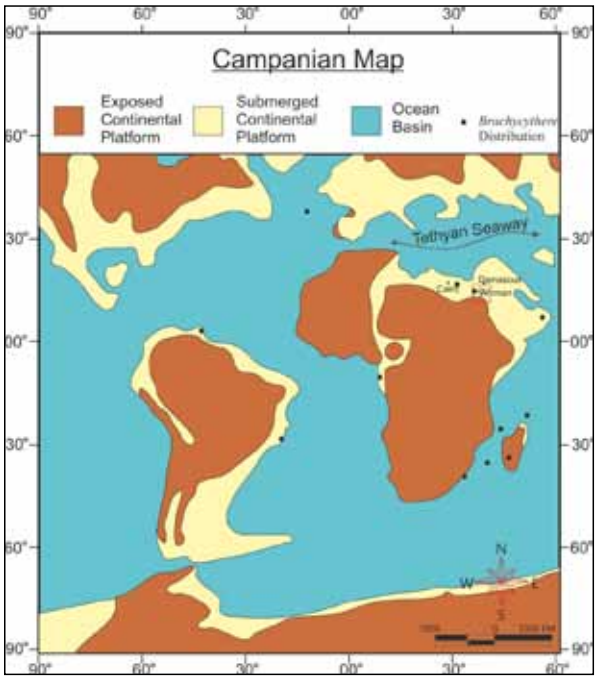

Figure 4. Reconstructed Tethyan Seaway map imposing the paleobiogeography of Brachycythere from Late Cretaceous (modified after Viviers et. al. 2000).

7. Conclusions:

Nine ostracod species were identified and described from the Late Santonian - Early Campanian succession of northwestern Jordan. The nine species belong to the following genera: *Cytherella*, *Bythocypris*, "*Togoina*", *Brachycythere*, *Cythereis*, "*Veenia*", *Ventrocythereis*, and *Cristaeleberis*. These species were correlated with the assemblage Zones S-3 (upper Santonian), Late S-4 (lower Campanian), and S-5 (Lower to Upper Campanian) that were defined by Honigstein (1984) in Israel. They were also an addition to paleobiogeographic constructions of the southern Tethyan realm. This study shows that *Brachycythere beershevaensis* is an excellent marker fossil up to now in Jordan, Egypt, and Israel for the Campanian age assignment. *Brachycythere* provides valuable information on the palaeoecology of shallow marine environments.

Acknowledgment:

Authors would like to thank Dr. Iyad Zalmout for his deep comments and improvement in the manuscript.

References

Abed, A. M., Kraishan, G., 1991. Evidence for shallow marine origin of a 'Monterey Formation type' chert-phosphorite-dolomite sequence Amman Formation, Late Cretaceous, central Jordan. Facies, 24, 25-38.

Abed, A.M., 1994. Shallow marine phosphorite-chert-palygorskite association, Late Cretaceous, Amman Formation, Jordan, In Iijima, A., Abed, A.M. and Garrison, R., eds., Siliceous, Phosphatic and Glauconitic Sediments of the Tertiary and Mesozoic: VSP, Zeist, Netherlands, p. 205-224., Microfacies and paleoenvironments of Wadi Sir Formation (Upper Cretaceous), North Jordan. Facies, 7, 229-236.

Abd-Elshafy, E., Ibrahim, N., Ied, I.M., 2002. Ostracod biostratigraphy and paleobiogeography of the upper Cretaceous in the northern part of the Gulf of Suez. Egyptian Journal of Paleontology, 2: 157-198.

Al-Harithi, T., 1986. Biostratigraphy and paleoecology of the Upper Cretaceous in N. Jordan, with help of small Mollusca. Ph.D. thesis. Hannover Univ.: 121; 18pls.

Anadon, P., Gliozzi, E., & Mazzini, I. (2002). Paleoenvironmental reconstruction of marginal marine environments from combined paleoecological and geochemical analyses on ostracods. GEOPHYSICAL MONOGRAPH-AMERICAN GEOPHYSICAL UNION, 131, 227-248.

Alexander, C.I., 1933. Shell structure of the ostracode genus Cytheropteron, and fossil species from the Cretaceous of Texas. Journal of Paleontology, 7: 181–214.

Al-Rifaiy, I.A., Cherif, O.H., & El-Bakri, B.A., 1993. Upper Cretaceous foraminiferal biostratigraphy and paleobathymetry of the Al-Baqa area, north of Amman (Jordan). Journal African Earth Science, 17(3): 343-357.

Apostolescu, V., 1961. Contribution à l'étude paléontologique (Ostracodes) et stratigraphique des bassins crétacés et tertiaires de l'Afrique occidentale. Review of the French Institute of Petroleum, 16 (7/8): 779-861.

Babinot, J.F., Colin, J.P., 1988. Paleobiogeography of Tethyan Cretaceous marine ostracods. In: Elsevier (Eds) Developments in Palaeontology and Stratigraphy, 11: 823-839. Elsevier.

Babinot, J.F., Colin, J.P., 1992. Marine ostracode provincialism in the Late Cretaceous of the Tethyan realm and the Austral Province. Palaeogeography, Palaeoclimatology, Palaeoecology, 92(3-4): 283-293.

Bandel, K., Geys, J., 1985. Regular echinoids in the Upper Cretaceous of the Hashemite Kingdom of Jordan. Ann. soc. Geol. Nord., 97- 115.

Bandel, K., Mikbel, S., 1985. Origin and deposition of phosphate ores from the Upper Cretaceous of Ruseifa (Amman, Jordan). Mitteilungen des Geologisch-Paläontologischen Instituts der Universität Hamburg, 59: 167- 188.

Bandel, K., 1981. New stratigraphical and structural evidence for lateral dislocation in the Jordan Rift Valley connected with a description of the Jurassic rock column in Jordan: Neues Jahrbuch Geologie und palaeontologie, Abhandlungen 161: 271-308.

Bandel, K., Khoury, H., 1981. Lithostratigraphy of the Triassic in Jordan. Facies, 4(1): 1-26.

Bandel, K., Shinaq, R., Nazzal, J., 1999. Palaeoecological and diagenetical significance of a silicified soft bottom fauna of Campanian age (Quatrana Unit, Jordan). Mitteilungen des Geologisch-Paläontologischen Instituts Universität Hamburg 83: 201-218.

Bassiouni, M.A.A., 1970. Ostracoda (Mauritsininae und Trachyleberidinae) und ihre Bedeutung fur die Biostratigraphie des Maastricht und des Alttertiar von Jordanien. Beihefte zum Geologischen Jahrbuch 106: 5–52.

Bassiouni, M.A.A., Luger, P., 1990. Maastrichtian to early Eocene ostracoda from southern Egypt. Palaeontology, palaeoecology, palaeobiogeography and biostratigraphy. Berliner Geowissenschaftliche Abhandlungen, Reihe A, 120: 755-928.

Bellion, Y., Donze, P., Guiraud, R., 1973. Répartition stratigraphique des principaux ostracodes (Cytheracea) dans le Crétacé supérieur du sud ouest constantinois.(Confins Hodna-Aurès, Algérie du nord). Bull. Serv. Géol. Algérie, 4: 1-136.

Bender, F., Mädler, K., 1969. Die sandige Schichtenfolge der Kreide mit einer Angiospermen-Flora in Südjordanien. Beiheft des geologischen Jahrbuch, 81: 35-92.

Bender, F., 1974. Geology of Jordan, Gerbrueder Borntraeger. Berlin. Germany.

Bold, W.A.van den, 1964. Ostracoden aus der oberkreide von Abu Rawash, Âgypten. Palaeontographica. Abteilung A, Paläozoologie, Stratigraphie, 123(4-6): 111-136.

Boukhary, M., Bassiouni, M.A.., Issawi, B., Sharabi, S., Mansour, H., 2013. Maastrichtian-early Paleogene ostracoda from the Kharga Oasis and the Nile Valley, Egypt. Micropaleontology 59, 223–248.

Butler, E.A., Jones, D.E., 1957. Cretaceous Ostracoda of Prothro and Rayburns salt domes, Bienville Parish, Louisiana. Department of Conservation, Louisiana Geological Survey.

Caus, E., Tambareau, Y., Colin, J.P., Aguilar, M., Bernaus, J.M., Garrido, A.G., Brusset, S., 2002. Upper Cretaceous microfauna of the Cárdenas Formation, San Luis Potosí, NE Mexico. Biostratigraphical, palaeoecological, and palaeogeographical significance. Revista Mexicana de Ciencias Geológicas, 19(2): 137-144.

Crane, M.J., 1965. Upper Cretaceous ostracodes of the Gulf Coast area. – Micropaleontology, 11(2): 191-254.

Damotte, R., 1995. The biostratigraphy and palaeobiogeography of Upper Cretaceous-basal Tertiary ostracods from North Africa, Mali and Congo. Cretaceous Research, 16(2-3): 357-366.

Damotte, R., Fleury, J.J., 1987. Ostracodes maastrichtiens et paleocenes du Djebel Dyr, pres de Tebessa (Algerie orientale). Géologie Méditerranéenne 14, 87–107.

Dingle, R. 1988. Marine ostracod distributions during the Early breakup of Southern Gondwanaland. In: Developments in Palaeontology and Stratigraphy 11: 841-854. Elsevier.

Donze, P., Colin, J.P., Damotte, R., Oertli, H.J., Peypouquet, J.P., Said, R., 1982. Le ostracodes du Campanien terminal a´ l'Eoce´neinfe´rieur de la coupe du Kef, Tunisie Nord-Occidentale. – Bulletin des Centres de Recherches Exploration-Production Elf-Aquitaine, 6: 273–307.

El-Nady, H.M, Abu-Zied, R., Ayyad, S., 2008. Cenomanian – Maastrichtian ostracoda from Gabal Arif El-Naga anticline, Eastern Sinai, Egypt. Revue de paléobiologi, (27) 2: 533 - 573.

El-Sogher, A., 1996. Late Cretaceous and Paleocene Ostracoda from the Waha Limestone and Hagfa Shale Formation of the Sirte Basin, Libya. In: Salim, M.J., Mouzughi, A.J., Hammuda, O.S. (Eds.), The Geology of Sirte Basin, Libya 1, 287–382.

Futyan, A., 1968. Benthonic foraminifera from the Upper Cretaceous- Lower Tertiary successions in East Jordan. – Ph. D. thesis. Univ. Coll. London: 353p 18 pls. Hannover 106:5-52.

Hewaidy, Abdel-Galil A.; Morsi, Abdel-Mohsen M.; Samir, Ahmed. 2021. Maastrichtian-Paleocene Ostracoda from Teneida section, Dakhla Oasis, Western Desert, Egypt: Systematics, Maastrichtian-Paleocene Ostracoda from Teneida section, Dakhla Oasis, Western Desert, Egypt: Systematics, biostratigraphy, paleobathymetry, and paleobiogeography. Journal of African Earth Sciences, Volume 174, article id. 104072.

Honigstein, A., 1984. Senonian ostracodes from Israel. Bulletin-Israel, Geological Survey, (78): 48 pp.

Honigstein, A., Almogi–Labin, A., Rosenfeld, A., 1987. Combined ostracod and planktonic foraminiferal biozonation of the Late Coniacian–Early Maastrichtian in Israel. Journal of Micropalaeontology, 6(2): 41-60.

Honigstein, A., lipson-benitah, S., Rosenfled, A., & Braun, M. (1993). Small-scale Cenomanian transgression pulses, indicated by ostracode and foraminifera assemblages, near Jerusalem, Israel. In International symposium on ostracoda. 11 (pp. 153-162).

Kolodny, Y., Garrison, R.E., 1994. Sedimentation and diagenesis in paleo-upwelling zones of epeiric sea and basinal settings: A comparison of the Cretaceous Mishash Formation of Israel and the Miocene Monterey Formation of California. Proceedings of the 29th International Geological Congress part C:133-158.

Lewy, Z. (1975): The geological history of southern Israel and Sinai during the Coniacian. Israel J. Earth-Sci, 24:19–43, Jerusalem.

Luger, P., 2003. Paleobiogeography of late Early Cretaceous to Early Paleocene marine Ostracoda in Arabia and North to Equatorial Africa. Palaeogeography, Palaeoclimatology, Palaeoecology, 196 (3):319-342.

Moore, R.C., 1961. Treatise on Invertebrate Palaeontology. Pt. Q, 3, Arthropoda, Crustacea, Ostracoda.,University Press of Kansas.

Morsi, A.-M.M., Hewaidy, A.-G.A., Samir, A., 2019: New Maastrichtian-early Eocene ostracod species from the Kharga Oasis area, Western Desert, Egypt. Revue de Micropaléontologie 65, 100385.

Morsi, A.-M.M., Hewaidy, A.-G.A., Samir, A., 2020. Maastrichtian Ostracods from the Dakhla Formation at the Kharga Oasis, Western Desert, Egypt: systematics and biostratigraphic significance. Annals Geol. Surv. Egypt. V. XXXVII, pp. 1 – 18.

Morsi, A.-M.M., 2000. Senonian ostracodes from east-central Sinai, Egypt; biostratigraphic and paleobiogeographic implications. Revue de Micropaleontologie 43, 47–70.

Mustafa, H., 2000. Fish Teeth from the Upper Um Ghudran Formation (late Santonian) of NW-Jordan. Neues Jahrbuch für Geologie und Paläontologie –Monatshefte, 10: 595-612, Stuttgart.

Nazzal, J., Mustafa, H., 1993. Ammonites from the Upper Cretaceous of north Jordan. Abhath Al Yarmouk 2: 87-120.

Okosun, E.A., 1992. Cretaceous ostracod biostratigraphy from Chad Basin in Nigeria. Journal of African Earth Sciences (and the Middle East), 14: 327-339.

Powell, J.H., 1989. Stratigraphy and sedimentation of the Phanerozoic rocks in central and south Jordan. Natural Resources Authority, Geological Mapping Division, Amman. 130 pp.

Puckett, T.M., 2002. Systematics and paleobiogeography of brachycytherine Ostracoda. Micropaleontology, 48: 1-87.

Reiss, Z., 1988. Assemblages from a Senonian high-productivity sea. Revue de Paleobiologie Special, 2: 323–332.

Reyment, R.A., 1960. The Cretaceous/Tertiary boundary of Nigeria. Reports of Geology Survey, pp.68-86.

Reyment, R.A., 1963. Studies on Nigerian upper Cretaceous and lower Tertiary Ostracoda. Part 2.

Reyment, R.A., 1980. Biogeography of the Saharan Cretaceous and Paleocene epicontinental transgressions. Cretaceous Research, 1: 299-327.

Rodriguez-Lazaro, J., & Ruiz-Muñoz, F. (2012). A general introduction to ostracods: morphology, distribution, the fossil record, and applications. In Developments in Quaternary Sciences (Vol. 17, pp. 1-14). Elsevier.

Seeling, J., Colin, J.P., Fauth, G., 2004. Global Campanian (Upper Cretaceous) ostracod palaeobiogeography. Palaeogeography, Palaeoclimatology, Palaeoecology, 213: 379-398.

Shahin, A., 2005. Maastrichtian to Middle Eocene ostracodes from Sinai, Egypt: Systematics, biostratigraphy, and paleobiogeography. Revue de Paléobiologie, 24(2), 749.

Shahin, A., El- Nady, H., 2001. Late Cretaceous- Early Tertiary ostracodes from northern Sinai, Egypt: Biostratigraphy and Paliobiogeography. Egypt Jour. Paleont. Vol. 1: 149-191.

Viviers, M.C., Koutsoukos, E.A.M., DA Silva-Telles, A.C., Bengtson, P., 2000. Stratigraphy and biogeographic affinities of the late Aptian–Campanian ostracods of the Potiguar and Sergipe basins in northeastern Brazil. Cretaceous Research, 21: 407–455.

JJEES

JJEES (2022) 13 (1): 16-25
ISSN 1995-6681

Jordan Journal of Earth and Environmental Sciences

Building Collapse in Nigeria and its Consequences on the Architect's Role as the Leader of The Building Team

Obi. I. Nicholas[1], Nwalusi, M. Dickson[2], Francis O. Okeke[3*]

[1,2,3] Dept. of Architecture, University of Nigeria

Received 11 April 2021; Accepted 6 June 2021

Abstract

The mishap of building collapse does not sound strange again in many sub-Saharan cities especially Nigeria due to the frequency of its occurrence, and architects are most vulnerable to blame because of their leadership position in building delivery. Evidence in literature has suggested a critical appraisal of built environment professionals' role to tackle the menace. However, the consequence of the role of architects as prime consultants hasn't been adequately investigated. Using a systematic review of literature for reported cases of building collapse in Nigeria between 2009 and 2019, the paper examines the causes of building collapse and enumerated specific areas members of the architecture profession in the building industry are implicated. The result reveals that the major causes of building collapse are the use of substandard materials, structural defects, and the use of incompetent personnel indicating a lapse in leadership and supervisory function. Although from direct observation, the study highlights deontology as the bane of building collapse in Nigeria and recommends among others that: Standard Organization of Nigeria (SON) should ensure that only certified building materials are allowed in the market; soil tests, environmental impact analysis, and structural analysis should be mandatory as well as proper supervision of construction works by competent professionals with strict law enforcement.

Keywords: *Architect, Building Collapse, Leadership, Nigeria, Professionals.*

1.0 Introduction

Among other requirements of a building, the structure is stable and the functionality of its intended use throughout its lifespan. Buildings are structures designed to support live loads such as weights of people, objects, rain, wind pressure, snow, in addition to their self-loads called dead loads, and failure in this aspect result to collapse. However, the incidence of building collapse is fast becoming a universal problem of which very little has been done to curb its occurrence, especially in developing countries. In Nigeria, it poses a serious challenge to the profession of architecture and other allied professionals and stakeholders in the building industry, including governments, private developers, landlords, and users (Chendo and Obi, 2015). Notably, cities in Nigeria like Abuja, Lagos, Port–Harcourt, Ibadan, Enugu, and Kaduna, to mention but a few, are witnessing a building collapse at alarming rates with many cases of collapsed buildings recorded in the recent past. Examples of collapsed buildings include; Ibadan multi-storey building in Mokota, Ibadan (Oyo State) 1974 (Olagunju et al., 2013), Mosque building, Osogbo, (Osun State), (1986), Saque Comprehensive Primary and Secondary School, Port Harcourt, (Rivers State), which resulted in the death of over 50 pupils in June 1990. Others include uncompleted two-storey building, Isinkan, Akure, (Ondo State) (1998); two-storey residential building, Funbi Fagun street, Abeokuta, (Ogun State) (1998); Nigeria Industrial Development Building (NIDB), Lagos (2006); a two-storey market plaza in Oshodi, Lagos (2010) (Olagunju et al., 2013). Prominent among the terrifying incidences of building collapse in Nigeria is the July 2006 collapse in Surulere, (Lagos State) where three buildings caved in, causing pandemonium among residents killing no fewer than 28 lives and leaving 50 others severely injured (Baje, 2019). Also in Lagos, about 37 people lost their lives in four-storey building mishap at Ebute Meta in 2006 (Baje, 2019). Another tragic collapse occurred in September 2014, where over 116 worshipers were killed in a six-storey building under construction which collapsed in the premises of the Synagogue Church of All Nations (SCOAN) in Lagos State (Nan, 2019). In another account in 2011, in Gimbiya Street, Area 11 Garki, Abuja, an uncompleted building collapsed killing five people including a pregnant woman, with over 40 squatters trapped in the house. It is also on record that no less than five worshippers died following the collapse of St. Anthony Catholic Church Cathedral in Oduma, Aninri Local Government Area of Enugu State (Olubi and Adewolu, 2018).

The review of the literature and anecdotal evidence revealed that between 1974 and 2019, which is 45 years, Nigeria have recorded over 221 cases of building collapse across its major towns and cities leading to the loss of many lives with several degrees of injuries recorded (Okeke et al., 2019). In fact, over the last four years, Yaqub (2019) alluded that Nigeria has recorded over 56 cases of building collapse and more still counting. Oyedele, (2018) further said that no state in Nigeria, out of the 36 states and the Federal Capital Territory (FCT), has been exempted from the event of building collapse in the last ten (10) years. In some years, building collapse occurred in more than ten (10) different

* Corresponding author e-mail: ogochukwu.okeke@unn.edu.ng

locations in Nigeria with casualties; according to Omenihu et al., (2016) from 1971 to 2016, a total of 1455 lives were lost in reported 175 occurrences of building collapse in Nigeria. It is therefore expedient that causes, implications, and mitigation steps of the nuisance be carefully examined.

Evidence in the literature suggests that while building collapse has been linked to inferno, acts of terrorism, global changes in the environment, and seismic activities in many western countries (World Bank, 2015), in countries of sub-Saharan Africa, most cases of building collapse have been attributed mainly to human factors such as design errors and negligence, and lack of institutional mechanisms and capacity to prevent the collapse of buildings. Other factors identified include Lack of geotechnics investigation, construction defects, quackery (Tanko et al., 2013; Agwu, 2014), and poor construction supervision linked to lack of physical development and building regulations enforcement.

Building collapse can be partial for example, Nigerian Industrial Development Bank (NIDB) Building on Broad Street, Lagos State in 2008, or complete, like the Lekki Garden building collapse in 2016. The site of building collapse is disheartened and very pathetic (see Figures 1-5 below), because most often it is associated with loss of life, investment, time, equipment, and waste of building materials. It also affects the reputation of the construction industry in the area of occurrence. The Nigeria Construction and Infrastructure Summit Group estimate that the nation loses between 2.03tn and 3.05tn naira annually to infrastructure deficit due to building failure (Okeke et al., 2020) as the rate of building collapse recorded is overwhelming. Below are scenes of building collapse sites.

Figure 1. Two -Storey Building that collapsed in Lagos, Nigeria (2019)
Source: Olasunkanmi, (2019)

Figure 2. Collapse of Two -Storey Building in Delta State, Nigeria (2015)
Source: Chido, (2015)

Figure 3. School Building Collapse in Lagos, Nigeria 2019
Source; Rayyan, (2019)

Figure 4. A Collapsed Building caused by Earthquake in Taiwan 2018
Source: the Associated Press, (2018)

Figure 5. Collapse of multistorey building in Agbama, Umuahia, Nigeria (table 1, No. 25)
Source: Babalola, (2015)

In building design and construction, architects establish realities, which once erected are not altered easily (Okeke et al., 2019). Consequently, the degree of pressure on the architect to deliver the projects from the moment he accepts commission has intensified in recent years due to the prevalent climate of the building industry. This has arisen due to greater complexity and scale of projects; more client-generated conditions of engagement with onerous implications for the architect, the emergence of hybrid and untested contract conditions, shifts in practice ethics which tend to confuse the traditional roles and responsibilities within the building team (RIBA, 2004). Based on the overwhelming ill effects of building collapse, scholarship in literature has suggested critical appraisal of built-environment professionals' role to tackle the frequent incidences. However, the consequences of the architect's role as the prime consultant have not been adequately explored. The study presumed that the

professional architect by right must exercise the "duty of care" he owes to all his design projects and the study aims to identify the major causes of building collapse in Nigeria and its implication to the architect's involvement as the leader of the project team. The specific objectives perused are:

- To identify the major causes of building collapses in Nigerian cities;
- To investigate the implication of building collapse to the Architects and other members of the building team;
- To suggest possible solutions to tackle the problems and issues that are likely to guide the architect and his team in addressing the problems.
- The study encountered a limitation of porosity of data on recent cases of building collapse as most incidence is no longer reported and or rarely investigated.

1.1 Context of Study

Nigeria is a West African country and has a diverse geography, with climates ranging from arid to humid equatorial (Okeke et al., 2020). On the global scale, Nigeria is the most populous black nation with its most diverse feature being its people. She occupies an area of 923,768 sq km, extending 1,127 km East-West and 1,046 km North-South (National Bureau of Statistics, 2010), with a population of over 198 million (National Population Commission, 2019). It lies between latitudes 4°N and 14°N, North Greenwich Mean Time (GMT and longitudes 3°E and 14°E East of Greenwich Mean Time (GMT) in the southeastern edge of the West African region with the Atlantic Ocean, Sahara Desert and Cameroon Mountains, which form the southern, northern and eastern boundaries respectively. (See Figure below)

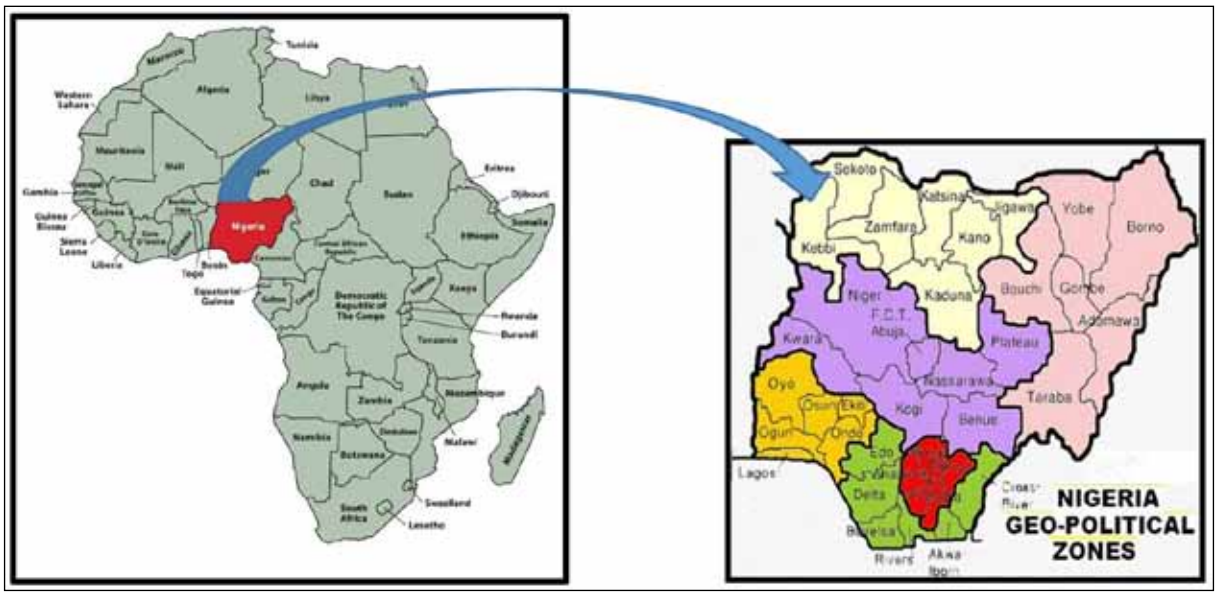

Figure 6. Map of Africa showing Nigeria and map of Nigeria showing 36 States that make up the 6 Geopolitical Zones
Source: Nigerian population commission, (2018)

1.2 Conceptual framework

The technique and architecture of buildings all over the world depend on the climatic boundary conditions, the culture, and the availability of raw materials within the locality (Okeke et al., 2019). Buildings provide shelter with protection from both natural and man-made elements (Okeke et al., 2021), and must be well conceptualized, designed, and erected to gain the desired comfort from the environment (Odeyemi, 2012). According to Ayinuola and Olalusi (2004), failure can be cosmetic when a building experiences an addition or subtraction of substances that affect its physical outlook, or structural when both physical outlook and structural stability have been affected. In line with the above concepts, Olagunju et al., (2013) defined building collapse as a total or partial failure of one or more components of a building, leading to the inability of the building to perform its principal function of stability, comfort, protection, satisfaction, and safety. It follows then that the building is said to have failed or collapsed when one or more elements of the structure cannot perform its original function efficiently due to the malfunction of the constituent materials. Furthermore, Omenihu et al., (2016) defined building collapse as the inability of a building component to withstand the loads it was designed for. Ede (2010) posits that collapse is a state of complete failure when the structure has factually given way and most of its members have carved in crumbled, and the building can no longer stand as originally built. Ayinuola and Olalusi, (2004) opined that failure is considered as occurring in a component when such component cannot perform its intended functions. In summary, the unplanned falling of a building is referred to as building collapse, while the planned falling of a building is referred to as demolition.

2.0 Literature Review

Evidence in the literature indicated that the rate of building collapse is increasing in many developing countries (Boateng, 2020), and owing to the regular occurrence of building collapse in Nigeria, research on this subject has been championed by mostly Nigerian Scholars (Okeke et al.,2020). Some elucidated factors that cause building collapse in Nigeria include poor structural design, use of unskilled workmen and use of substandard material, and lack of adequate management and supervision (Ayeni

and Adedeji, 2015; Hilary et al., 2018; Odeyemi, et al., 2019). Oloyede et al., (2010) attributed causes of building collapse to negligence in some vital areas in construction such as soil investigation, design for building loads, wind loads, earthquakes, uneven terrain, and use of substandard building materials, poor supervision, and overall poor workmanship. Ede, (2010a) identified other factors which he termed the "Nigerian factor" enumerating corruption, lawlessness, and the "jack of all trade" posture of Nigerian building professionals who take all forms of responsibility in the building process. Tanko et al., (2013) revealed that quackery is the cause of the most frequent building failure in Nigeria. However, the majority of investigations revealed the contrary; that sub-standard or poor quality of building materials is the main cause of building failure and collapse in Nigeria (see table 2). Ayinuola and Olalusi (2004), blame parties in the building industry, clients, architects, engineers, town planners in the local authorities, and contractors stating that they have contributed to building failures in various dimensions. Adebayo, (2006) noted that building collapse incidences can be controlled or minimized if the client is ready to pay for high-quality materials and expert professional services. In 2006, the Nigerian government regulatory body of engineers, Council of Registered Engineers in Nigeria (COREN) reported an outcome of an investigation panel for three cases of collapsed buildings in 2005. It was discovered that no registered engineer was involved. Ayedun et al., (2012) compiled findings on collapsed buildings in Lagos State between the years 2000 and 2010 (10years), out of the 54 collapsed buildings 37 (68.52%) failed and collapsed due to structural related issues. Oseghale et al., (2015) opined that weakening of reinforced concrete could occur from corrosion of the reinforcement due to carbonation and chloride ingress through cracking from overloading of the concrete structure and construction defects. The findings of Oseghale et al., (2015) and Folagbade (2001) revealed that poor structural design, use of substandard building materials, non-compliance with approved building design, poor workmanship, lack of qualified and experienced professionals to ensure quality construction are the major causes of building collapse in Nigeria. Ayinuola and Olalusi (2004), reasoned that building failures occurred due to inadequate knowledge of building structural performance and unexpected environmental phenomena. Fagbenle & Oluwunmi, (2010) blamed the high frequency of structural collapse on the low level of compliance with approved architectural and structural drawings before construction, ineffective monitoring by the concerned government agencies, and the low level of awareness of the existing building regulations by clients and contractors. This submission was buttressed by Mrabure and Awhefeada, (2020) and stressed that there is a need to enforce the provision of these laws. Windapo, (2006) stated that over the years, Lagos residents have witnessed consistent building collapse leading to fatalities, litigations, and regulatory actions, pains, injuries, delayed schedules, bad reputations, and loss of properties. Most collapsed buildings were found to be constructed with low-quality building materials, while incompetent craftsmen rather than professionals were engaged. Also, the existing building codes, meant to guide builders were rendered ineffective because of a lack of political will to enforce the same by the Town Planning Authorities. On the other hand, most investigations, as well as research on the causes of building failure, tended to focus on Architects, Engineers, Surveyors, and Builders; hence several architectural and design elements are seen to be mentioned in many articles and linked to failure causes. However, many have no connection with building stability or otherwise; the building can only collapse when one or more of its essential components failed and these components are part of the structural frame. The time-tested method is not always followed on many projects. There is no control over the building process in Nigeria. An empirical ascertainment of the causes of building collapse in Nigeria was carried out by Ayedun et al., (2012). The study identified the use of substandard building materials, poor workmanship by contractors, use of an incompetent contractor, faulty construction methodology, heavy downpour, non-compliance with specification/standards by developers/ contractors, inadequate/lack of supervision/inspection/ monitoring, structural defects, defective structural design, illegal conversion /alteration/additions to existing structures and dilapidating structures as the major causes of building collapse in Lagos State, Nigeria. Again, the research of Hamma-adama et al., (2020) from academic literature identified three leverage points as differential settlement, structural failure, and structural issues, all connected to the field of civil engineering as the leading cause of frequent building collapse in Nigeria.

In the study conducted by Qurix and Doshu (2020) aimed at exploring major causes of building collapse in Nigeria as perceived by building industry professionals, policymakers, and the public; it was discovered that the leading cause is the change of use without following professional protocols. Furthermore, it was reported that the Client's undue interference, made at an advanced construction stage without consultants' advice is a contributory factor to building collapse (Odunisi, 2019; Imafidon and Ogbu, 2020). Fakere et al., (2012), reviewed extensively, building collapse concerning the role of building materials during construction. It was discovered that building materials such as reinforcing steel, cement, sand, granite, sandcrete blocks, and concrete play a huge important role in either the collapse or stability of buildings in Nigeria. It was concluded that 10-25% of buildings that collapse in Nigeria are as a result of the use of poor quality building materials. Okeke et al., (2020) investigated the cause of building collapse in Nigeria and discovered that negligence on the part of a government agency has fueled the incessant building collapse in the country. Ayodeji (2011), in a study, termed sustainable construction practices revealed that the quality of materials and workmanship in the Nigerian building industry is not satisfactory and that the problem lies in the use of inappropriate materials supplied to the site, inadequate materials, and inefficient supervision of the site workers. Usman et al., (2010) revealed that building Collapse is an occurrence that has been frequent over the decades caused by many factors which have their great impact on lives and

properties of man, judging from reported cases of building collapse in Nigerian cities between 2000 till 2015. Ayedun et al., (2012) gave an account of some collapsed buildings in Lagos between the years 2000 and 2010 with their locations and suspected causes of their collapses (Table 2). Windapo and Rotimi, (2012) examine contemporary issues in building collapse and its implications for sustainable development in Nigeria and establish that the approach to construction by industry stakeholders does not match sustainable principles, and contributes to the general underperformance of buildings.

3.0 Research Methodology

The study investigated building collapse in Nigeria and its consequences on the Architect's role as the leader of the building team. It utilized Primary data based on anecdotal pieces of evidence, authors' observations in the field of practice, and also secondary data from journals, conferences, and technical reports of previous works of other authors on the subject matter. A systematic review of related literature was adopted possibly to achieve the objectives set out in the study. Papers reviewed were identified via searchers on online databases such as Google Scholar and Science Direct among others. Reported causes of collapsed buildings in Nigeria between 2009 and 2019 were identified and using content analysis, descriptive statistics, and percentages, data collected were analyzed. Research results revealed that the majority of the cases were due to the use of substandard building materials and a few cases owing to natural occurrence. This invariably indicates that the leadership role of the architect in the building team is lax.

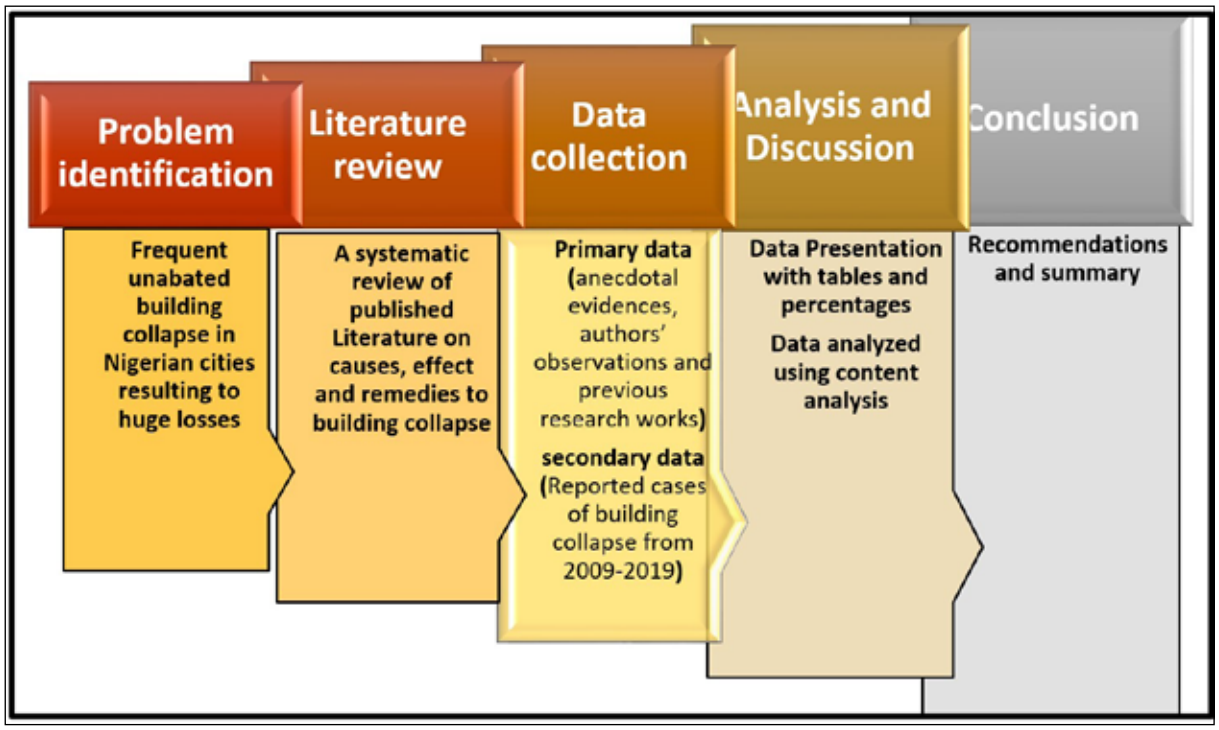

Figure 7. research methodology flow chart

4.0 Data Presentation, Analysis, and Discussions

Table 1. Records of building collapse in Nigeria from 2009 to 2019
Source; Source: Babalola (2015); Omenihu et al., (2016)

sn	Location	Date of collapse	Type of building	Causes of Collapse	Casualty
1	Ogbomosho Oyo state	February 2009	Six storey Lautech Teaching hospital under construction	Substandard material[1] Poor supervision[3]	5 died
2	Ogbomosho Oyo state	Mar-09	Four storey building under construction	Not reported[7]	5 died
3	Lagos	Jun-09	Two storey building	Not reported[7]	7
4	Aghaji crescent GRA Enugu	Aug-09	A fence wall	No proper drainage[3]	1
5	Oke padre street Itamorin Abeokuta	18th October 2009	Uncompleted residential building	Use of substandard materials[1] Hasty construction[3]	3 died 11 were injured
6	Garki Abuja	Nov-09	2-storey commercial building	Structural failure[2] Substandard material[1]	-
7	Isopakodowo street, Cairo oshodi Lagos	26th April 2010	Residential building under construction	Use of substandard material[1]	4 died 12 were injured
8	Adenike Street off new market oniru estate VI Lagos	2nd June 2010	Uncompleted storey building	Use of substandard materials[1]	1 died 2 injured
9	Plot 702 Port-Harcourt crescent Garki 11 Abuja	Jul-10	6 suspended floors for commercial purposes with a basement	Substandard materials[1] Use of unqualified professionals3	-
10	2 Okolie street off Gimbiya street, Abuja	11th August 2010	Uncompleted four storey building	Substandard materials[1] Disregard for building regulations[4]	23 died 11 were injured
11	Tinubu street VI Lagos	28th September 2010	4-Storey Building	Structural defect[2]	3
12	No 9B Adenubi close ikeja Lagos State	13th March 2011	5- storey hotel under construction	Poor quality concrete1	2

13	Oba ile Housing Estate Akure	2011	The collapse of a hotel Building under construction	Substandard materials[1]	–
14	Mararaba (near Abuja)	The collapse	The collapse of a 2- storey Zenith Bank Plc	No Geotechnical investigation[6], Undersized[1] Large span slab, No specific floor thickness on drawing[6]	2 died 11 were injured
15	No 6 Magaji close idumota Lagos	Jul-11	3-storey building	Not reported[7]	18
16	Aderibigbe street, Maryland Lagos	Oct-11	A penthouse	Structural failure[2]	2
17	No 3 Ademola Awosike Road Kubwa Extension III, Abuja	8th August 2012	The collapse of 2-storey building under construction	Poor quality material[1] poor workmanship[3], weak foundation[1], failure of structural element[2]	3 died 9 injured
18	Gwarinpa Estate Abuja	28th January 2012	The collapse of two storey building	Structural Defect[1], Demolition operation[3]	3
19	Apo Mechanic Village Abuja	13th June 2012	1-storey commercial building under construction	No qualified professional on-site, poor supervision[3], use of poor quality material[1]	–
20	Hadeja Road by Ibrahim Taiwo Road Gombe	Jul-12	101 year old 3-storey commercial/residential	age, Lack of maintenance[6]	1
21	Muri Okunola street Eti-Osa LGA of Victoria Island Lagos	4th November 2012	Collapsed building under construction	Structural failure[2] Poor construction[3]	3 dead 50 trapped
22	Jakande estate in Oke-Ake-Afa, Isolo Lagos	20th November 2012	Collapsed of a building (in use)	Structural Failure[2], Occupants ignored governments safety warning[4]	3
23	!74 Corporation drive Dolphin Estate, Ikoyi Lagos	20th November 2012	Collapsed of a building	Structural Failure[2]	–
24	Ojodu, Lagos	8th May 2013	2-storey Building under construction Illegal approval	Structural failure[2]	1
25	Agbama, area, Umuahia	15th May 2013	Building under Construction	Not Reported[7]	7
26	Ojodu, Lagos	May-13	Three |storey building	Not reported[7]	2
27	Agege motor road, Mushin Lagos	11th June 2013	Three storey building	Unauthorized conversion. Use of quacks [3]	1
28	Ishago road, Surulere Lagos	21st July 2013	2-storey uncompleted building under construction	Non-compliance to regulatory authority warnings[4] Inferior Building materials[1]	4
29	Ebeute-meta, Lagos	11th July 2013	Residential Building	Structural Defect[2]	7
30	Maitama, Abuja	6th September 2013	Building Collapse	Not reported[7]	3
31	Nyanya, Abuja	27th September 2013	Storey Building of Government secondary school	Not reported[7]	8 injured
32	Lagos Island	25th September 2013	Three storey building fell on a bungalow	Not reported[7]	2
33	Amassoma in Southern Ijaw LGA of Bayelsa State	5th October 2013	Lecture theatre building at the permanent site of the Niger Delta University	Use of substandard material[1] No compliance with the standard procedures in the use of materials[4]	-
34	Ologuneru in Ido LGA	May 3rd, 2014	An uncompleted	Not reported[7]	2
35	Akure, Ondo state	9th May 2014	A hostel building under construction	No geotechnical report Use of quacks[3]	2
36	Agudama-Epie, near Yenagoa	19th May 2014	Uncompleted Church building	Heavy downpour[5]	20 injured
37	Onitsha, Anambra state	2nd June 2014	An uncompleted four storey building	Structural failure[2]	4
38	Pedro police station, somolu Lagos	30th June 2014	2-storey barrack building	Not reported[7]	-
39	Ejigbo, Osun State	10th July 2014	School building complex few hours before commissioning	Not reported[7]	2 injured
40	Bucknor estate, Jakande-Isherioshun Rd.Ejigbo/isolo Lagos State	30th July 2014	The collapse of three storey building	Structural failure[2]	-
41	Osogbo, Osun State	19th August 2014	One storey building Heavy downpour		1 injured
42	Lagos	12th September 2014	The collapse of a warehouse at synagogue church	Demolition process[3]	4
44	Benin	30th September 2014	The collapse of liberty power bible church	Structural defects[2] Use of substandard material[1]	-
45	Ebute Meta Lagos	15th July 2015	3-storeyResidential Building	Structural defects[2]	4 rescued
46	Swamp street Odunfa Lagos island	21st October 2015	3-storey Residential Building	Structural defects[2]	4 rescued
47	Lekki, Lagos	9th March 2016	Five storey Building Under	Heavy rainfall[5] foundation failure[2]	34
48	Mile 12, Lagos	19th March 2016	Two storey building	Structural defects[2]	1 dead 1 injured
49	Malete, Kwara State	2016	Three storey building	Not reported[7]	–
50	Lagos Island	27th August 2017	Residential Building	Heavy downpour5 Vibration3	8
51	Zulu Gambari Road, Ilorin	18th August 2017	Four Storey Building	Not Reported[7]	3 Injured
52	Abuja	18th August 2018	An abandoned Building	Old age, Illegal conversion[6]	2 Dead 3Injured
53	Port-Harcourt	November 19th, 2018	7- Storey Building under construction	Not Reported[7]	15 dead 31, rescued
54	Lagos	February 3rd, 2019	3-storey Building	Not reported[7]	2 dead 1 injured
55	Ita-faji, Lagos Island	13th March 2019	3-storey building	Old age[6] Non-compliance to regulatory authority warnings[4].	20 dead 41 Injured
56	Sogoye, Bode Area of Ibadan	15th March 2019	3- Storey building under construction	Concrete was not allowed to cure before continuing the construction[1]	–

Table 2. Selected Collapsed Buildings in Lagos from 2000 to 2010
Source; Ayedun, et al., (2012)

S/N	Year	Location, of Building	Casualties	Suspected Cause of Collapse
1	2000	.Eleganza Building, Ikota Ajah	deaths,25 injured ,2	Structural failure[2]
2	2000	St., Dennis, Catholic Church, Bariga	deaths 3	Structural failure[2]
3	2000	Semi street, Surami, Itire,14	1death,1 injured	.Structural, slab deterioration[2]
4	2000	Ogba,Road, Agege,14	N/A	Flooding[5]
5	2001	Karunwi, Central Mosque, Mushin	deaths 7	.Structural defects[2]
6	2002	storey building along Allen Avenue 3	N/A	Structural failure[2]
7	2003	Buildings at 28 Idumagbo, street 2 (and10, Pedro street (same day	deaths, several injured 30	The explosion from fireworks materials[6]
8	2004	Building, at Ilasamanja	N/A	Use, of substandard materials[1]
9	2004	Alias, street, Lagos Island ,10	N/A	Dilapidation/Lack, of Maintenance[3]
10	2005	Princess Street, Lagos Island 6	N/A	Poor construction Materials[1]
12	2006	.6A, Milverton Close, Ikoyi	N/A	Dilapidation[6]
13	2007	The building at Ebute Metta	.Several deaths	Unauthorized conversion/poor supervision[3]/use of substandard materials[1]
14	2010	Uncompleted storey building at Adenike .street, Oniru Estate, Victoria Island	dead,2 killed 1	Use of substandard materials[1]Non .compliance with Approved Building Plan[4]
15	2010	,storey building at,24, Ali Street 4 .Victoria Island	killed. Several injured 3	Structural overloading[2]

4.1. Results

The occurrences of building collapse in Nigeria from 2009 to 2019 were investigated. This investigation was based on available published statistics of researchers evident in literature, because the national procedures/actions followed in investigating the cases of building collapse in Nigeria is setting up a panel for an investigation that is usually bureaucratic, time-consuming, politically influenced, and sometimes end up not yielding substantial findings. The locations, date of occurrence, the building types, the suspected causes of the collapse, and the casualty Figures were obtained and reported in Tables 1 & 2. The result presented in the graphical illustration below shows that the leading cause of building collapse within the period under investigation is the use of substandard materials while natural disasters account for the least cause compared to other developed cities.

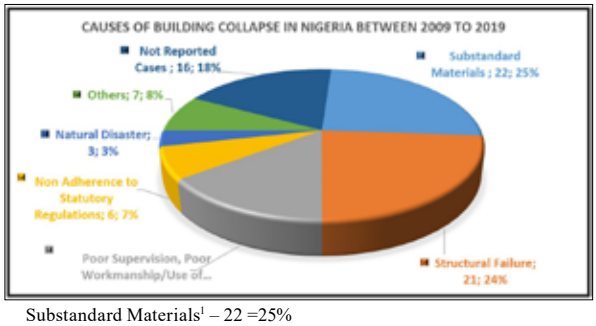

Substandard Materials[1] – 22 =25%
Structural Failure[2] – 21 =23.9%
Poor Supervision, Poor Workmanship/Use of Quacks[3]- 13 =14.8%
Non Adherence to Statutory Regulations/Warnings and compliance with Approved Building Plan[4] – 6 = 6.8%
Natural Disaster[5] – 3 =3.4%
Others[6] - 7 =7.9%
Not Reported Cases[7] - 16 = 18.2%

Total cases identified =22(25%) +21(23.9%) +13(14.8%) +6(6.8%) +3(3.4%) +7(7.9%) +16(18.2%) = 88 (100%)

4.2 Analysis

A summary of the main causes of building collapse in Nigeria is presented below:

Substandard materials recorded the highest number of cases amounting to 25% and are considered as a major challenge facing the stakeholders of the building industry. It manifests in form of poor concrete mix, poor cemented block units, use of untested materials, and use of low-quality materials. This is followed by Structural Failure, 23.9% while Poor Supervision, Poor Workmanship/Use of Quacks collectively recorded 14.8%. Non Adherence to Statutory regulations and None Compliance with Approved Building plans to account for 6.8% of the whole cases. Natural disasters recorded the lowest 3.4 %. Other cases such as No Geotechnical investigation, no specific floor thickness on drawing, Old age/lack of maintenance, Explosion from fire, and Dilapidation recorded 7.9%. Generally, 18.2% belong to None Reported Cases. This study observed that building collapse is not common in bungalows, however, occurs more frequently in storey buildings and that it is an event that repeats itself every year. Under location, the trend highlights Lagos state with numerous reported occurrences probably due to nearness to the sea, high population with demand for housing, or huge causalities of happenings.

5.0 Discussions

The erection of a building or structure undergoes a building process of various stages from the pre-design stage to post-construction and occupancy. According to Fowode (2016), building projects start well before ground is broken. It is pertinent to think of building construction as a series of activities that result in the structure's actualization. Therefore, it requires the services of a team of experienced professionals in the building industry to avoid failure.

5.1 Functions of Building Design Team: The land Surveyor

determines the shape, geographical orientation, and size of the site. The Architects' duties involve the design, coordination, and supervision of the building project. Structural engineers are in charge of structural design and supervision of structural specifications. The town planners ensure that the building codes and regulations such as setbacks, maximum heights of buildings, building lines, and plot coverage are incorporated in the building site. Quantity Surveyors estimate the probable amount that will complete the house and issue payment valuations at interims The Estate Surveyors take control of the building for management after it has been completed. These professionals ensure that buildings are professionally built to avoid the incessant collapse in Nigeria although the efforts of these professionals in arresting the frequency of building collapse have not been effective and at minimal given the current trend of building failure within the country.

5.1.1 Identified Areas of Loopholes arising from the Building team

Client: Changes and variations at an advanced stage of construction; Changes to standard conditions of contract, specifications, regulations, and bye-laws Interference in the contract roles and duties of contract Consultants and administrators; Giving the contract to inexperienced ill-equipped contractors

Contract consultants: (architects, engineers, surveyors, town planners, quantity surveyors) Errors and design inadequacies; Use of inexperienced and incompetent personnel and undefined delegation of responsibilities; Inadequate or incomplete information; Lack and or poor co-ordination of contract issues; Taking commission beyond the scope to minimize cost

Government Agencies: Approving drawings prepared by unregistered consultants through bribery and corruption; Selling retained drawings meant for other sites to prospective clients without considering the nature of the new site; weak monitoring and supervision of site work.

Contractors: Use of inexperienced and incompetent personnel and undefined delegation of responsibilities; Inadequate or incomplete information; Lack and or poor co-ordination of contract issues; Taking commission beyond scope and capacity of the firm

Sub-Contractors: Poor standards of workmanship; Conflicts with main contractors

5.2 Implications of the Architect's duties and responsibilities as the leader of the building team and co-coordinator of other allied professional input

Under this criteria, architect's managerial roles as spelled out in the standard form of building contracts (SFBC, 1996) include, site investigation, preparation of sketch plans, sketch design proposals, design details and working drawing, specifications, advice to the client, co-ordination of other consultants' services, issuing and preparation of variation, certificates, and overall supervision. Enormous responsibilities rest on the shoulders of the architect who among other players in any building project has a total appetite to actualize and deliver his design drawings because a failed building project is regarded as the abortion of an architect's brainchild. Judging from the above, it is therefore of paramount importance that an architect imposes firm management disciplines on his activities through the establishment of a clear management structure and responsibility. From the result of the study, substandard materials recorded the highest number of cases with 25%. These findings, therefore, indicate the architect or his team and at large the architectural profession of laxity in their overall supervisory role and contract administration in building projects. The role of the Architect as a leader is also to refuse the use of none certified materials because according to the ethics of the profession, the prime consultant (architect) owes a duty of care and diligence to the building and the environment. Furthermore, observation and the author's personal experience in the building industry over the years and in conjunction with the research results have proved that deontology is an ethical issue boarding around corruption as the bane of building collapse in Nigeria. Laws and adequate frameworks exist, however lack of implementation and its enforcement fuels the unethical practice. This finding corroborates the result of Ede (2010), who discovered that the 'Nigerian factor' such as lawlessness, corruption, and the assumption that any Engineer in the construction industry can undertake all forms of responsibility in the building process. By deontology, we mean the normative ethical position that judges the morality of an action's adherence to rules or obligations rather than either the inherent goodness or the consequences of those actions. Stakeholders in the building and construction industry now result in 'cutting corners' for selfish reasons. If the weak framework of the Government and its agencies has allowed substandard building material to flood the market, the architect as a leader in the building team should not permit its use on construction sites or grant approval for such material on building projects. Potential areas of loopholes that should be guided by the architect as viewed by this study include:

- **Management of Project:** Management disciplines on the part of the architect entail his ability to manage his activities in project administration.
- This can be achieved through proper checks and responses arising from reports and drawings as they come or leave the office. Accepting commission within the scope and capability of the firm.
- **Management of Staff:** Delegation of roles of members of staff should be following levels of experience and competence to ensure adequate skilled supervision. Be always accessible to all the staff under his control. Some firms resort to employing the services of school leavers to manage big projects thereby acting as principal architects. Establish regular systems of project monitoring on a feedback basis including regular inspections (RIBA, 1998; 2004).
- **Dealing with other consultants:** Ensure that the consultants appointed by the client are adequate for the project and that the terms of appointment do

not override the leadership role of the architect. Do not delegate to other consultants' services that you are bound by contract to execute and for which in any event you are accountable. In the same vein, do not take up the services of other consultants even if you think you are capable because you will be liable to claims arising from such actions in the event of any collapse. Architects venturing into the design of structural drawings may result in a faulty design capable of causing collapse.

- **Dealing with project Site:** Check appropriate site information provided by the client
- Any departure from the original brief must be agreed upon with the client in writing
- **Planning Permission:** Architects should not allow any work to commence until planning permission is granted. Refusal on the ground of defective structural drawing may lead to building failure if the building has gone to the advanced stage.
- **Construction of building:** Check the accuracy of technical details before the commencement of works**.** The specification should be made in clear language in a standard format and must conform to the latest code and standards.
- **Building Contract:** Care must be taken when selecting contractors on behalf of the client. Be especially wary of contractors selected by the client
- **Commencement of works:** Contracts are often started with incomplete drawings, incomplete details, soil tests, foundations details due to pressure from the client. The problems that can follow this action can lead to building failure and bring serious trouble for the architect. Do not permit a contract to commence in advance of adequate information. Do not alter design or details or permit some without the client's written consent
- **Project Management:** If you are appointed project manager for a project of which you are not the architect, ensure that you do not interfere in architectural matters. Confine strictly with management duties.
- **Materials:** Structural defects caused by wrong concrete mix invariance to structural engineer's specification must be avoided. Substituting lower-quality materials should be avoided.
- **Inspection and Supervision:** There should be clarification between the two terminologies. Inspection means looking at something critically to ensure whether it meets prescribed criteria. For architects, it means a periodic inspection of the works in progress to establish whether it is being carried out generally following the contract in terms of progress and quality of work, that is, an inspection cannot guarantee detection of every defect. The best way an architect should carry out an inspection is when unaccompanied by the contractor. Where work is in variance with the contract, an architect should issue an instruction to the contractor on how to deal with it.

Supervision means a continuous overviewing of progress. It implies that architects supervise the works of their employees. There is widespread misunderstanding of the term supervision and it should never be used in connection with the architect's leadership role during the building works (RIBA, 2004).

6.0 Recommendations

Based on the findings, the following are recommended:

Substandard Materials

i. Standard organization of Nigeria, (SON) should monitor the standard of blocks molded-in block industries and impose minimum standards in terms of sand-cement ratios and scrutinize building materials that are supplied for use in Nigeria and ensure that only certified building materials are allowed in the market.

ii. The standard organization of Nigeria should be vigilant to ensure that building materials imported into the country conform to standard requirements.

iii. There is a need to empower and restructure materials testing laboratories in all Geo-political zones of the country.

iv. Building professionals and contractors should ensure proper and efficient checking of materials brought to site and carry out tests such as cube test for concrete, tensile strength for steel bars, slump test for in-situ concrete in a building project following Engineer's specification.

v. The design team in any building project should ensure that building materials supplied to the site by the domestic or nominated supplier are under the contract specification.

vi. The national regulations regarding building materials are revised and consider the international standards to be adopted

vii. Build on tested engineering properties of available local building materials in Nigeria.

Structural Failure

i. There is a need to organize periodic public awareness campaign through electronic and print media to sensitize the public on the advantages of using professionals as a way of realizing safe buildings. Structural Engineers should be engaged in all building projects above two floors.

ii. The building construction process involves professionalism in the planning, design, and execution of the project. Engineering consultants must be involved in the design and supervision of buildings

iii. Imposing additional floors beyond original design provision should be avoided

iv. Reduce the level of exposure of structures to risk by imbibing maintenance culture, seek advice from

experts when changing the form and use of buildings, and insist on material and soil tests for multistory buildings.

v. Regulatory professional bodies such as the Engineering Regulatory and Monitoring (ERM) unit of COREN and their corresponding associations should on regular basis organize workshops for stakeholders in the building industry to update their knowledge and highlight the dangers and penalties associated with collapsed buildings.

Poor Supervision, Poor Workmanship/Use of Quacks

i. All building professionals play key roles to actualize their respective obligations during building production, using the wrong professionals at any stage of the building process puts the building in danger

ii. Construction should involve the collaboration of different professionals who have been registered by law practice the art of the building process.

iii. Professionals in the building industry should maintain their integrity and professional ethics and work by standard practice procedures laid down by the standard form of building contracts SFBC and Joint Contract Tribunal JCT/80 especially when they play in the hands of ignorant clients

iv. Only workers or building operatives with the appropriate training and experience should be allowed to engage in building works especially on the structural members.

Non Adherence to Statutory Regulations/Warnings and Compliance with Approved Building Plan

i. It is the duty of the architect as the prime agent of the client to detect or rather direct the client to use the right professionals. This he achieves by at last ensuring that the Structural and Services drawings brought to his office are stamped and signed by professionals registered by their respective professional bodies before proceeding to plan authority for "building permit".

ii. Urban or Town development agencies at various levels of government (Commission, Board, and Authority) should enforce control of building works in their localities as laid down on Urban and Regional Planning Decree 88, of 1992 and as in section 13 of the National Building Code 2006.

iii. Proper planning, supervision, and monitoring of construction activities should be institutionalized by policymakers to ensure that all buildings are constructed according to design, specifications, and planning regulations

iv. All building plans tendered by any developer for approval must comply with the Nigerian new building code and local bye-laws and regulations.

v. Soil Tests, Environmental Impact Analysis, and Structural Analysis need to be made mandatory for all institutional, industrial, and commercial buildings and submitted along with the building plans to Town Planning Authorities by all building developers.

Natural Disaster

i. Building on flood plains or flood-prone areas should be avoided because flood weakens soil structure and foundation.

ii Building on the hillside is likely to collapse due to erosion. Ensure that the soil surrounding the building is well protected with concrete or with stone pitching. All stakeholders in the construction industry should adhere strictly to the provisions of the building code.

7.0 Conclusion

The study investigated the frequent causes of building collapse in Nigeria and enumerated specific areas members of the architecture profession and other stakeholders in the building industry are implicated. The research results revealed that the majority of the cases were due to the use of substandard building materials and a few cases owing to natural occurrence. This invariably indicates that the leadership role of the architect in the building team is lax. The responsibility of the Architect as dictated by his professional ethics and his position as the coordinator of other allied professionals is always at stake when things are not followed according to standard procedures. This paper thinks that the building project delivery though is a collective responsibility of the stakeholders involved in the building process, the architect who stands out as the first target of blame during incidences of building collapse should ensure that his duties are discharged diligently as backed by relevant existing laws. The professional architect also should guide against deontology an ethical issue in construction. It recommends an overhaul of planning and implementation policies for building development regulations (e.g. building codes), with strict enforcement of laws, and that the Nigerian government, as a major construction stakeholder should initiate sustainable construction measures and ensure this as best practice for the construction industry.

Funding

No funding was received for the study.

Conflict of interest:

The authors declare no conflict of interest

Acknowledgments

The authors wish to acknowledge the technical assistance of Prof. I G Chendo of the Department of Architecture, University of Nigeria.

References

Adebayo, S.O (2006) Improving Building Techniques "Proceedings of Workshops on Building Collapse: Causes, Prevention, and Remedies. The Nigerian Institute of Builders, Lagos State.

Agwu, M.O. (2014) Perception survey of poor construction supervision and building failures in six major cities in Nigeria, British Journal of Education society and Behavioural Sciences. 4 (4) 456–472.

Arayela,O and Adam, J.J. (2001). Building Disasters and Failures in Nigeria. Causes and Remedies. Journal of the Association of Architectural Educators in Nigeria (ARCHES). 1(6), (2001)

Ayedun, C., Durodola, O. and Akinjare, O. (2012). An empirical ascertainment of the causes of building failure and collapse in Nigeria, Mediterranean Journal of Social Science. 3 (1) 313–322. DOI:10.5901/mjss2012.03.01.313

Ayeni, D.A. and Adedeji, M.D. (2015). Strategies for Mitigating Building Collapse in Nigeria: Roles of Architect and other Stakeholders in the Building Industry. Civil and Environmental Research, 140–146.

Ayinuola, G.M. and Olalusi, O.O (2004). Assessment of building failure in Nigeria, African Journal of Science and Technology. 5 (1) 73-78

Ayodeji, E.O. (2011). An examination of causes and effects of building collapse in Nigeria. Journal of Design and Built environment. 9(1) 37-47

Babalola, H.I (2015) Building Collapse: Causes and Policy Direction in Nigeria. International Journal of Scientific Research and Innovative Technology, 2(8), 1–8.

Baje, A. (2019) Lagos building collapse; another avoidable tragedy. The Guardian News, 10 April 2019.

Boateng, F.G. (2020). Building safe and resilient cities; lessons from Ghana, in S. Awaworyi Churchill (Ed.), Moving from the Millennium to the Sustainable Development Goals, Palgrave Macmillan, Singapore,

Chendo, I.G. and Obi, N.I. (2015) Building collapse in Nigeria: the causes, effects, consequences and remedies, International Journal of Civil Engineering, Construction and Estate Management. 3 (4) 41–49. ISSN2055-6586.

Chido, O. (2015) Church exonerates self over collapsed Delta hotel. The guardian news. 13th September 2015. Available online @ https://guardian.ng/news (Accessed 1st July 2020)

Ede, A.N. (2010) Building collapse in Nigeria: the trend of casualties in the last decade (2000-2010), International Journal of Civil & Environmental Engineering. 10 (6), 32–42.

Ede, A.N. (2010a) Structural Stability in Nigeria and Worsening Environmental Disorder: The way forward. The West African Built Environment. Conference Research Conference, Accra, Ghana, July, (2010) PP. 489-498

Fagbenle, O.I. and Oluwunmi, A.O. (2010). Building failure and collapse in Nigeria: the influence of the informal sector, Journal of Sustainable Development. 3(4), 268–276.

Fakere, A.A., Fadairo, G., and Fakere, R.A (2012). Assessment of building collapse in Nigeria: A case of a naval building, Abuja, Nigeria. International Journal of Engineering and Technology, 2 (4), 584-591.

Folagbade, S.O. (2001). Case studies of building in Nigeria, in Proceedings of a Workshop on Building Collapse Causes, Prevention, and Remedies, The Nigerian Institute of Building, Ondo State Chapter, October 2001, pp. 23–24.

Fowode, K.V. (2016) Building collapse and safety concern in Lagos, Guardian (April 12, 2016).

Hamma-adama, M., Iheukwumere, O. and Kouider, T. (2020) Analysis of Causes of Building Collapse: System Thinking Approach. Jordan Journal of Civil Engineering 14(2) 188-197

Hilary, I.O., Chukwuemeka, I.O., Nkolika, J.P., James, D.O., Patience, I.A. and Abiodun, A.O. (2018) Systematic review of building failure and collapse in Nigeria, International Journal of Civil Engineering Technology 9 (10) 1391–1401.

Imafidon, M.O and Ogbu, C.P (2020). A taxonomy of building collapse causes in Lagos state Nigeria. Nigerian Journal of Technology (NIJOTECH). 39(1). 74 – 86. http://dx.doi.org/10.4314/njt.v39i1.8

Mrabure, K O and Awhefeada U.V (2020). The menace of building collapse incidences in Nigeria. The need for strict enforcement of applicable planning laws. Commonwealth law bulletin Doi: https//doi.org/10.1080/03050718.2020.1804421

NAN (2019). Synagogue church building in perfect condition before the collapse, the witness said. The Guardian News, 21 June 2019.

National Bureau of Statistics (NBS). Nigeria Poverty Profile Report 2010.

National Population Commission (NPC). Nigeria and ICF, 2019. Nigeria Demographic and Health Survey 2018. Abuja, Nigeria, and Rockville, Maryland, USA: NPC and ICF.

Odeyemi, S.O. (2012). Effect of Types of Sandcrete Blocks on the Internal Microclimate of a Building. Journal of Research Information in Civil Engineering (RICE), Department of Civil Engineering, University of Ilorin, Ilorin, Nigeria, 9(1), 96–107.

Odeyemi, S.O., Giwa, Z.T. and Abdulwahab, R. (2019) Building collapse in Nigeria (2009-2019), causes and remedies – a review, Journal of Science and Engineering Production. 1 (1) 122–135.

Odunisi, W. (2019). 'Building Collapse in Nigeria'. Daily Post, 2019.

Okeke, F.O., Chendo I. G. and Ibem, E.O. (2021) Imprints of security challenges on the vernacular architecture of northern Nigeria: a study on Borno State. IOP Conference Series: Earth Environmental Sciences. vol. 665 (012021) doi:10.1088/1755-1315/665/1/012021

Okeke, F.O., Chendo, I.G. and Sam-amobi, C.G. (2019) Resilient architecture; a design approach to counter-terrorism in building for the safety of occupants. IOP. Conference Series Material Science and Engineering 640 (12003) doi:10.1088/1757-899X/640/1/012003

Okeke, F.O., Chukwuali, B.C., and Idoko, A.E (2019) Environmentally responsive design; A study of Makoko floating school building, International Journal of Development and Sustainability, 8(8). 476-487.

Okeke, F.O., Ibem, E.O., Udeh, C.A and Ezema, E.C. (2020) City as Habitat: Assembling the fragile city. Civil engineering Journal. 6(6) 1143-1154. http://dx.doi.org/10.28991/cej-2020-03091536

Okeke, F.O., Okeke, F.I and Sam-Amobi, C.G (2019) Building Collapse in Nigeria and Development Control, the Missing Link. West Africa Built Environment Research (WABER) 2019 Conference Proceedings (August 5, 2019): Accra, Ghana, pp 242-256 doi: https://doi.org/10.33796/waberconference2019.17

Okeke, F.O., Sam-Amobi, C. and Okeke, F.I (2020). Role of local town planning authorities in building collapse in Nigeria: evidence from Enugu metropolis. Heliyon 6(7) https://doi.org/10.1016/j.heliyon.2020.e04361

Olagunju, R.E., Aremu, S.C., and Ogundele, J. (2013) Incessant Collapse of Buildings in Nigeria: An Architect's View. Journal of Civil and Environmental Research. 3(4), ISSN 2225-0514

Olasunkanmi, A. (2019). One feared dead, four rescued as another two storey building collapses in Lagos. Vanguard News 2nd November, 2019. Available online @ https://www.vanguardngr.com/2019/11/ (Accessed 1st July 2020)

Oloyode, S.A., Omogun, C.B and Akinjare, O.A (2010) Tracking Causes of Building Collapse in Nigeria. Journal of Sustainable Development. 3(3), 127-132

Olubi, A. R. and Adewolu, T. O (2018). Impacts of Building Collapse on Sustainable Development in Nigeria. Journal of Culture, Society and Development Vol.44, 35-50. www.iiste.org

Omenihu, F.C. Onundi, L.O. and Alkali, M.A (2016). An analysis of building collapsed in Nigeria (1971-2016): challenges for stakeholders, Ann. Borno 26 (June 2016) 113–140.

Oseghale, G.E., Ikpo, J.I. and Ajayi, O.D. (2015) Causes and

Effects of Building Collapse in Lagos State, Nigeria. Civil and Environmental Research, 7(4), 34–43.

Oyedele, O.A (2018) A study of control measures of building collapse in Lagos State, Nigeria FIG congress 2018; embracing our smart world where the continents connect: enhancing the geospatial maturity of societies Istanbul, Turkey May 6-11(2018) 1–2.

Qurix,W.B and Doshu, R.G.(2020) Mitigating building collapse in Nigeria ARTEKS : Jurnal Teknik Arsitektur, 5(3), (2020) 449-458 doi: 10.30822/arteks.v5i3.596

Rayyan, A. (2019) Over 100 pupils perish in Lagos school building collapse. Daily Nigerian News 13th March 2019 Available online @ https://dailynigerian.com (Accessed 1st July 2020)

RIBA, In Association with Ray, C.and Alaime, H of RIBA Publications and Neil, T.P (1998, 2004). Managing Director, RIBA Indemnity Research Limited.

Standard Form of Building Contract, SFBC, (1996).

Tanko, J.A., Ilesanmi, F.A., and Balla, S.K. (2013). Design Error and Construction Defects. A Report on Building Collapse. Department of Civil Engineering, Modibbo Adama University of Technology, Yola, Nigeria

The Associated Press Two Canadians were found dead in a hotel partially toppled by the Taiwan earthquake. Toronto Star 9th February 2018. Available online @ https://www.thestar.com/news/world/2018/02/09/2 (Accessed 1st July 2020)

Usman, N., Chen, J. and Lodson, J. (2010) Environmental Sciences and the Challenges of collapsed buildings in Nigeria. Journal of Environmental Sciences and Agriculture in Developing Countries 2(2) (2010)

Windapo, A.O. (2006). The Threat of Building Collapse on Sustainable Development in the Built Environment, In proceedings of the sustainable Development conference Jos, Nigeria 9-12th August 2006. 59-65

Windapo, A.O. and Rotimi, J.O. (2012) Contemporary Issues in Building Collapse and Its Implications for Sustainable Development, Buildings 2 (2012), 283-299; DOI: 10. 3390/buildings ISSN 2075-5309

World Bank, (2015) Building Regulation for Resilience: Managing Risks for Safer Cities, Author, Washington, DC, 2015.

Yaqub, M (2019) Almost 60 Buildings Collapsed in Nigeria in 4 Years. But No One Is Taking it seriously, 2019. Available online at, https://www.africanliberty.org/2019/03/22/. (Accessed 19 June 2019).

JJEES

JJEES (2022) 13 (1): 26-36
ISSN 1995-6681

Jordan Journal of Earth and Environmental Sciences

Estimation of Surface Soil Particles Using Remote Sensing-based Data in Al-Ghab Plain, Syria

Alaa Khallouf [1,2*], Sameer Shamsham[2], Younes Idries[3]

General Commission for Scientific Agricultural Research (GCSAR), Damascus, Syria.
Department of Soil and Land Reclamation- Faculty of Agriculture- Al-Baath University, Homs, Syria.
General Organization of Remote Sensing (GORS), Damascus, Syria.

Received 17 October 2020, Accepted 2 July 2021

Abstract

This study focuses on digital soil mapping and its role to predict topsoil texture particle distribution. The study was carried out by collecting 146 surface soil samples (0-30 cm) from Al-Ghab plain, Hamah governorate, and 40 environmental covariates were derived from Landsat 8 OLI, and Digital Elevation Model (DEM). The surface soil particle models were obtained by Multiple Linear Regression (MLR) via R programming software, SAGA-GIS, and ArcGIS. Statistical analysis and results demonstrate no outlier in the data. Normal distribution for all covariates was examined, where skewness and kurtosis values were highly varied and ranged from 2.398 to 4.1090, and -1.772 to 20.1603 respectively, indicating that some predictors are highly skewed. Therefore, Tukey's ladder of power transformation was applied for all environmental predictors to be normally-distributed or close to normal distribution. All normal or close to normal data of environmental variables were used in MLR prediction models and cross-validation. Three MLR methods including forwarding selection, backward elimination, and stepwise selection were implemented for predictors selection. Relative importance also was calculated to estimate the contribution of each regressor in ML. The backward elimination method for the three soil texture particles sand, silt, and clay has the highest R^2 values (31.3, 28.6, 45.5%) respectively, and with the lowest values of mean absolute error (MAE) Root Mean stander error (RMSE), so it is the best prediction method for soil particles the study area.

Keywords: Backward elimination, Cross-validation, Forward selection, Multiple Linear Regression (MLR), Stepwise selection, Surface soil texture.

1. Introduction

Sustainable development as an overall goal usually deals with several issues at the regional and global levels involving land degradation, high food demand, water scarce, and climate change. Addressing these problems needs continuous and up-to-date soil information (McBratney, 2014; Zhang et al, 2013). Soil texture affects tightly many physical and chemical soil characteristics such as water and ventilation features, soil porosity, its fertility status, drainage characteristics, etc. (Makabe et al., 2009; Akpa et al., 2014). Soil texture and soil organic matter content are regularly used as the most significant parameters of hydrological characteristics and soil Cation Exchange Capacity (CEC) prediction (Wösten et al., 2001; Seybold et al., 2005). Besides, soil texture is a strong indicator to anticipate the soil erosion hazard conditions and eroded soil amount (Le Bissonnais 1996; Warrington et al., 2009). Therefore, accurate and reliable soil texture maps are crucial needs for hydrological and environmental modeling, land management practices, and environment protection, particularly when budget, labor, and time are limited (Zhao et al., 2009). The traditional survey process has been subjected to many limitations; firstly, the changes in environmental conditions are not easy to observe, mainly when the processing of many variables works concurrently; secondly, the entire steps must be repeated for any updating process, that leads to ineffective soil survey updates (Zhu et al., 2010). Remote sensing data was used for the first time to predict soil properties in the 1960s (McBratney et al., 2003). Digital soil mapping (DSM), which means the spatial prediction of soil properties in unobserved locations using statistical assumptions, have increasingly been applied recently since their early development at the beginning of the 19th century (Webster and Oliver, 2007). DSM relies on defining the relationship between soil attributes with some terrain characteristics which are usually derived from the Digital Elevation Model (DEM) such as Slope, Aspect, Curvature, Length of slope (LS), and others, in addition to derived remote sensing indices from satellite images. This approach was significantly used during the past three decades in predicting soil properties and has been achieved required rapidness and accuracy (Chen, et al., 2008; D'Acqui et al., 2010). Many studies examined the relation between soil reflection of the visible and near-infrared bands (400-2500 nm) and surface soil texture (Al-Abbas et al., 1972; Suliman and Post, 1988; Zhang et al., 1992; Sullivan et al., 2005). Liao et al. (2013) applied remote sensing data of Landsat7 ETM - digital number (DN) of six bands (Bands 1–5 and Band 7)- as covariates for estimation of surface soil particles distribution in the city of Pingdu lands, Shandong Province, China. Correlation analysis revealed that surface soil particles were

* Corresponding author e-mail: alaakhallouf@gmail.com

highly correlated with Landsat ETM data. Multiple Linear Regression (MLR) is one of the major statistical models that is commonly used to describe the relationship between environmental covariates and soil particles (Lagacherie et al., 2008; Mitran et al., 2018). Al-Ghab Plain is a highly valuable agricultural area in Syria, where various strategic crops such as wheat, sugar beets, cotton, tobacco, sesame, sunflower, soybeans, olives, and vegetables are grown. Therefore, land use planning procedures require beneficial and accurate soil data. Thus, the main objectives of this study are: (i) setting a digital map of the spatial distribution of sand, silt and, clay in the Al-Ghab Plain area and, (ii) fitting the best model for estimating the distribution of soil particles.

2. Material and Methods

2.1 Site description:

Al-Ghab Plain is located in the northwestern of Hamah governorate in the middle of Syria (Figure 1) and it extends between 36º 19` 12``36º 23` 45`` E and 35º 44` 40 ``- 35º 16` 34``N. It covers about 477 km^2 with altitude ranges between 146-176 m above sea level (asl). Al-Ghab plain is described as one of the Pliocene lakes. At the end of the Pliocene period, vigorous movement occurring along the already existing faults formed the actual landscape, although the movement continued during the Quaternary period. According to the existing geological map, a major part of the plain was covered by peat on the subsoil of gray plastic marl or white lime ooze. Gravels, sand, marls, and coquina are found in small parts in old riverbeds or lakeshore. White limestone and dolomite formations occur in the eastern border of the plain with basalts on the northeastern boundary (FAO, 1972). The Orontes river passes from south to north which is forming many terraces and irrigation channels. The climate of Al-Ghab plain belongs to the Mediterranean climate which is described as cold and rainy winters, hot and dry summers with two transitional seasons (spring and fall) (Moses, 1978). The soil climate is classified based on USDA as Xeric for soil moisture and Thermic for soil temperature regime (Ilaiwi, 1985).

2.2 Soil sampling and laboratory analyzing:

The study was conducted by collecting 146 surface soil samples (0-30cm) during 1-23/4/2020 (Figure 1), and their geographic locations were recorded by using the Global Positioning System (Garmin GPS, accuracy ± 5 m). The collected soil samples were air-dried, ground, and sieved through a 2mm sieve. The hydrometer method was used to estimate soil particle distribution (sand, silt, and clay as percentage) (Gee and Bauder, 1986).

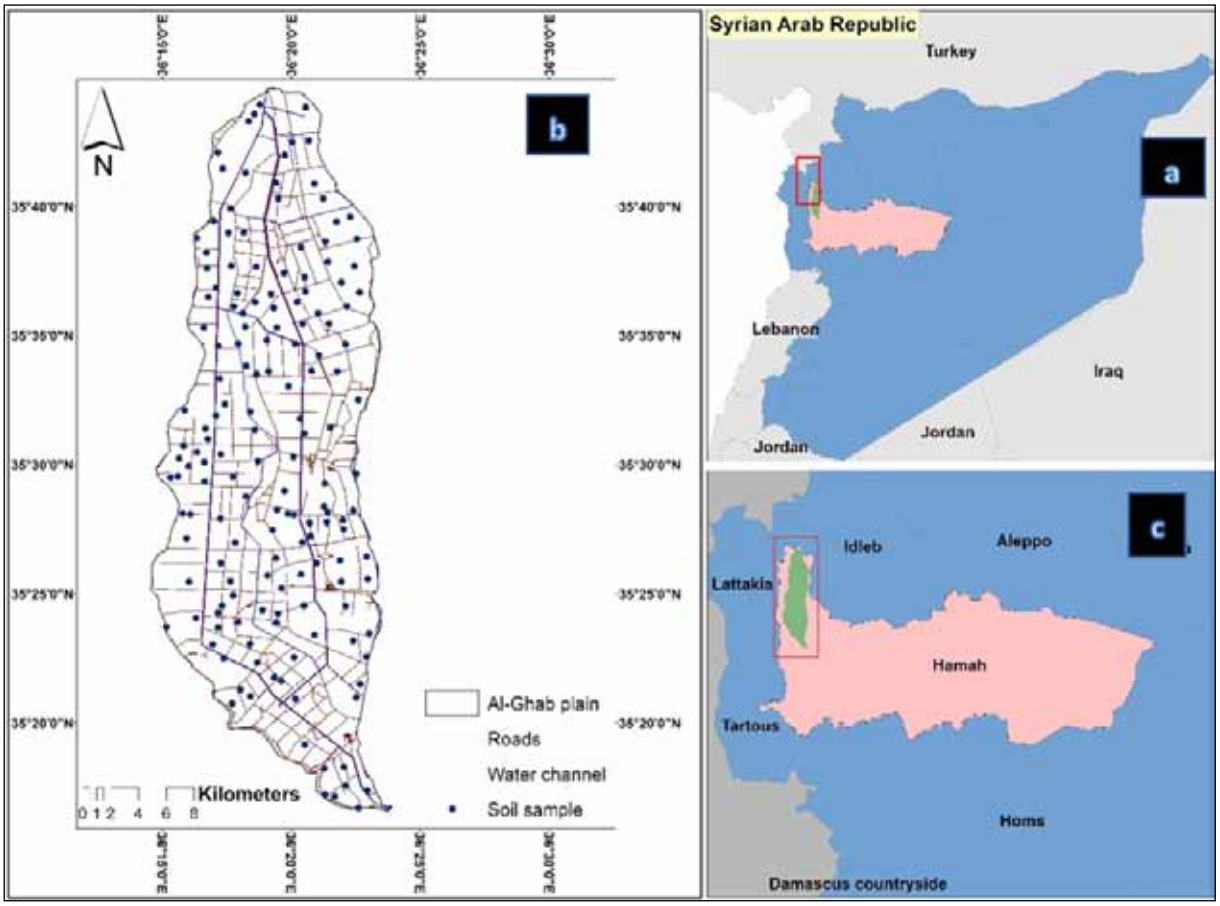

Figure 1. (a) Location of studied area to Syria, (b) soil samples distribution, (c) Location of the studied area to Hamah governorate

2.3. Remote sensing data and derived covariates:

To predict the relationship between surface soil distribution and the environmental predictors (variables) mainly topographic factors, hydrology, and vegetation cover indicators, in total 40 parameters were derived from Landsat8 OLI and Digital Elevation Model (DEM) but only 37 parameters were convenient for predicting soil texture (Table.1). Firstly, the satellite image was downloaded from https://earthexplorer.usgs.gov/, its date 18/4/2020 and re-projected, then bands reflectance was obtained.

The remote sensing imagery of Landsat8 OLI involves reflectance of bands (2to7), or some vegetation indices such as NDVI, SAVI, OSAVI, MSAVI, GS, etc…. Also, some transformations including principle component analysis PCA as PCA1 for reflectance bands 2,3,4; PCA2 for bands 5,6,7; and environmentally considered bands, finally tasseled cap transformation (brightness, greenness, and wetness). On the other hand, a 30 m-resolution DEM (Ministry of Economy, Trade, and Industry of Japan and the United States National Aeronautics and Space Administration, 2009), was sink-filled and SAGA-GIS was used to derive 13 environmental parameters (Table.1) using the basic terrain analysis, terrain-hydrology analysis, and morphometry analysis (Olaya, 2006).

Table 1. input environmental variables and derived covariates

Parameters	Description	Formula	Reference
Landsat8 band2	blue band (B)		
Landsat8 band3	green band (G)		
Landsat8 band4	red band (R)		
Landsat8 band5	near infra-red band (NIR)		
Landsat8 band6	short wave infra-red1 band (SWIR1)		
Landsat8 band7	short wave infra-red2 band (SWIR2)		
PCA1	principle component analysis	Derived from of bands 2,3,4	Frazier and Cheng, 1989
PCA2	principle component analysis	Derived from of bands 5,6,7	Frazier and Cheng, 1989
PCA3	principle component analysis	Derived from of bands 2,3,4,5,6,7	Frazier and Cheng, 1989
SR	Simple ratio	NIR/R	Malthus et al,1993
DVI	Difference Vegetation Index	NIR-R	Foody et al., 2001
OSAVI	Optimized Soil Adjusted Vegetation Index	(NIR -R) / (NIR + R + 0.16)	Nikolakopoulos, 2003
SAVI	Soil Adjusted Vegetation Index	[NIR-R)/(NIR+R+L)] × (1+L)	Pettorelli et al., 2005
MSAVI	Modified Soil Adjusted Vegetation Index	[NIR-R)/(NIR+R+L)] × (1+L)	Bannari et al 1995
TVI	Transformed Vegetation Index	(SWIR1-R)/(SWIR1+R)	Bannari et al 1995
MNDVI	Normalized Difference NIR/MIR Modified Normalized Difference Vegetation Index	(NIR-MIR)/(NIR+MIR)	Jürgens,1997
GVI	Green Vegetation Index	-0.29 (G) -0.56(R)+0.6(IR)+0.49(IR)	Leblon, 1993
OI	Simple Ratio Red/Blue Iron Oxide	R/B	Hewson et al.,2001
SRRed/NIR	Simple Ratio Red/NIR Ratio Vegetation-Index	R/NIR	Bannari et al 1995
SCRI	Surface clay index	SWIR2/SWRI1	Bannari et al 1995
SARVI2	Soil and Atmospherically Resistant Vegetation Index2	2.5(NIR-R)/(1+NIR+6R-7.5B)	Heute et al,1997
Wetness	The humid band derived from tasseled cap		Bahtti et al., 1991
Brightness	Brightness derived from tasseled cap		Bahtti et al., 1991
Greenness	Greenness band derived from tasseled cap		Bahtti et al., 1991
ASPECT	facing direction		Castro-Franco et al,2018
GENERALCUR	General curvature		Ließ et al,2012
LONCUR	Long curvature		Ließ et al,2012
LSFACTOR	Length of slope steepness		Castro-Franco et al,2018
PROFILECUR	Profile curvature		Ließ et al,2012
PLANCUR	Plan curvature		Ließ et al,2012
MRVBF	Multi-resolution Valley Bottom Flatness Index		Dobarco et al,2016
MRRTF	Multi-resolution of ridge top flatness index		Dobarco et al,2016
FLOWLINE	Flow line		Zevenbergen et al.,1987
MAXCUR	Maximum curvature		Ließ et al,2012
TWI	Topographic Wetness Index		Dobarco et al.,2016
SLOPE	Slope		Castro-Franco et al, 2018
DEM	Digital Elevation Model		Pinheiro et al, 2018

2.4. Descriptive statistics of environmental covariates and data transformation:

R programming software was used to calculate the criteria of descriptive statistics for both soil particles and environmental predictors. It includes the mean, minimum, maximum, standard deviation (SD), coefficient of variation (CV), skewness, and kurtosis. The CV% is usually used to explain the variance of each soil characteristic and predictors. The CV% was classified into: high variance (% CV> 35%), medium variance (15< %CV <35), low variance (% CV <15) (Wilding, 1985). The normal distribution test was applied for all variables by plotting histogram test companion package), skewness, and kurtosis were determined by using (moments package). For non-normal distributed variables, Tukey`s ladder of power transformations was applied (Mondejar and Tongco, 2019) by using the equation:

$$y=\begin{cases} x^{\lambda \text{ if } \lambda>0} \\ \log x \text{ if } \lambda=0 \\ -(x^{\lambda}) \text{ if } \lambda<0 \end{cases} \quad \text{..... (1)}$$

Where λ is the power used to convert the factor closer to the normal distribution (Mangiafico, 2016; Scott, 2018). in this study λ values were (-2, -1, -1/2, 0, 1/2, 1, 2) (Tukey, 1977)

The transformation was performed for non-normal distributed variables for the Value of skewness to be close to zero and Kurtosis ranges between 1 to3.

2.5. Multiple Linear Regression predictive model:

Multiple Linear Regression predictive (MLR) has been widely utilized for estimating soil characteristics based on environmental covariates, where the correlation between predictors was examined. MLR equation is defined as:

$$Y`=\beta_0+\sum_{j=1}^{p} Xj\beta j \quad \text{..... (2)}$$

where: Y`: dependent variable, β_0: constant, Xj the matrix of the input independent covariates, and is the unknown coefficients for the involved predictors (McDonald, 2014).

Three methods of MLR involving Backward elimination, Forward Selection, and stepwise regression were applied in SAGA-GIS and a 95% confidence level was used for fitting the estimation model. All selected methods of MLR were subjected to Kolmogorov-Smirnov (Lilliefors) test.

2.6. Model fitting and validation:

The determination coefficient (R^2) is used as a function of goodness of fitting linear models for cross-validation and it is expressed as:

$$R^2=\frac{\sum_{i=1}^{n}(\hat{y}i-y`)^2}{\sum_{i=1}^{n}(yi-y`)^2} \quad \text{..... (3)}$$

The predictive model's performance was examined via cross-validation technique [5-fold method in R (Carte Package)] (Kuhn and Johnson, 2013), since the validation dataset was unavailable, in addition to the limited soil samples number (Ballabio et al., 2016). The accuracy of models was determined by calculating the coefficient of determination (R^2), the mean absolute error (MAE), and the root mean squared (RMSE) as following equations:

$$MAE=\frac{\sum|\hat{y}i-yi|}{n} \quad \text{..... (4)}$$

$$RMSE=\sqrt{\frac{\sum_{n=i}^{1}(yi-\hat{y}i)^2}{n}} \quad \text{..... (5)}$$

where $\hat{y}_i$: is the predicted value, y_i: is the observed value, y`: is the mean of observed values, and n:is the number of observed points.

2.7. Relative importance of environmental variables:

Relative importance is a topic that has seen a lot of interest in recent years, particularly in applied work. Relative importance (RI) is described as "the quantification of individual regressor's part to a multiple regression model" (Gromping, 2006). RI is typically implemented as part of the model-building procedure, e.g., forward variable selection or backward elimination, …etc. It is an alternative to the multiple regression techniques and it addresses the multi-collinearity problems and also helps to calculate the importance rank of variables. It helps to answer " Which variable is the most important and rank variables based on their contribution to R-Square". RI was obtained using R (Relaimpo package) and its values are calculated as percentages of 100% (Mondejar and Tongco, 2019).

2.8. Map generating:

Soil texture maps were generated based on the best MLR predicting model by using R (Automap package) and saved all maps as a raster (FAO,2018).

3. Results and discussion:

3.1. Descriptive statistics of environmental variables:

The former step in this study was examining data including descriptive statistics and transformation. Table.2 shows the summary statistics for untransformed data. The results showed high CV% and it ranges between 1.41 to 284.08%, with medium CV% for soil particles sand, silt, clay (21.5, 30.6, 18.3%) respectively, while CV% values were high for OSAVI, slope, LS factor, and Aspect (284.08, 245.46,104.29, and 100.63%) respectively. On the other hand, skewness, and kurtosis values range from 2.39 to 4.10; -1.77, and -20.16 respectively, these results imply that some predictors are highly skewed, and this is not appropriate to the normal assumption. It is obvious in Table.2 that the three soil particles were normally distributed, since skewness values for soil particles as a flowing: -0.154, 0.504, 0.762, and kurtosis values were -0.69, 0.768, 0.593 respectively, whereas results of some predictors were non-normally distributed based on histogram test and skewness and kurtosis values. Therefore, Tukey`s ladder of power transformation was applied to transform the environmental predictors into normally or close to a normal distribution as shown in Table. 3. The histogram, skewness, and kurtosis tests were applied for transformed data of non-normally distributed predictors.

Table 2. Descriptive statistics of environmental variables

Parameters	Minimum	Maximum	Mean	Standard Deviation	CV%	Skewness	Kurtosis
Sand %	22.0000	57.0000	38.874	7.9929	21.5	-0.154	-0.69
Silt%	10.0000	52.0000	27.361	10.1320	30.6	0.504	-0.77
Clay%	18.0000	62.0000	33.765	8.9702	18.3	0.762	0.59
Landsat8 band2	0.0033	0.0061	0.004	0.0005	2.24	0.995	2.21
Landsat8 band3	0.0166	0.0279	0.020	0.0020	4.47	0.703	1.12
Landsat8 band4	0.0325	0.0698	0.044	0.0069	8.31	0.791	1.20
Landsat8 band5	0.0317	0.1267	0.057	0.0156	12.49	0.966	2.35
Landsat8 band6	0.0350	0.1382	0.072	0.0222	14.90	0.098	-0.54
Landsat8 band7	0.0288	0.1061	0.061	0.0200	14.14	0.151	-0.97
PCA1	0.0282	0.0484	0.035	0.0036	6.00	0.736	1.12
PCA2	0.0567	0.2047	0.110	0.0319	17.86	0.120	-0.52
PCA3	0.0739	0.2277	0.129	0.0328	18.11	0.149	-0.43
SR	0.2491	0.2725	0.260	0.0037	6.08	-0.022	0.36
DVI	1314.44	1324.294	1319.367	2.5066	158.32	-0.056	-1.09
OSAVI	1244.56	1278.028	1261.294	8.0699	284.08	0.003	-0.91
SAVI	0.0000	0.5403	0.327	0.0904	30.07	-0.620	0.74
MSAVI	0.1058	0.6499	0.378	0.1059	32.54	-0.389	0.09
TVI	-0.0071	0.3780	0.218	0.1052	32.43	-0.622	-0.66
MNDVI	0.0000	0.3050	0.042	0.0568	23.83	1.983	5.25
GVI	0.0067	0.0948	0.040	0.0200	14.14	0.029	-0.77
NDVI	0.0000	0.3682	0.112	0.0698	26.42	0.722	1.24
MVI	0.0000	0.3502	0.141	0.1058	32.53	0.072	-1.18
ASPECT	0.0000	360.0000	118.055	118.4584	100.63	0.620	-0.87
GENERALCUR	0.0000	0.0089	0.001	0.0018	4.24	2.032	3.71
LONCUR	0	0.0066	0.001	0.0011	3.32	1.947	4.88
LSFACTOR	0	25.8273	10.95	11.502	104.29	0.229	-1.77
PROFILECUR	0	0.0034	0	0.0006	2.45	2.069	5.78
PLANCUR	0	0.1333	0.007	0.0204	14.28	4.109	20.16
MRVBF	5.5045	79.6704	57.786	20.4601	452.3	-0.834	-0.39
MRRTF	0.0872	8.9686	6.697	2.6469	162.69	-0.983	-0.19
FLOWLINE	0.6381	1.0385	0.968	0.0846	29.09	-1.768	3.13
MAXCUR	0.8736	1.1477	1.115	0.0818	28.60	-2.398	3.95
TWI	0.301	1.0404	0.523	0.1816	42.61	0.094	-0.84
SLOPE	0	0.9989	0.342	0.2706	245.46	-0.138	-1.2
DEM	0.3094	0.3152	0.311	0.001	3.16	0.711	1.14
OI	0.3179	0.8751	0.492	0.101	31.78	0.806	1.19
SRRed/NIR	0.4513	1.0142	0.655	0.1527	39.08	0.874	-0.29
VARIgreen	0	0.2188	0.067	0.0415	20.37	0.695	1.2
SCRI	0	0.4669	0.136	0.1104	33.23	0.898	0.38
SARVI2	0.285	0.2986	0.29	0.0018	4.24	1.277	5.84
Wetness	-0.06426	0.008739	-0.02631	0.018262	13.51	-0.075	-1.007
Brightness	0.087	0.2293	0.133	0.0275	16.58	0.313	0.18
Greenness	0	0.0006	0	0.0002	1.41	-0.352	-0.89

The results are shown in Table.3 reveals that all transformed data of predictors are normal or near to normal distribution, and values of skewness and kurtosis range -0.834 to 0.995 and -1.204 to 2.206 respectively. Consequently, all environmental predictors were used in MLR modeling with normal or close to normal distribution.

Table 3. The transformation data for some non-normally distributed using Tukey's method

soil variables	Trans formation-mode	Min	Max	Mean	Standard Deviation	CV%	Skew	Kurtosis
band3	Log(x)	0.017	0.028	0.02	0.08	3.65	0.703	1.115
band2	Log(x)	0.003	0.006	0	0.06	4.72	0.995	2.206
SR	X^2	0.249	0.273	0.26	0.07	6.23	-0.022	0.361
PCA1	Log	0.028	0.048	0.03	0.07	5.24	0.736	1.115
SAVI	Log(x)	0	0.54	0.33	0.09	12.25	-0.62	0.744
General curvature	Log(x)	-2.653	-2.051	-2.5	0.2	4.65	0.69	-1.036
Profile-curvature	-1/x	-3.654	-2.465	-2.96	0.16	12.58	-0.473	2.125
Plan curvature	Log(x)	-1.722	-0.875	-1.37	0.23	15.26	0.809	0.785
MRVBF	Log(x)	5.504	79.67	57.79	20.46	48.62	-0.834	-0.391
Max- curvature	-1/x	0.273	0.332	0.33	0.02	25.62	-0.407	2.01
TWI	Log(x)	0.301	1.04	0.52	0.18	3.69	0.094	-0.838
SLOPE	Log(x)	0	0.999	0.34	0.27	17.82	-0.138	-1.204
DEM	Log(x)	0.309	0.315	0.31	0.02	6.36	0.711	1.142
Greenness	Log(x)	0	0.001	0	0	10.28	-0.352	-0.892

3.2 Multiple linear regression modeling:

Table.3 shows the MLR results for the three methods that were chosen namely forward selection, backward elimination, and stepwise selection. All selected methods of MLR were subjected to Kolmogorov-Smirnov (Lilliefors) test. Homoscedasticity and normality test of residuals were determined to confirm the homogeneity of variance assumption (Heil and Schmidhalter, 2017), where the Lilliefors value is more than 0.05 that indicates enhancing in normality and stability of variance for both independent and dependent variables (Tsai et al., 2017), minimizing errors, and unbiased estimation (Zhang et al., 2013).

3.3 Cross-validation of MLR selected methods

Cross-validation of selected methods was carried out and R^2, MAE, RMSE, Homoscedasticity, and normality tests for residuals including skewness, kurtosis, and Lilliefors were calculated for estimating the accuracy of the model's performance. Homoscedasticity and normality tests of residuals were determined to confirm the homogeneity of variance assumption (Heil and Schmidhalter, 2017). The results in Table.4 show that the backward elimination method has achieved the best model performance in comparison with forwarding selection and stepwise methods, where the MAE, RMSE values were less than other methods in all soil particles predicted models. However, the backward elimination method has the highest R^2 for sand, silt, and clay (31.3, 28.6, 45.5%) respectively. Figure 2 illustrates the scatter plots of residuals and predicted values of homoscedasticity test, it is clear that the homoscedasticity was not broken by any all three MLR methods for soil texture particles, since linearity theory was met having no identifiable pattern and the residuals randomly scattered, in addition to the almost of residuals were symmetrically clustering towards the center of the plot. Graphically, Figure 3 explains clearly the test of normality of residuals for three MLR methods where most of the points are placed almost directly either below or above closely to the reference line with no evidence of outlier's presence (Mondejar and Tongco, 2019). It is also obvious that the most of points of the sand regression models were located very close to the reference line. These results were statistically confirmed in Table.4, where the regression models of sand particles were the least in both skewness and kurtosis values. Table 4 also shows that the distribution of the residuals was statistically near to normal distribution based on the Lilliefors normality test.

Table 4. Cross-validation of the selected methods of MLR

Soil particle	Regression model	Predictors number	MAE	RMSE	R^2	Residuals normality		
						skewness	kurtosis	Lilliefors
sand	Forward	2	5.9	7.11	20.2	-0.215	-0.815	0.96
	Backward	10	5.4	6.6	31.3	-0.192	-0.49	0.57
	Stepwise	2	5.9	7.11	20.2	-0.215	-0.851	0.96
silt	Forward	2	7.3	8.85	23.1	0.479	-0.428	0.97
	Backward	6	7.05	8.52	28.6	0.322	-0.365	0.7
	Stepwise	2	7.3	8.85	23.1	0.479	-0.428	0.97
clay	Forward	3	5.71	7.21	34.8	0.344	-0.089	0.055
	Backward	14	5.79	7.01	45.5	0.283	-0.281	0.073
	Stepwise	3	5.71	7.21	34.8	0.344	-0.089	0.055

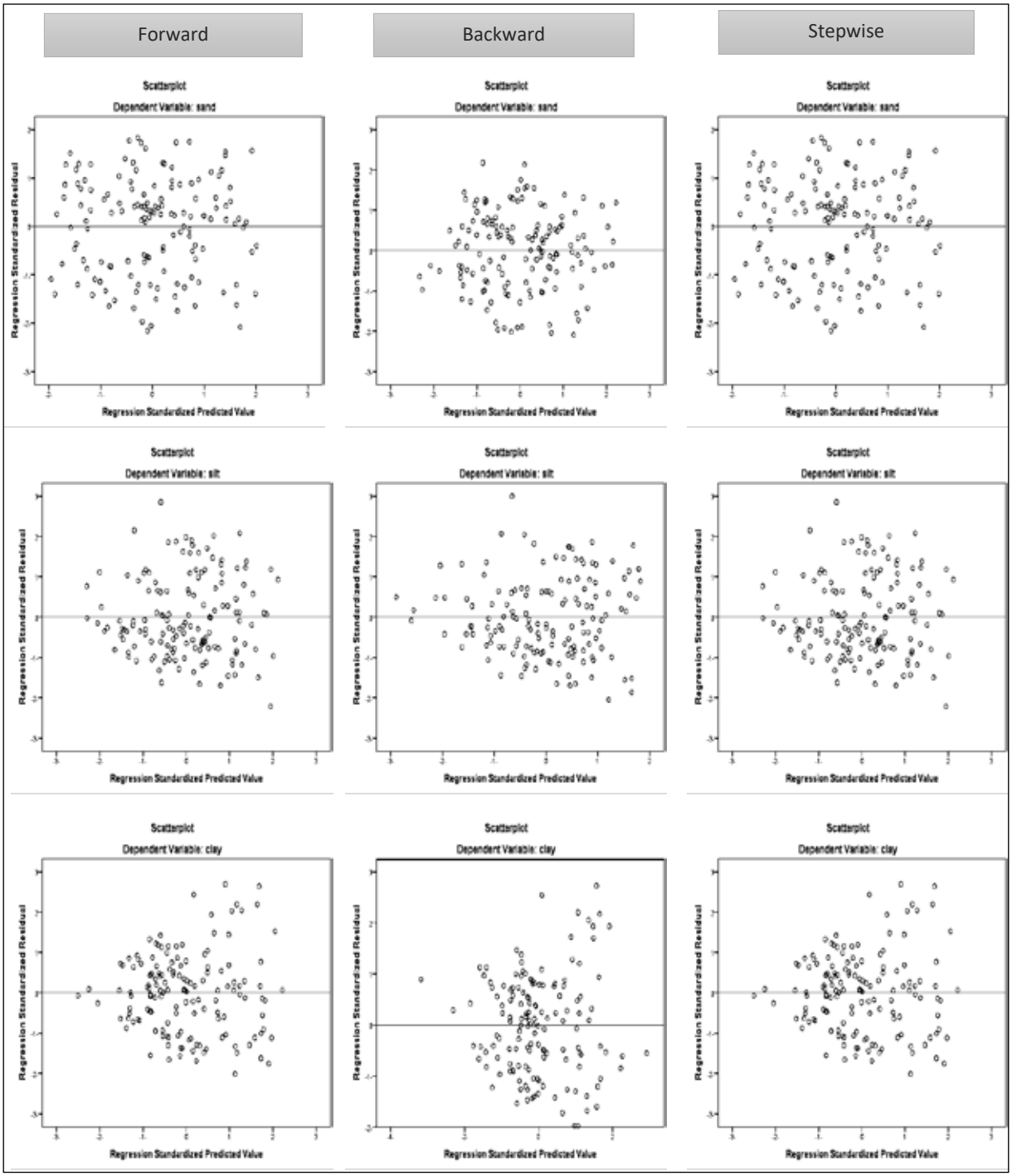

Figure 2. Residuals plots of MLR models based on selection methods

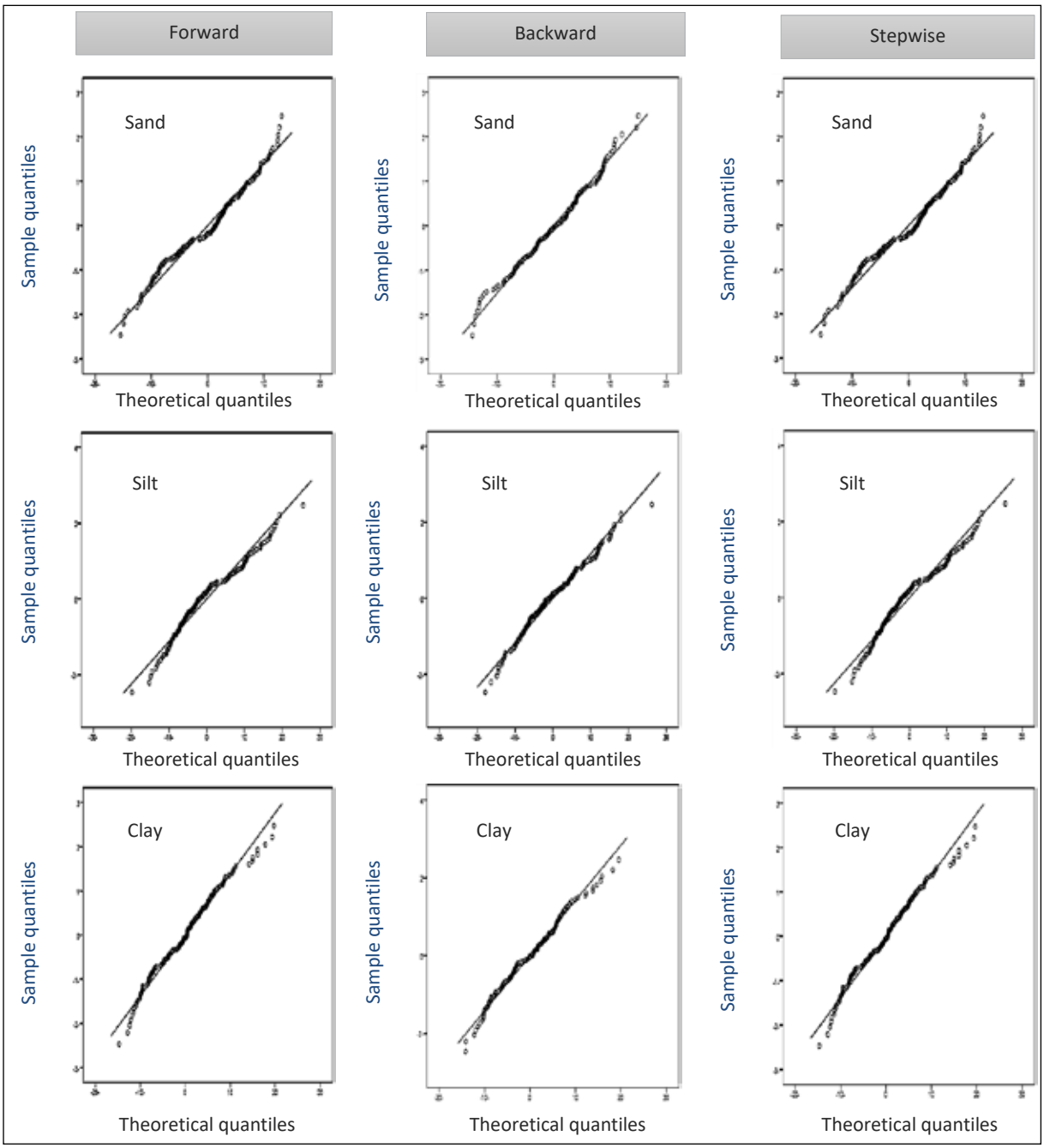

Figure 3. QQ plot of residuals for MLR selected methods

3.4 Relative importance of environmental covariates:

Figure 4 demonstrates that TWI, PCA1, SARVI, MAX-CUV, MRVBF, SCRI, OSAVI, MSAVI, Wetness, and NDVI were the most significant environmental covariates for predicting surface soil texture particles. In the sand predicting model, 10 predictors for the backward elimination method, since TWI, PCA1, SARVI, SRRED/NIR, and slope were the most important predictors with RI values 18.47, 15.4, 12.79, 11.32, and 9.6 % respectively. These results agreed with Mehrabi-Gohari et al. (2019) results since TWI was the most significant auxiliary variable to predict sand fraction distribution. Whereas Mondejar and Tongco (2019) found that stream proximity index (SPI) was the most crucial variable affected in sand fraction prediction. In Figure 4, the silt regression model is predicting silt values by using 6 predictors. Similarly, TWI, MAX-CURV, and MRVBF were the most critical variables for silt regression predicting models. In many studies, TWI and MrVBF were considered as a significant predictive variable in the prediction model of the silt fraction (Mehrabi-Gohari et al., 2019; Jafari et al., 2012), while Mosleh et al. (2016) reported steam power index, and plan curvature were the most auxiliary variables to silt prediction. For the clay predictive model, Figure 5 demonstrates that 14 environmental variables were considered in the predictive model since GSAVI, MSAVI, and DVI respectively were found the most significant variables of clay fraction prediction. These results agreed with Mehrabi-Gohari et al. (2019) results. Topography factors can influence soil physicochemical properties (soil depth, texture, and mineral contents), incoming solar radiation, precipitation and affect crop production. As an increased topography/elevation significantly increased soil

moisture, precipitation, soil significantly lower at the higher elevations, whereas bulk density, pH, and soil temperature were significantly lower at higher elevations (Abate and Kibret, 2016).

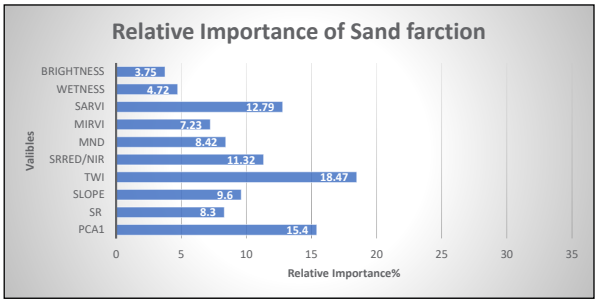

Figure 4. Relative importance of environmental covariates for soil texture prediction

3.5. Predictive soil texture maps:

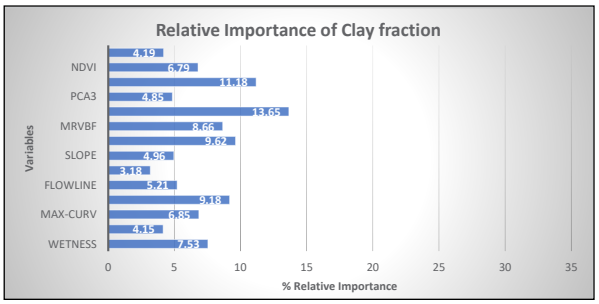

Figure 5. Relative importance of environmental covariates for soil texture prediction

Figures 6, 7, and 8 show the spatial distribution of sand, silt, and clay fraction based on the backward estimation predictive model. Sand content ranges from 20.7 to 59.6%, with a high concentration in the west northern part of Al-Ghab plain. Silt also ranges from 11.2 to 46.9% since most northern lands are high content of silt. The high content of clay (43.4-60.7%) is in the south and southeastern lands of Al-Ghab plain.

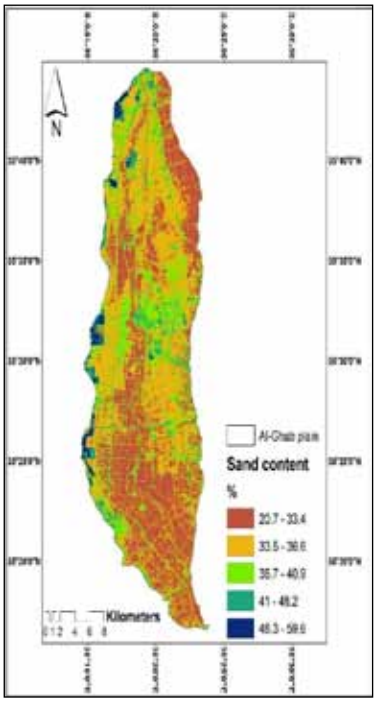

Figure 6. Sand spatial distribution

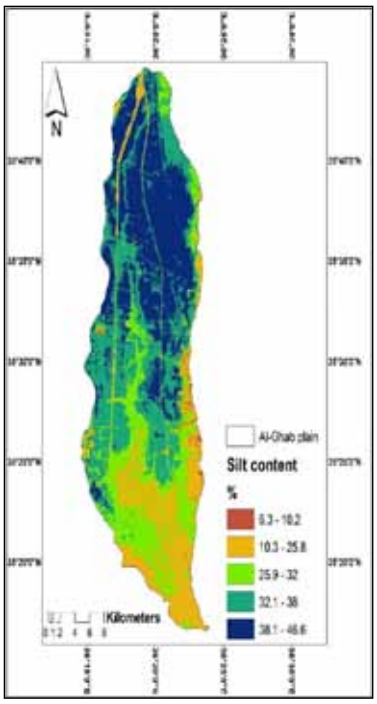

Figure 7. Silt spatial distribution

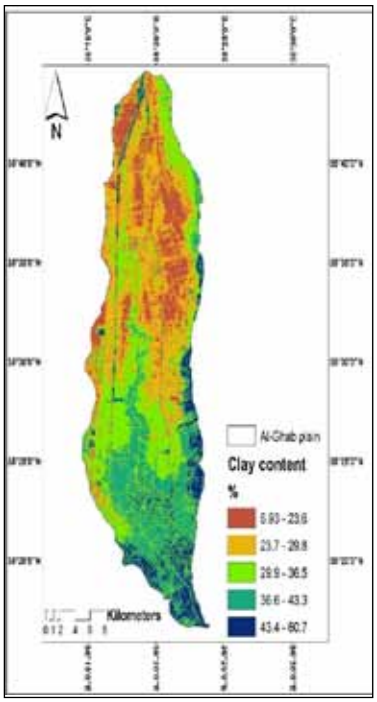

Figure 8. Clay spatial distribution

4. Conclusions:

Soil texture is one of the most crucial soil properties because it affects many soil functions involving the availability of water, nutrients, and many physical soil properties. In this study, 40 environmental RS-based covariates were derived from Landsat 8 OLI and DEM with a spatial resolution of 30 m. Multiple linear regression was used to determine the relationship between soil texture particles and environmental variables. The results revealed that backward elimination was the best predictive model for the three soil particles (sand, silt, and clay) with the highest R^2 values (31.3, 28.6, 45.5%) respectively, and with the lowest values of MAE and RMSE. On the other hand, TWI,

MRVBF, GSAVI, and MSAVI were the most significant predictors to predict topsoil texture fractions with a high relative importance percentage.

References

Abate, N, and Kibret, K (2016). Effects of Land Use, Soil Depth, and Topography on Soil Physicochemical Properties along the Toposequence at the Wadla Delanta Massif, Northcentral Highlands of Ethiopia. Environment and Pollution; 5(2): 57-71.

Akpa, S.I.C.; Odeh, I.O.A.; and Bishop, T.F.A. (2014). Digital mapping of soil particle-size fractions for Nigeria. Soil Sci. Soc. Am. J., 78: 1953–1966.

Al-Abbas, A.H., Swain, P.H., and Baumgardner M.F. (1972). Relating organic matter and clay content to the multispectral radiance of soils. Soil Sci, 114: 477–485.

Bahtti A.U., Mulla, D.J., and Frazier, B.E. (1991). Estimation of soil properties and wheat yields on complex eroded hills using geostatistics and thematic mapper images. Remote sens. Environment, 31: 181-191.

Ballabio, C., Panagos, P., and Monatanarella L. (2016). Mapping topsoil physical properties at a European scale using the LUCAS database. Geoderma, 261:110–23.

Bannari, A., Morin, D., Bonn, F., and. Huete, A. R. (1995). A review of vegetation indices.

Ben-Dor, E, Inbar, Y., and Chen, Y. (1997). The reflectance spectra of organic matter in the visible near-infrared and short-wave infrared region (400–2500 nm) during a controlled decomposition process. Remote Sens. Environ, 61: 1–15.

Ben-Dor, E, Irons, J., and Epema, G. (1999). Soil spectroscopy. In Manual of Remote Sensing, 3rd ed., Ed. Rencz A., John Wiley, and Sons, New York. 111–188 p.

Ben-Dor, E. and Banin, A. (1995). The near-infrared analysis is a rapid method to simultaneously evaluate several soil properties. Soil Sci. Soc. Am. J, 59: 364–372.

Ben-Dor, E., Goldshleger, N., Eshel, M., Mirablis, V., and Bason, U. (2008). Combined active and passive remote sensing methods for assessing soil salinity. In Remote Sensing of Soil Salinization: Impact on Land Management, Ed. Metternicht G, Zinck A, CRC Press, Boca Raton, FL, USA. 235–258.

Brown, D.J., Shepherd, K.D., Walsh, M.G., Dewayne, M., and Reinsch, T.G. (2006). Global soil characterization with VNIR diffuse reflectance spectroscopy. Geoderma, 132, 273–290.

Castro-Franco M, Domenech, M.B., Borda, M.R. and Costa, J.L. (2018). A spatial dataset of topsoil texture for the southern argentine pampas. Geoderma Reg, 12:18–27.

Chen, F., Kissel, D.E., West, L.T. and Adkins, W. (2000). Field-scale mapping of surface soil organic carbon using remotely sensed imagery. Soil Sci. Soc. Am. J 64: 746–753.

Chen, F., Kissel, D.E., West, L.T., Adkins, W., Rickman D., and Luvall, J.C. (2008). Mapping soil organic carbon concentration for multiple fields with image similarity analysis. Soil Sci. Soc. Am. J, 72: 186–193.

D'Acqui, L.P., Pucci, A., and Janik, L.J. (2010). Soil properties prediction of western Mediterranean islands with similar climatic environments employing mid-infrared diffuse reflectance spectroscopy. Eur. J. Soil Sci, 61: 865–876.

Dobarco, M.R., Orton, T.G., Arrouays, D., Lemercier, B., Paroissien, J.B. and Walter, C, et al. (2016). Prediction of soil texture using descriptive statistics and area-to-point kriging in region Centre (France). Geoderma Reg, 7:279–92.

FAO (Food and Agriculture Organization). (1972). report on the soil survey of Ghab Valley. Damascus, Syria.

FAO (Food and Agriculture Organization). (2018) Soil organic carbon mapping cookbook. Rome, Italy.

Foody, G.M., Cutler, M., Mcmorrow, J., Pelz, D., Tangki, H., Boyd, D.S. and Douglas, I. (2001). Mapping the biomass of Bornean tropical rain forest from remotely sensed data. J. Global Ecology Biogeography, 10: 379-387.

Frazier, B.E., and Cheng, Y. (1989). Remote sensing of soils in eastern Palouse region with LandSat thematic mapper, Remote sense. Environment, 28: 317-325.

Gawlik, B.M., Bo, F., Kettrup, A., and Muntau, H. (1999). Characterization of the second generation of European reference soils for sorption studies in the framework of chemical testing – Part I: Chemical composition and pedological properties. Sci. Total Environ, 229: 99–107.

Gee, G.W., and Bauder, J.W. (1986). Particle-size analysis. p. 383–411. In A. Klute (ed.) Methods of soil analysis. Part 1. 2nd ed. Agron. Monogr. 9. ASA and SSSA, Madison, WI.

Gromping, U. (2006). Relative importance for linear regression in R: the package relaimpo. J Stat Softw, 17:1–27.

Hassink, J. (1992). Effects of soil texture and structure on carbon and nitrogen mineralization in grassland soils. Biol. Fert. Soils, 14: 126–134.

Heil, K., and Schmidhalter, U. (2017). Improved evaluation of field experiments by accounting for inherent soil variability. Eur J Agron, 89:1–15.

Henderson, T.L., Szilagyi, A., Baumgardner, M.F., Chen, C.T., and Landgrebe, D.A. (1989). Spectral band selection for classification of soil organic matter content. Soil Sci. Soc. Am. J, 53: 1778–1784.

Hewson, R. D., Cudahy, T. J., and Huntington, J. F. (2001). Geologic and alteration mapping at Mt Fitton, South Australia, using ASTER satellite-borne data.

Huete, A. R., Liu, H. Q., Batchily, K, and Leeuwen, W.V. (1997). A comparison of vegetation indices over a global set of TM images for EOS-MODIS.

Hunt, J.r., Raymond, E., Daughtry, C. S., Eitel, T., Jan, U. H., and Long, D. S. (2011). Remote Sensing Leaf Chlorophyll Content Using a Visible Band Index.

Ilawi, M. (1985). Soil map of Syria and Lebanon (ACSAD)Map.

Jafari, A.; Finke, P.A., Wauw, J.V., Ayoubi, S., and Khademi, H. (2012). Spatial prediction of USDA-great soil groups in the arid Zarand region, Iran: Comparing logistic regression approaches to predict diagnostic horizons and soil types. Eur. J. Soil Sci, 63: 284–298.

Jürgens, C. (1997).The modified normalized difference vegetation index (mNDVI) - a new index to determine frost damages in agriculture based on LANDSAT TM data.

Kuhn, M., and Johnson, K. (2013). Applied predictive modeling. 1st ed. New York: Springer.

Lagacherie, P., Baret, F., Feret, J.B, Madeira Netto, J., and Robbez- Masson, J.M. (2008). Estimation of soil clay and calcium carbonate using laboratory, field, and airborne hyperspectral measurements. Remote Sens. Environ, 112: 825–835.

Le Bissonnais, Y. (1996). Aggregate stability and assessment of crushability and erodibility: 1. Theory and methodology. Eur. J. Soil Sci, 47: 425–437.

Leblon, B. (1993). Soil and vegetation optical properties. In: Applications in Remote Sensing, Volume 4, The International Center for Remote Sensing Education. Wiley Press, New York, USA.

Liao KH, Xu SH, Wu JC, Zhu Q. (2013). Spatial estimation of surface soil texture using remote sensing data. Soil Sci Plant Nutr. 59:488–500.

Ließ, M., Glaser, B., and Huwe, B. (2012). Uncertainty in the spatial prediction of soil texture comparison of regression tree

and Random Forest models. Geoderma, 170:70–9.

Mangiafico, S.S. (2016). Summary and analysis of extension program evaluation in R, version 1.18.1. New Brunswick: Rutgers Cooperative Extension.

Makabe, S., Kakuda, K., Sasaki, Y., Ando, T., Fujii, H., and Ando, H. (2009). Relationship between mineral composition or soil texture and available silicon in alluvial paddy soils on the Shounai Plain, Japan. Soil Sci. Plant Nutr, 55: 300–308.

Malthus, T. J., Andrieu, B., Danson, F. M., Jaggard, K. W., and Steven, M. D. (1993). Candidate high spectral resolution infrared indices for crop cover. Remote Sensing of Environment.

Manrique, L.A, Jones, C.A., and Dyke, P.T. (1991). Predicting cation exchange capacity from soil physical and chemical properties. Soil Sci. Soc. Am. J, 55: 787–794.

McBratney, A.B., Santos, M.M., Minasny, B. (2003). On digital soil mapping. Geoderma, 117(1–2):3–52.

McBratney, A. (2014). Field DJ, Koch A. The dimensions of soil security. Geoderma, 213: 203–13.

McCarty, G.W., Reeves, G.B. III, Reeves, V.B., Follett, R.F., and Kimble, J.M. (2002). Mid-infrared and near-infrared diffuse reflectance spectroscopy for soil carbon measurement. Soil Sci. Soc. Am. J, 66: 640–646.

McDonald, J.H. (2014). Handbook of biological statistics. 3rd ed. Baltimore: Sparky House Publishing.

McKenzie, N.J., Ryan, P.J. 1999. Spatial prediction of soil properties using environmental correlation. Geoderma, 89(1-2): 67-94.

Mehrabi-Gohari, E., Matinfar, H. R., Jafari, A., Taghizadeh-Mehrjardi, R., and Triantafilis J. (2019). The Spatial Prediction of Soil Texture Fractions in Arid Regions of Iran. Soil Syst, 3: 65 doi:10.3390/soilsystems3040065.

Mitran, T., Mishra, U., Lal, R., Ravisankar, T., Sreenivas, K. (2018). Spatial distribution of soil carbon stocks in a semi-arid region of India. Geoderma Regional, 15:1–9

Mondejar, J.P., and Tongco A. F. (2019). Estimating topsoil texture fractions by digital soil mapping - a response to the long-outdated soil map in the Philippines. Sustainable Environment Research, 29:31, doi.org/10.1186/s42834-019-0032-5.

Moses, A. (1987). The climate of Syria, Damascus university publication 123. p

Mosleh, Z., Salehi, M. H., Jafari, A., Borujeni, I. E., and Mehnatkesh, A. (2016). The effectiveness of digital soil mapping to predict soil properties over low-relief areas. Environ Monit Assess 188:195. DOI 10.1007/s10661-016-5204-8.

Nikolakopoulos, K.G. (2003). Use of vegetation indexes with ASTER VNIR data for burnt areas detection in Western Peloponnese, Greece. IEEE Int. Geoscience and Remote Sensing Symp., September 21-25, Toulouse, France.

Oberthür, T., Dobermann, A., and Neue, H.U. (1996). How good is a reconnaissance soil map for agronomic purposes? Soil Use Manage, 12: 33–43.

Olaya, V. (2006). Basic Land-Surface Parameters. In: Hengl, T., Reuter, H.I. [Eds.]: Geomorphometry: Concepts, Software, Applications. Developments in Soil Science, Elsevier, 33: 141-169.

Pettorelli, N., Vik, J.O., Mysterud, A., Gaillard, J.M., Tucker, C.J. and Stenseth, N.C. (2005). Using the satellite-derived NDVI to assess ecological responses to environmental change. J. Trends Ecology Evolution, 9:503-510.

Pinheiro, H.S.K., de Carvalho, W., Chagas, C.D., dos Anjos, L.H.C., and Owens, P.R. (2018). Prediction of topsoil texture through regression trees and multiple linear regressions. Rev Bras Cienc Solo, 42:1–21.

Rawls, W.J, Brakensiek, D.L., and Saxton, K.E. (1982). Estimation of soil water properties. Trans. ASAE, 25: 1316–1320, 1328.

Scott D.W. (2018). Tukey ladder of powers. In: lane DM, editor. Introduction to statistics. Online Statistics Education: A Multimedia Course of Study. http:// onlinestatbook.com/ Online_Statistics_Education.pdf. Accessed 21 Dec. 2018.

Seybold, C.A., Grossman, R.B., and Reinsch, T.G. (2005). Predicting cation exchange capacity for soil survey using linear models. Soil Sci. Soc. Am. J, 69: 856–863.

Sudduth, K.A., and Hummel, J.W. (1991). Evaluation of reflectance methods for soil organic matter sensing. Trans. ASAE, 34: 1900–1909.

Suliman, A.S., and Post, D.F. (1988). Relationship between soil spectral properties and sand, silt, and clay content of the soil on the University of Arizona Maricopa Agricultural Center. Proc. Hydrology and Water Resources in Arizona and the Southwest. J. Arizona Nevada Acad. Sci, 18: 61–65.

Sullivan, D.G., Shaw, J.N., and Rickman, D. (2005). IKONOS imagery to estimate surface soil property variability in two Alabama physiographies. Soil Sci. Soc. Am. J, 69: 1789–1798.

Tsai, AC, Liou, M., Simak, M., and Cheng, P.E. (2017). On hyperbolic transformations to normality. Comput Stat Data An, 115:250–66.

Tukey, J. W. (1977). Exploratory Data Analysis. Reading, Massachusetts: Addison-Wesley.

Warrington, D.N., Mamedov, A.I., Bhardwaj, A.K., and Levy, G.J. (2009). Primary particle size distribution of eroded material affected by the degree of aggregate slaking and seal development. Eur. J. Soil Sci, 60: 84–93.

Webster R, Oliver MA. (2007). Geostatistics for environmental scientists. Chichester: John Wiley & Sons, Ltd.

Wilding, L. P. (1985). Spatial Variability: its documentation, accommodation, and implication to soil surveys. In Nielsen, DR. Bouma, J. (Eds.). Soil Spatial Variability, Pudoc, Wageningen, Netherlands.

Wösten, J.H.M., Pachepsky, Y.A., and Rawls, W.J. (2001). Pedotransfer functions: Bridging the gap between available basic soil data and missing soil hydraulic characteristics. J. Hydrol., 251: 123–150.

Zevenbergen, L.W., and Thorne, C.R. (1987). Quantitative analysis of land surface topography. Earth Surface Processes and Landforms, 12: 47-56.

Zhang, R., Warrick, A.W., and Myers, D.E. (1992). Improvement of the prediction of soil particle size fractions using spectral properties. Geoderma, 52: 223–234.

Zhang, S.W., Shen, C.Y., Chen, X.Y., Ye, H.C., Huang, Y.F. and Lai, S. (2013). Spatial interpolation of soil texture using compositional kriging and regression kriging with consideration of the characteristics of compositional data and environment variables. J Integr Agr, 12:1673–83.

Zhao, Z.Y., Chow, T.L., Rees, H.W., Yang, Q. Xing Z.S., and Meng, F.R. (2009). Predict soil texture distributions using an artificial neural network model. Comput. Electron. Agr, 65: 36–48.

Zhu, Q., and Lin, H.S. (2010). Comparing ordinary kriging and regression kriging for soil properties in contrasting landscapes. Pedosphere, 20: 594–606.

JJEES

JJEES (2022) 13 (1): 37-47
ISSN 1995-6681

Jordan Journal of Earth and Environmental Sciences

Petrographical and Petrophysical Studies of Some Upper Cretaceous Rocks, Western Desert, Egypt

Hesham Abuseda[1] and Abdel Moktader El_Sayed[2]

[1]Production Department, Egyptian Petroleum Research Institute (EPRI), 11727, Cairo, Egypt.
[2]Department of Geophysics, Faculty of Sciences, Ain Shams University, 11566 Cairo, Egypt.

Received 20 June 2021; Accepted 27 July 2021

Abstract

The petro-graphically studied sandstone samples are principally made out of detrital quartz and quartz overgrowth, plagioclase, microcline, kaolinite, iron oxide, and pyrite. Muscovite, biotite, apatite, and calcite, are present as accessory minerals. The sedimentary structures show that the deposition environment was in a relatively low-energy, sub- to the intertidal zone. The petrophysical properties indicate a moderate degree of diagenesis and cementation for the investigated sandstones that results in favorable reservoir conditions. Most samples belonging to the Bahariya Formation showed a strong influence on most petrophysical parameters. It causes a higher internal surface (S_{por}), higher electrical resistivity, higher magnetic susceptibility, increased p-wave velocity, a small reduction in porosity, and reduced rock permeability. Magnetic susceptibility has proved to be a key parameter in evaluating the investigated sandstone samples' porosity and permeability. Iron oxide cement that has been precipitated in the pore space control porosity, specific internal surface, and permeability. The permeability–formation resistivity factor relation reflects the effect of porosity changes, as indicated by Archie's law. The pore volume-related internal surface shows an inverse relation to permeability for both Bahariya and Abu Roash formations. Since it is known that (S_{por}) is related to the inverse to the effective pore radius. The formation factor's determination from the Börner equation has been determined and is slightly lower than in the measured formation factor. It was shown that the Wyllie equation fails to provide a reliable prediction of porosity for saturated samples from compressional wave velocity data.

Keywords: Permeability, Porosity, Susceptibility, Spectral Induced Polarization.

1. Introduction

The Abu Sennan concession lies in the Western Desert, Egypt, which is considered one of the most important oil and gas provinces. The Abu Sennan concession is located between latitudes 290 32' and 290 35' N and longitudes 280 30' and 280 35' E. (see Figure 1). It's lies 260 km west of Cairo and about 160 km south of the Mediterranean coast. The South West Sennan (SWS) oil field is in the Abu Sennan concession. The Upper Cretaceous (Cenomanian) Bahariya Formation is counted among the most important hydrocarbon reservoirs in the Western Desert. Several authors studied the subsurface Bahariya Formation from the stratigraphic, tectonic, and sedimentological points of view (Soliman and Hassan, 1970; El Gezeery et al., 1972; Franks, 1982, Dominik, 1985; and Catuneanu et al., 2006). It is made up of sandstones, siltstones, shale, and limestone. Catuneanu et al., 2006 described the Bahariya depositional environment as an overall transgression with coastal backstepping comprising several coarsening-upward cyclothems and the deposition of fossiliferous glauconitic siltstones and sandstones. Hence, the environment was a shallow marine with tidal flat to marine shelf settings. The stratigraphic sequence of the SWS field can be described by the generalized stratigraphic column of the northern part of the Western Desert shown in Figure 2. The Khoman, Abu Roash, and Bahariya formations form the Upper Cretaceous section in the stratigraphic column. The Bahariya is the lowermost Formation, which covers the lower Cretaceous Kharita Formation. The Abu Roash Formation overlies it that consists of limestone, shale, and sand interbeds, which were deposited under restricted marine conditions Abuseda et al., 2016. The present study is mainly devoted to the analysis of core samples recovered from four wells, SWS-7, SWS-13, SWS-15, and SWS-21, related to the Bahariya Formation, and two wells SWS-8 and SWS-21 related to Abu Roash Formation have been investigated to establish useful relations between petrophysical parameters and reservoir properties. The samples' mineralogical composition was analyzed by microscopy of thin sections and scanning electron microscope (SEM). Different petrophysical methods were applied to identify the sample's physical parameters related to reservoir properties.

* Corresponding author e-mail: heshamabuseda@epri.sci.eg

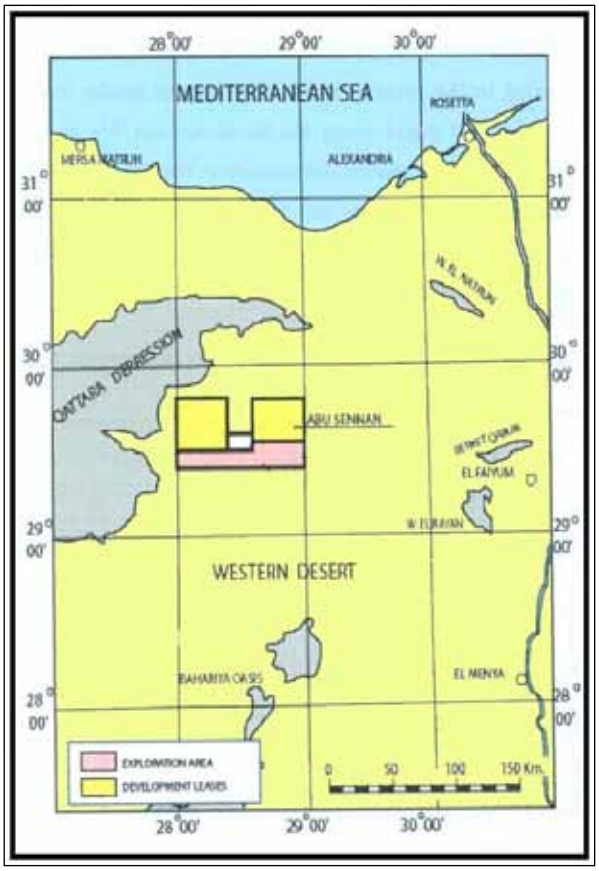

Figure 1. location map of the study area.

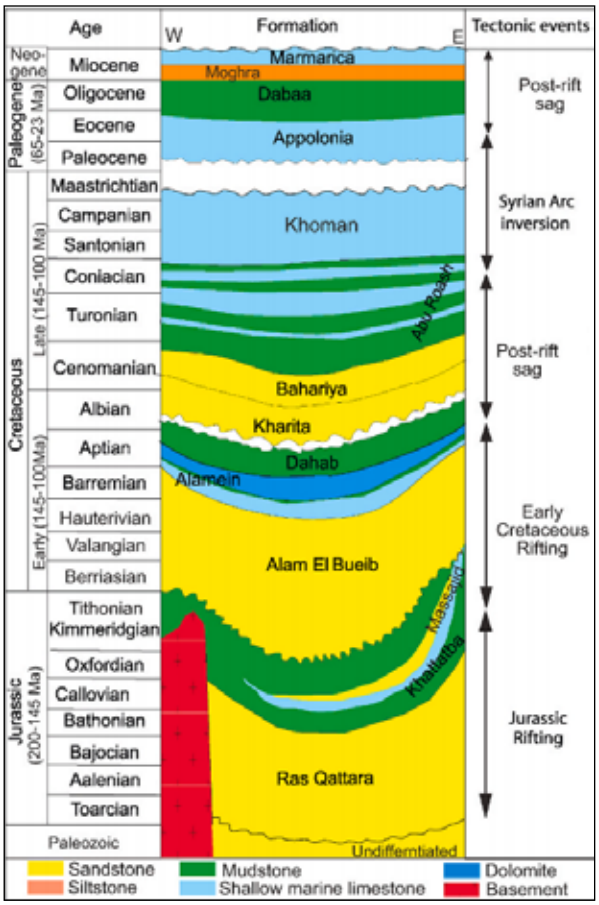

Figure 2. Stratigraphic column of the Western Desert (Selim et al., 2021).

2. Mineralogical investigations

The petrography and mineralogy of the present studied samples were examined using a polarizing microscope and the description was based on the study of the petrography and facies types. The sedimentary structures and mineralogical composition correspond to the results of Athmer (2006) and Halisch et al. (2009). The mineralogical composition and the sedimentary structures studied by Abuseda et al., 2016 show that the sedimentary structures show characteristic deposition features in a relatively low-energy, sub- to the intertidal zone. To identify the mineralogical composition of sandstones of the SWS field, a variety of thin sections were prepared for transmitted light microscopic investigations. These investigations reveal that the mineralogical composition for studied sandstone samples is mainly composed of detrital quartz and quartz overgrowth, kaolinite, plagioclase, and microcline, pyrite. Muscovite, biotite, zircon, glauconite, rutile, apatite, and diagenetic calcite, are present as accessory minerals. The mica minerals have a fibrous shape and are located tangential between quartz grains, which indicate deep burial Figure 3, showing a primary inter-particle porosity (yellow arrow) and the (red arrows) indicate tangential mica between quartz grains. Cementation minerals are kaolinite, calcite, and subordinate quartz overgrowths Figure 4, with associated secondary microporosity (Alsuwaidi et al., 2021). Most of the quartz overgrowth surfaces are clean of further cement forming diagenetic minerals (Farouk et al., 2018). Non-weathered tight glauconite grains, as well as disintegrating glauconite grains with secondary intraparticle microporosity, indicate moldic porosity. Feldspar appears as plagioclase and microcline, which often are heavily etched or decomposed to honeycomb structures. Muscovite is mostly aligned along with the sedimentary beddings. Due to their oxidation, the layers contain minor iron hydroxides and quartz overgrowths Figures 5 & 6. Abundant chlorite cementation increases the magnetic susceptibility, the specific internal surface, and grain density and, on the other hand, decreases porosity and permeability.

3. Petrophysical investigation

Petrophysics is considered a cornerstone and magic key for solving geophysical problems and introducing theories. Therefore, the study of rock physics provides multidisciplinary concepts and tools to facilitate and enhance geophysical interpretation. Laboratory investigations were carried out to determine standard parameters for reservoir characterization, such as porosity, density, permeability, and special core analysis, such as specific surface area, compressional wave velocity, and complex electrical resistivity. We combined the knowledge and data of geology, mineralogy, and petrophysics to get access to form a detailed reservoir description.

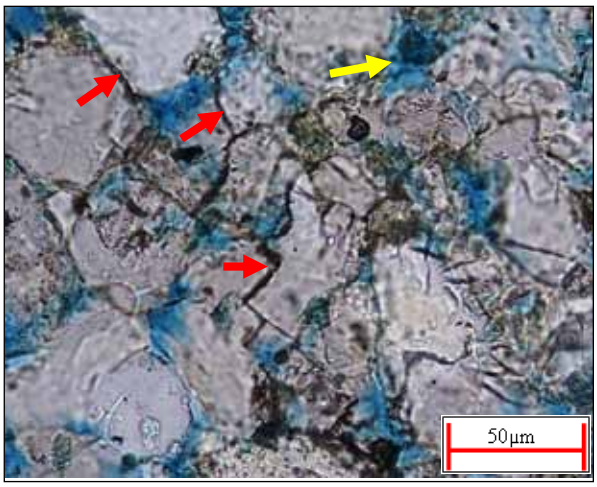

Figure 3. Thin section image of sample 15_28H1 (PPL X40) Bahariya Formation. They are showing primary interparticle porosity (yellow arrow). The red arrows indicate tangential mica between quartz grains.

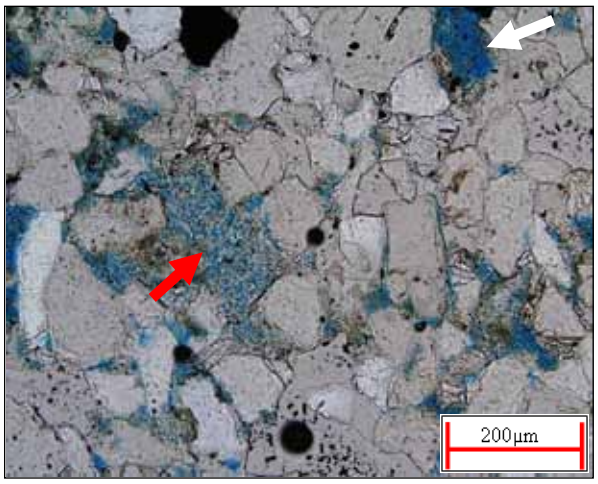

Figure 4. Thin section image of sample 15_43H1 (PPL X40) Bahariya Formation. They are showing pore filling kaolinite (red arrow) with associated secondary microporosity.

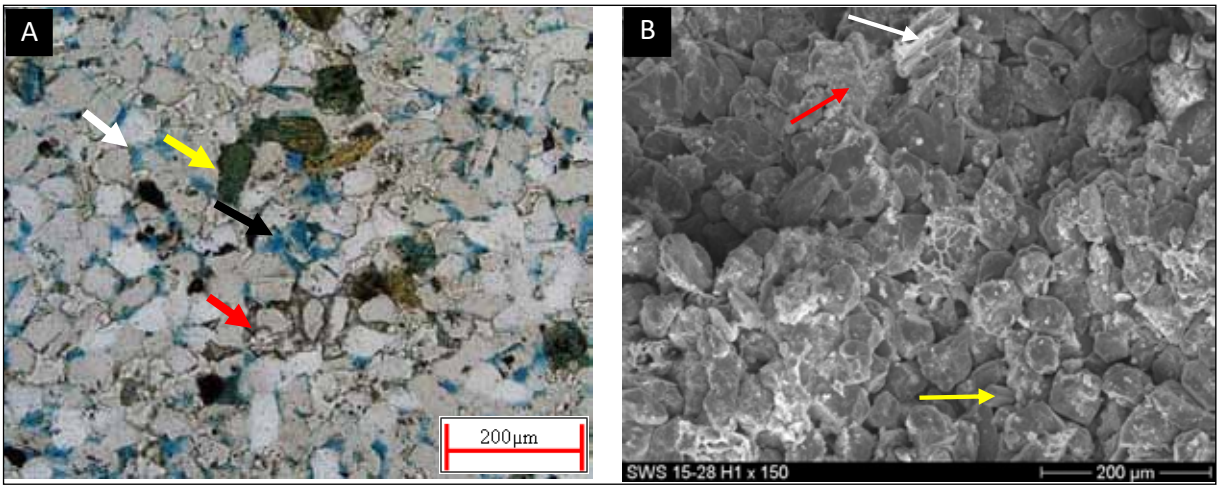

Figure 5. Thin section image of sample 15_28H1 (PPL X10) Bahariya Formation. (A) Primary interparticle porosity (white arrow), secondary moldic porosity (black arrow), secondary intraparticle microporosity within a glauconite grain (yellow arrow), and carbonate cement (red arrow). (B) SEM image showing a moderate increase of specific internal surface by glauconite grains (red arrows) and feldspar honeycombs (white arrow). Pore-lining cement of Fe-rich chlorite is missing or less. Most of the quartz overgrowth surfaces (yellow arrow) are clean of further cement forming diagenetic minerals.

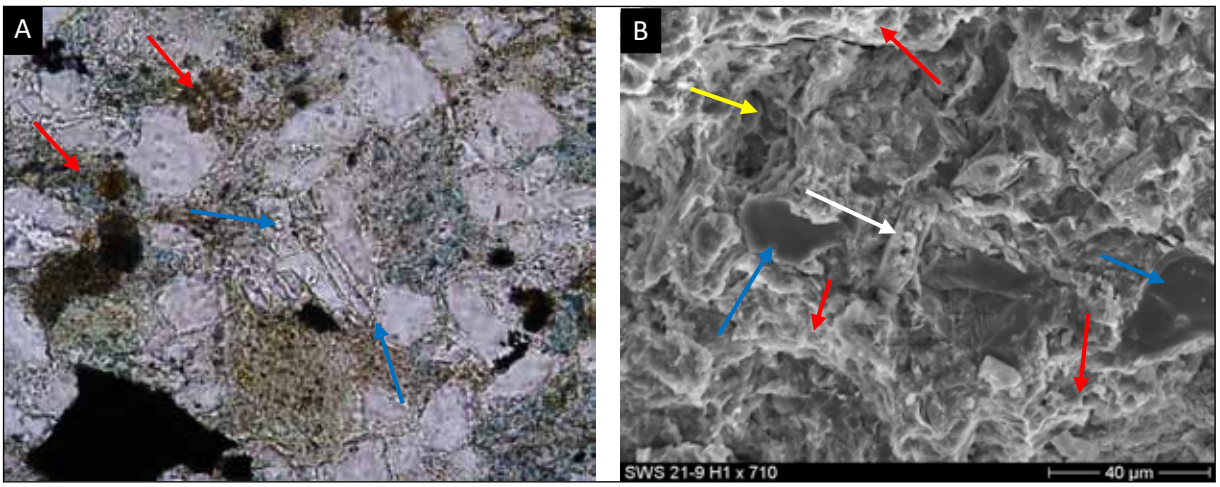

Figure 6. Thin section image of sample 21-9H1 (PPL X10) Abu Roash Formation. Silty quartz and quartz swimming in shale (blue arrows) stained by iron oxide (red arrows). (B) SEM image showing a strong increase of specific internal surface by pore-lining cement of Fe- oxide (red arrows) and clay matrix (white arrow). The amount of quartz overgrowth surfaces (blue arrows) cleans of further cement forming diagenetic minerals is rather low. The yellow arrow indicates a pyrite

3.1. Methods and Techniques:

- Petro-physical properties

3.1.1. Sample preparation:

Samples were drilled as cylinders of 2.5 cm diameter and different lengths (2 to 4 cm) using a diamond drilling machine. The studied samples have been cleaned by organic solvents using soxhlet extractor apparatus; the particular solvent used was selected not to alter or destroy the samples pore framework. Samples were dried to remove pore water and cleaning solvent. It dried in an oven to a constant weight of 100 C^0. Before and after a subsequent 4 hours drying period, samples were at a constant weight, and repeatable weight (+/- 1%) could be determined. After constant weights had been achieved, all the samples were cooled to room temperature in moisture-free desiccators.

3.1.2. Porosity and density

Several methods have been proposed and explained in different literature for rock porosity determination. In the laboratory, measurement of rock porosity requires the determination of only two of the three-volume parameters: they are pore volume (V_p), grain volume (V_g), and bulk volume (V_b), with the latter being the sum of the previous two parameters. In the present study, the rock porosity and grain density were determined by the Archimedes method with weighting the sample three times: in a dry state, in a fully saturated state, and finally in a water basin. Bulk density is defined as the mass of the unit volume of a rock in its natural state and expressed as:

$$d_b = \frac{m}{v} \quad \text{..... (1)}$$

with bulk density g/cm³, mass of the sample g, and volume of the samples cm³.

The grain density is a sensitive tool to indicate the mineral composition of the rock. It also helps in the evaluation of the cement materials and the presence of impurities. It has been calculated from the porosity test (Archimedes method) by using the following equation:

$$d_g = \frac{m_d}{V_g} \quad \text{..... (2)}$$

with grain density g/cm³, dry mass of sample g, and volume of grains cm³.

Porosity is the most important parameter for evaluating the storage capacity of a porous medium. Porosity (Φ) is defined as the ratio of the volume of pore space Vp to the total volume V of the rock sample:

$$\Phi = \frac{Vp}{V} \quad \text{..... (3)}$$

with volume of pore space cm³, volume of the samples cm³, and porosity.

3.1.3. Specific surface area

Porosity describes the volume of the voids (pores, cracks, fissures, fractures, etc.) related to the considered rock volume. The specific internal surface describes the surface area of these voids to $S_{tot.}$ (μm^{-1} the total rock volume) with S_{por} μm^{-1} (the pore volume) with S_m μm^{-1} (the volume of the solid matrix) and S_{ma} m^2/g (the mass of the dry rock). The following equations can be used to transform the quantities mentioned above:

$$S_{por} = d_{grain}\left(\frac{(1-\Phi)}{\Phi}\right)S_m$$

$$S_{tot} = \Phi.S_{por} = (1-\Phi).S_m \quad \text{..... (4)}$$

$$S_{ma} = \frac{S_m}{d_m} \quad \text{..... (5)}$$

with density of the solid matrix material.

The specific internal surface depends mainly on the shape and size of pores and the matrix-pore interface's microstructure and morphology. The specific internal surface varies over a wide range. The "micromorphology" of the pore surface strongly influences the value of the specific internal surface. The specific internal surface increases with the decrease of the mean pore or grain size as a general tendency. The presence of clay particles and the growth of various types of surface structures in the pore space increases the internal surface (Schön, 1996).

3.1.4. Permeability

The permeability of a rock is defined as a measure of a porous material's ability to transmit fluid. Permeability is a phenomenon that can be described by Darcy's law for viscous fluids in porous media. A rock's permeability is controlled by many factors such as rock pore geometry, cementation, rock texture, grain size, grain shape, and roundness.

Molecular slip can contribute to the flow of gases when the pore dimensions approach the gas molecules' mean free path. The apparent permeability k_a becomes dependent on the mean absolute gas pressure (Klinkenberg, 1941)

$$k_a \quad k\left(1 \quad \frac{\alpha}{p}\right) \quad \text{..... (6)}$$

The constant called Klinkenberg constant. The Klinkenberg constant s often expressed as a function of the true permeability k. The Klinkenberg effect might even lead to a "gas chromatographic" separation of gases of different molecular weights in porous rocks. In geohydrology, a simplified version of Darcy's law is commonly used.

3.1.5. Magnetic Susceptibility

The magnetic properties of rocks are controlled by those mineral constituents which have a magnetic effect. The fraction of these minerals concerning the total rock volume may be small. Magnetic properties describe the behavior of any substance under the influence of a magnetic field. Magnetic phenomena arise from the motion of electrically charged particles within the substance. Schön (1996) describes three main groups of materials about the magnetic properties: diamagnetic behavior, Paramagnetic behavior, and Ferro-, antiterror and ferrimagnetic behavior. Diamagnetic and paramagnetic substances show only weak effects in the presence of an applied magnetic field. In both cases, the strength of the induced magnetization M (magnetic dipole moment per unit volume) is directly related to the strength of the applied magnetic field H:

$$M = \kappa.H. \quad \text{..... (7)}$$

with the factor of proportionality κ being the magnetic susceptibility.

3.1.6. Formation Resistivity Factor

The formation resistivity factor was discussed by many authors, such as Wyllie and Spangler, 1952; El Sayed, 1981; Tiab and Donaldson, 2015; Glover, 2009; Abuseda et al., 2016 and others. They concluded that the formation resistivity factor is a function of the effective electric current flow path and the effective cross-sectional area available for electric conduction.

Archie (1942) first defined the property of a porous medium known as "formation resistivity factor" as:

$$\text{True formation resistivity} = \frac{R_W}{rho_0} \quad \text{..... (8)}$$

with the photo being the resistivity of a sample that is completely saturated with brine of resistivity R_w.

The fundamental formation resistivity factor F porosity relation, as introduced by Archie (1942), is

$$F = \Phi^{-m} \quad \text{..... (9)}$$

with m being the cementation factor.

Wyllie and Gregory (1953) investigated the influence of particle size and cementation on the formation resistivity factor of various materials. Observed formation resistivity factor for artificially cemented aggregates showed that the cemented aggregates exhibit a greater change in porosity than the unconsolidated aggregates. Wyllie and Gregory (1953) concluded that the general form of the relation between formation factor and porosity is:

$$F = a\Phi^{-m} \quad \text{..... (10)}$$

with a being another free parameter that depends on lithology.

At high water salinity, the measured ratio is a good estimate of the true formation factor.

3.1.7. Compressional wave velocity

The elastic properties and the velocity of elastic waves in rocks are controlled primarily by the rock-forming minerals and constituents' elastic properties, their fractional volume, their contact, cementation or bonding properties, pressure, and temperature. The mineralogical composition of sedimentary rock has a strong influence on its velocity. For certain rock types, porosity is often the dominant influence. The elastic properties of porous clastic and carbonate rocks are mainly controlled by porosity and matrix composition. The matrix composition also influences the contact conditions, cementation, and grain bonding (Schön, 1996). In the present work, compressional wave velocity was measured at room temperature and ambient pressure on cylindrical samples using USLT 2000 (Inspection Technology). The acoustic velocity was determined for fully saturated sandstone rock samples at ultrasonic frequencies of 500 kHz. Porosity is one of the most important characteristic parameters in the evaluation of potential reservoirs. The porosity can be derived from the knowledge of the interval velocity. The average time equation of Wyllie et al., (1956 and 1958) has been used to obtain porosity from acoustic velocity logs. The equation for P-wave velocity (Vp) in water-saturated rock is:

$$\frac{1}{V_p} = \frac{\Phi}{V_f} + \frac{(1-\Phi)}{V_m} \quad \text{..... (11)}$$

$$\Phi = \frac{V_f}{V_p}\left(\frac{V_m - V_p}{V_m - V_f}\right) \quad \text{..... (12)}$$

with: V_p the compressional wave velocity, V_m the velocity of the solid material, V_f the velocity of the pore fluid, and Φ the porosity of samples.

This simple equation appears adequate for fully saturated sandstone in the middle range of porosity (10% < Φ < 25%).

4. Results and Discussions

The minima, maxima, average values, and standard deviations of all measured parameters are calculated for all studied samples are compiled in Table (1).

Table 1. Compilation of minimum, maximum, average values, and standard deviations of measured petrophysical parameters.

Parameters	Bahariya Formation				Abu Roash Formation			
Parameters	Min.	Max.	Mean	Std. dev.	Min.	Max.	Mean	Std. dev.
dry (g/cm^3)	2.00	2.42	2.17	0.14	1.94	2.59	2.18	0.18
drain (g/cm^3)	2.52	2.84	2.65	0.08	2.24	2.73	2.57	0.15
Porosity *Φ*	0.12	0.24	0.18	0.04	0.05	0.26	0.15	0.07
Permeability (MD)	0.06	133.65	44.35	51.28	0.05	25.36	11.27	12.11
F	12.45	62.40	26.23	13.22	13.27	38.01	22.66	13.40
κ (10^{-6} SI)	25.19	1175.05	235.18	253.96	7.33	906.98	177.88	152.10
VP (m/s)	2053	3880	2851	435	2190	3887	2875	413
S_{por} (1/μm)	1.35	147.91	40.33	45.94	13.01	43.79	24.92	13.67
s' (mS/m)	5.64	26.39	13.20	6.76	1.93	13.43	8.98	4.93
s'' (mS/m)	0.04	0.32	0.15	0.08	0.02	0.26	0.17	0.11
σ'$_{surf}$ (mS/m)	0.99	22.77	8.06	7.35	4.27	7.60	5.95	1.66
r (Ωm)	38.75	181.86	99.06	42.87	98.90	103.85	100.69	2.19

4.1. Bulk density - porosity relationship

The bulk density - porosity relationship for the studied samples is shown in Figure 7. An inverse relationship for all studied Bahariya Formation wells encountered in SWS-7, SWS-13, SWS-15, SWS-21, and Abu Roash Formation in wells SWS-8, SWS-21 is characterized by a coefficient of correlation (R^2 = 0.78 and 0.76) for the Bahariya Formation and the Abu Roash Formation respectively.

The following equations control the bulk density - porosity relationship Figure 7:

For the Bahariya Formation $\Phi = 0.68 - 0.23\ d_b$ .....(13)

For the Abu Roash Formation $\Phi = 0.79 - 0.29$ DB .....(14)

with the bulk density d_b given in g/cm³ and the porosity Φ as fraction value.

4.2. Porosity - Permeability relationship

The permeability of a rock may be affected by many geological factors. High rock porosity does not guarantee that a significant permeability exists. The pores must be interconnected, and the pore throats must be large enough to permit the flow of fluids. A pore network is made up of larger spaces referred to as pores, which are connected by small spaces referred to as pore throats. In other words, the volume of pore space is reflected by the measured porosity, while the measured permeability of the rock reflects the size of pore throats. The geometric relationship between pore spaces and pore throats controls the relationship between porosity and permeability. The relationship between porosity and permeability has been studied by many authors, (e.g., Carman, 1937; Timur, 1968; Scheidegger, 1974; El Sayed, 1981; Herron, 1987; Adler et al., 1990; Schön, 1996; and Tiab and Donaldson, 2015). In the present work, porosity–log permeability cross plots exhibiting the investigated samples are shown in Figure 8. This figure's data points follow the expected positive trend between porosity and permeability for all studied samples. The relationship is characterized by a weak coefficient of correlation (R^2 = 0.43) for the Bahariya and a high correlation coefficient (R^2 = 0.88) for the Abu Roash Formation, indicating the inhomogeneity of the Bahariya Formation. The samples generally show lower porosity and permeability for all samples indicating that clay pore filling causes a decrease in porosity and permeability. The following equations control them:

For Bahariya Formation $\ln(k) = 61.79\ \Phi - 9.69$ .....(15)

For Abu Roash Formation $\ln(k) = 50.38\ \Phi - 9.56$ .....(16)

with the Permeability K in mD and the porosity Φ as fraction value.

4.3. Internal surface (S_{por}) - permeability relationship

The internal surface (S_{por}) - permeability relationship for the studied samples is shown in the Figure 9. The Bahariya Formation relationship is characterized by a coefficient of correlation (R^2 = 0.70) and a weak coefficient of correlation (R^2 = 0.28) for the Abu Roash Formation. The internal surface (S_{por}) - permeability relation shows a reverse trend with a general permeability decreases with increasing internal surface (S_{por}). Generally, the internal surface (S_{por}) decreases with increased permeability. The following power-law equation controls the relationship:

For Bahariya Formation $\ln(K) = 5.90 - 1.57 \ln(S_{por})$ ...(17)

with S_{por} Internal surface in 10^6 * 1/m.

4.4. Porosity - Formation resistivity factor relationship

The porosity-formation resistivity factor cross plot for the studied samples is shown Figure 10. The data shows a reverse trend for all samples. The relations are characterized by the coefficient of correlation (R^2 =0.70) for the Bahariya Formation, but it was (R^2 = 0.99) for the Abu Roash Formation. It shows a good possibility to calculate the formation factor from porosity data. Larger values of the formation factor reflected the samples' lower porosity, while the calculated cementation factor for the Bahariya Formation (m=2.05) was higher than the cementation factor for the Abu Roash Formation (m=1.83). The iron oxide improves the cementation exponent of the Bahariya sandstone due to its high electrical conductivity. The formation resistivity factor - porosity relationships are controlled by the following equations:

For Bahariya Formation $\log F = 3.96 - 2.05 \log \Phi$ ..(18)

For Abu Roash Formation $\log F = 3.75 - 1.83 \log \Phi$.(19)

The above equations (18 & 19) are very important for outlining these formations' water and hydrocarbon saturation during well logging processing and interpretation.

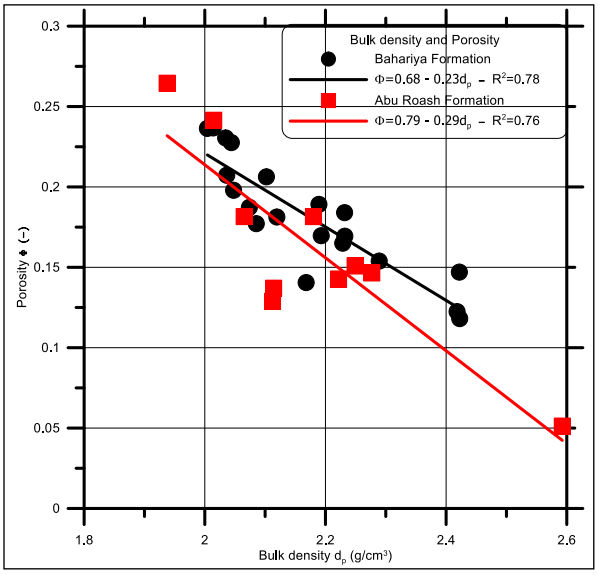

Figure 7. Bulk density versus Porosity for the studied samples.

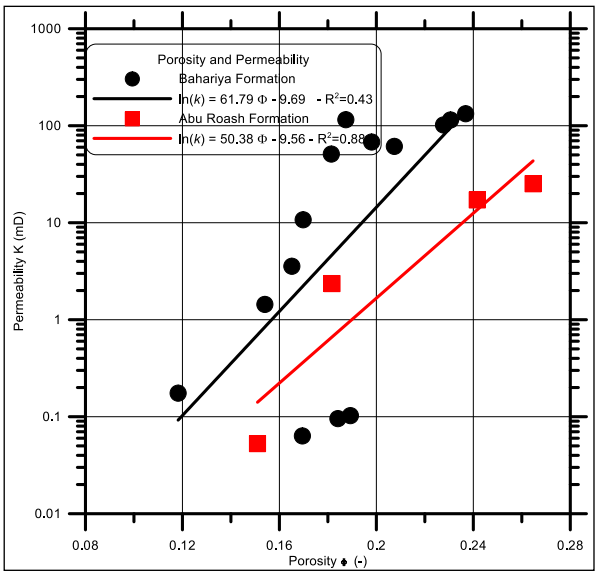

Figure 8. Porosity versus Permeability for the studied samples.

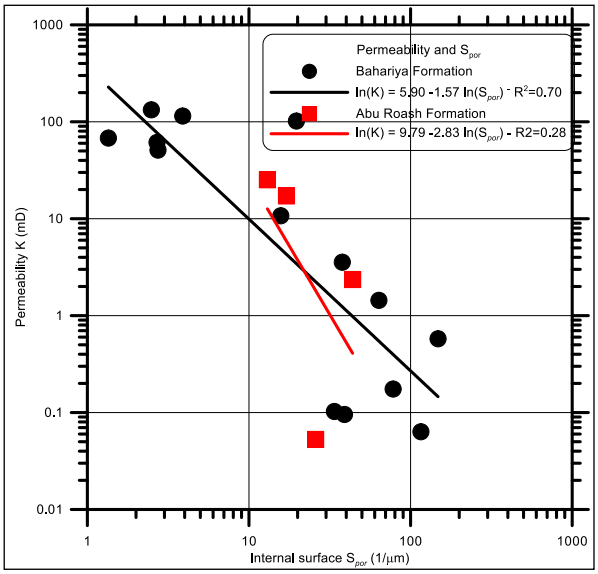

Figure 9. Internal surface S_{por} versus permeability for the studied samples.

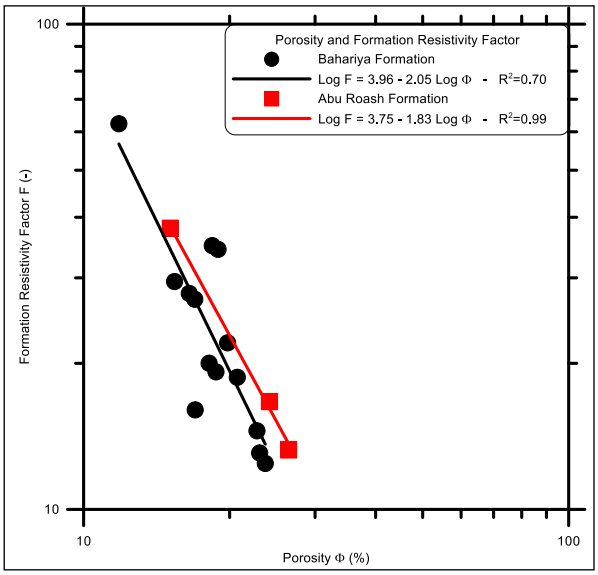

Figure 10. Porosity versus Formation resistivity factor for the studied samples.

4.5. Permeability - Formation resistivity factor relationship

The formation resistivity factor - permeability cross plot for the studied samples is shown in Figure 11. The data in this Figure show a reverse relation for all samples. The relations are characterized by a coefficient of determination of 0.69 for the Bahariya Formation, but the determination coefficient is 0.98 for Abu Roash Formation. The formation resistivity factor - permeability relationships are controlled by the following equations:

For Bahariya Formation $\ln(K) = 19 - 5.46 \ln(F)$ .....(20)

For Abu Roash Formation $\ln(K) = 19.66 - 6.18 \ln(F)$ ..(21)

4.6. Magnetic susceptibility - Grain density relationship

The susceptibility - grain density cross plot for all samples is shown in Figure 12. The relationship is characterized by the coefficient of correlation (R2 = 0.66) for Bahariya Formation and is characterized by a coefficient of determination of 0.61 for Abu Roash Formation. Figure 12 indicates a positive trend of increasing magnetic susceptibility with increasing grain density for all samples. The susceptibility - grain density relationship is controlled by the following equations:

For Bahariya Formation $\ln(d_g) = 0.02 \ln(\kappa) + 0.86$ ...(22)

For Abu Roash Formation $\ln(d_g) = 0.03 \ln(\kappa) + 0.80$ ...(23)

with d_g grain density in g/cm³ and κ magnetic susceptibility in 10^{-6} SI.

The magnetic susceptibility is a reliable indicator of the presence of iron oxide minerals. The reason for the wide variation in grain density has been identified as the increase in grain density caused by iron oxide cement, as indicated in the Figures 5 and 6.

4.7. Magnetic susceptibility and porosity relationship

The susceptibility - porosity cross plot for the samples is shown in Figure13 (the resulting correlation is characterized by a coefficient of determination of 0.51 for the Bahariya Formation and a very weak coefficient of determination for the Abu Roash Formation. The relation indicates a decreasing porosity with increasing magnetic susceptibility. The best-fitting equation reads:

For Bahariya Formation $\ln(\Phi) = -0.14 \ln(\kappa) - 1.07$ ...(24)

The reduction in porosity of samples suggests that diagenetic iron oxide precipitated as pore-lining cement, as can be observed in Figure 6.

4.8. Magnetic susceptibility – Permeability relationship

The susceptibility - permeability cross plot for the samples is shown in Figure 14. The resulting correlation is characterized by a coefficient of determination 0.77 and 0.84 for Bahariya and Abu Roash Formation, respectively. The susceptibility - permeability relationship shows a general increase of permeability with decreasing magnetic susceptibility for all samples, which is controlled by the equations:

For Bahariya Formation $\ln(K) = 13.96 - 2.62 \ln(\kappa)$ ...(25)

For Abu Roash Formation $\ln(K) = 46.60 - 9.19 \ln(\kappa)$ ...(26)

with K Permeability in mD.

The precipitation of pore-lining iron oxide in the pore space affects the permeability, too. Considerable reduction of permeability is observed for the samples of higher magnetic susceptibility.

4.9. Magnetic susceptibility - Specific Internal surface (S_{por}) relationship

The relation between magnetic susceptibility and specific internal surface S_{por} is displayed in Figure 15. A clear trend is observed. The Figure indicates a positive trend in increasing magnetic susceptibility with the larger values of the specific internal surface for all samples. The power-law can describe the trend:

For Bahariya Formation $\ln(S_{por}) = 1.48 \ln(\kappa) - 4.22$ ...(27)

For Abu Roash Formation $\ln(S_{por}) = 1 \ln(\kappa) - 2.07$ ...(28)

The relationship between susceptibility and the specific internal surface is characterized by a coefficient of determination of 0.82 for Bahariya sandstone samples and a coefficient of determination of 0.99 for Abu Roash Formation.

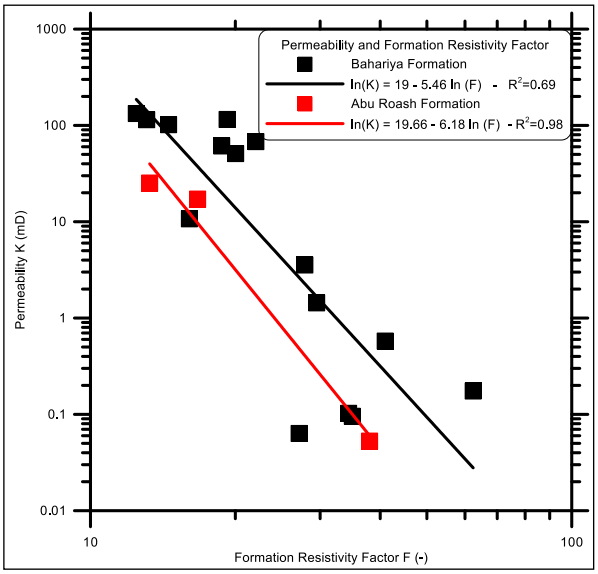

Figure 11. Permeability versus Formation resistivity factor for the studied samples.

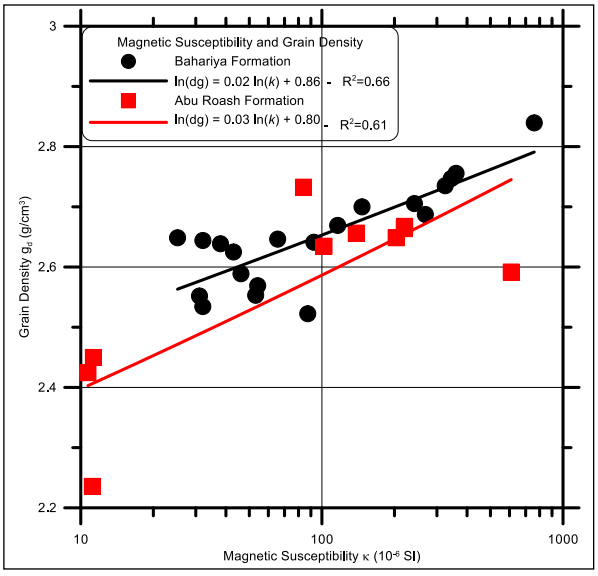

Figure 12. Magnetic susceptibility versus Grain density for the studied samples.

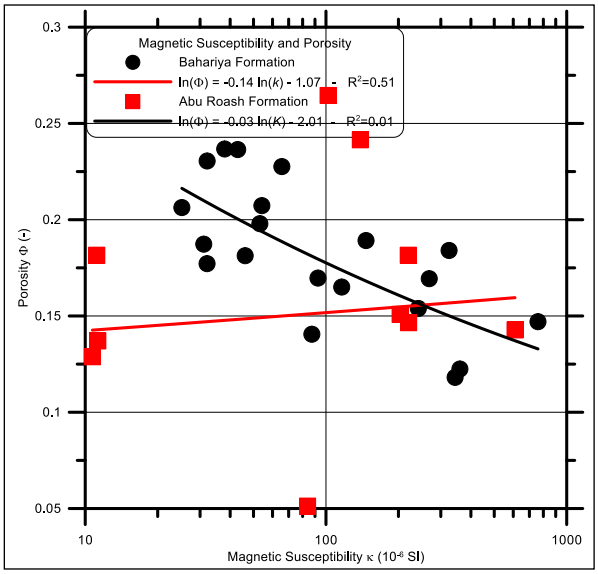

Figure 13. Magnetic susceptibility versus Porosity for the studied samples.

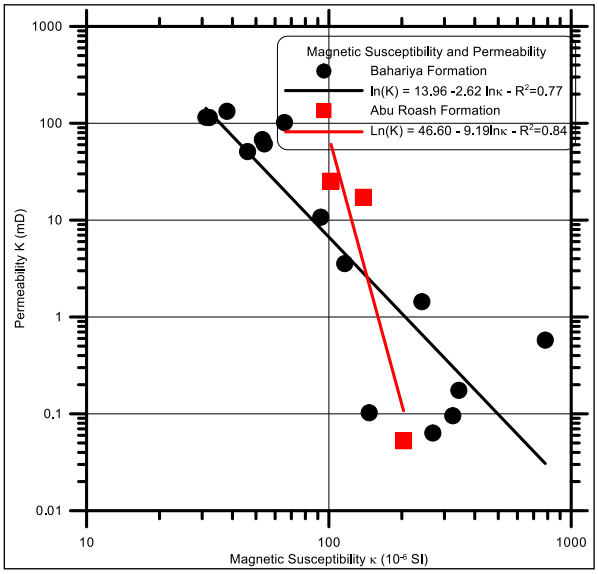

Figure 14. Magnetic susceptibility versus permeability for the studied samples.

4.10 P-wave velocity - porosity relationship

The p-wave velocity - porosity relationship for samples is shown in Figure 16. The relationship is characterized by a coefficient of correlation (R^2 = 0.49). For Bahariya Formation, but the coefficient of correlation (R^2 = 0.77) for Abu Roash Formation. The p-wave velocity - porosity shows a reverse relation. P-wave velocity decreases with increasing porosity. The following equation controls the relationship:

For the Bahariya Formation $\Phi = 0.35 - 5.73\ V_p$. .....(29)

For the Abu Roash Formation $\Phi = 0.54 - 0.0001\ V_p$. ...(30)

with: V_p compressional wave velocity.

5. Petrophysical Models

5.1. Electrical parameters versus formation resistivity factor

Most models for the complex electrical conductivity of a porous material at low frequencies (e.g., less than 100 Hz) are based on a parallel addition of two conduction terms representing (a) an electric contribution via conduction through the interconnected pore space and (b) a mineral surface conduction contribution (Vinegar and Waxman, 1984). Polarization is associated with surface conductivity at low frequencies. For a fully saturated medium:

$$\sigma_0 = \sigma_w \cdot \frac{1}{F} + \sigma_i \quad \text{..... (31)}$$

with F formation resistivity factor and σ_w fluid conductivity.

Empirical and mechanistic formations for the surface conductivity exist but are not established as Archie's law. These formulations describe the surface conductivity in terms of (a) the volume normalized surface area or the cation exchange capacity and (b) factors such as the surface charge density and surface charge mobility (Waxman and Smits, 1968; Rink and Schopper, 1974; Vinegar and Waxman, 1984). Complex conductivity measurements can determine the imaginary part. Assuming a fixed ratio l between the imaginary part and real part of interface conductivity. Börner et al. (1996) report a variation of l between 0.01 and 0.15, and the true resistivity factor can be easily approximated using the following formula:

$$F = \frac{\sigma_w}{\sigma_0 - \sigma_i'/l} \quad \text{..... (32)}$$

In this study, the resistivity amplitudes at a frequency of 1.0 Hz have been used. The measurements were performed under ambient conditions at a constant temperature of about 20 °C. The samples were fully saturated with a sodium chloride solution of 0.526 g/l resulting in a water conductivity of 0.1 S/m. Surface conductivity (σ'_{surf}), and imaginary part of conductivity cross plot for all samples for σ_w 100 mS/m. The data are explained by a single linear relationship with the gradient l = 0.032 for Bahariya Formation and gradient l = 0.038 For Abu Roash Formation. The equivalent relationship between surface conductivity (σ'_{surf}) and normalized chargeability m_n linear relation is again observed. The gradient is equal to l_{mn} = 0.22 for Bahariya Formation and gradient l = 0.23 For Abu Roash Formation. The higher value for the gradient in normalized chargeability is expected as m_n represents the total additive polarization across the measured frequency range.

Knowing the value of l provides opportunities to improve the petrophysical interpretation of electrical measurements. The inherent ambiguity of resistivity measurements results from the dependence of the measurement on the pore fluids' properties, interconnected pore volumes, and interconnected posurfacesace. It is common practice to estimate F from measurements of σ' and σ_w at a single salinity under the assumption that the fluid's salinity is sufficiently high such that $\sigma_{surf.}$ is negligible. Given an IP measurement, assuming l is known. According to Börner et al. (1996), a predicted value of the form factor can be determined. Figure 17 shows the result obtained using equation 33 and assuming a single value of l = 0.032 for Bahariya Formation and l = 0.038 for Abu Roash Formation. Estimated data result and relationship between surface conductivity (σ'_{surf}) and an imaginary part of conductivity cross plot. It should be noted that the variation of the formation resistivity factor calculated from the Börner formula is slightly lower than in the measured formation resistivity factor.

5.2 Model of Wyllie equation

The porosity can be derived from the knowledge of the interval velocity. The average time equation of (Wyllie et al., 1956 and 1958) has been used to obtain porosity from acoustic velocity logs. This simple equation appears adequate for clean sandstone in the middle range of porosity (10% < Φ < 25%). The equations 11 and 12 for p-wave velocity in water-saturated rock. Using equation (12) to determine the acoustic porosities of the sandstone samples. The velocity of quartz = 6040 m/s is used as the velocity of the solid material VM. For the fully saturated samples, the pore space is filled with tap water, and the fluid velocity is assumed to be equal to the velocity of freshwater Vf = 1500 m/s. The comparison between the measured porosity and the acoustic porosity calculated from the Wyllie equation is shown in Figure 18. It should be noted that the variation of the acoustic porosity is larger than in the measured porosity. A strong overestimation of the acoustic porosity is observed for all samples.

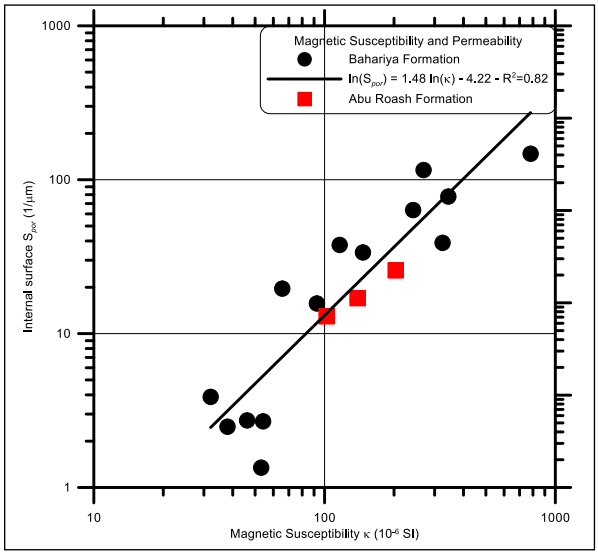

Figure 15. Magnetic susceptibility versus specific internal surface S_{por} for the studied samples.

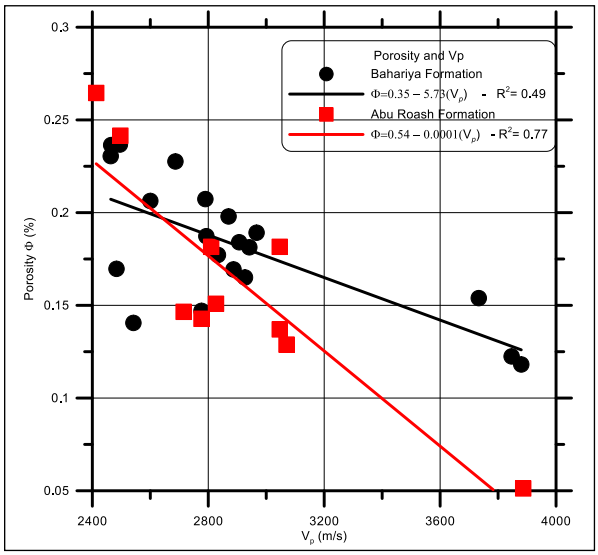

Figure 16. P-wave velocity versus porosity for the studied samples.

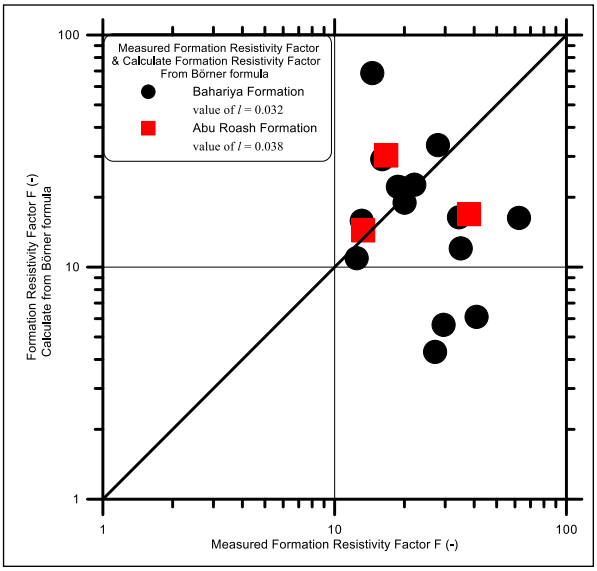

Figure 17. Measured formation resistivity factor versus calculate formation resistivity factor from Börner formula.

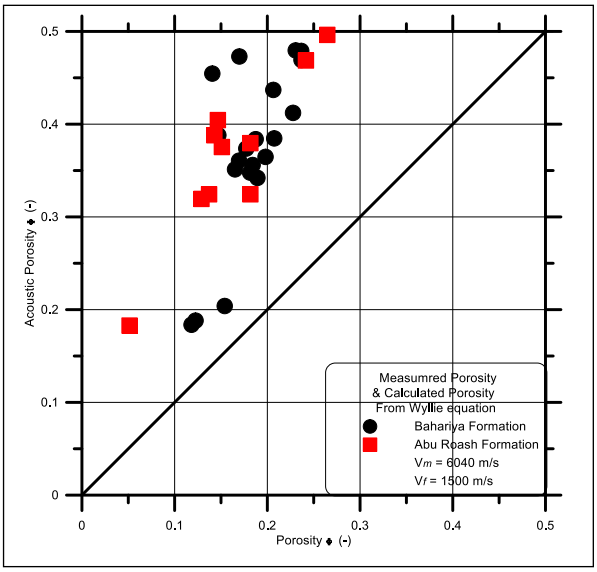

Figure 18. Measured porosity versus calculate porosity from Wyllie equation.

6. Conclusions

The Bahariya and Abu Roash formations represent an important Cretaceous oil and gas reservoir in Egypt. The samples of this study originate from the Abu Sennan concession in the South West Sennan oil field is in the Western Desert of Egypt. The mineralogical composition for studied sandstone samples belonging to the Bahariya and Abu Rawash formations is mainly composed of detrital quartz and quartz overgrowth, kaolinite, plagioclase microcline, iron oxide, and pyrite. Muscovite, biotite, zircon, rutile, and apatite, as well as diagenetic calcite, are present as accessory minerals. The sedimentary structures show characteristic features of deposition in a relatively low-energy, sub- to the intertidal zone. Most of the samples conspicuous flaser bedding develop on tidal flats during the turn from flood to the ebb tide when transport energy reaches its lowest level so that fine material like clay and silt sinks and gets deposited between sand ripples, as demonstrated.

Most samples belonging to the Bahariya Formation were laminated and showed a strong influence on most petrophysical parameters. It causes a higher internal surface (S_{por}), higher electrical resistivity, higher magnetic susceptibility, increased p-wave velocity, a small reduction in porosity, and reduced rock permeability. The wide variation in grain density has been identified as the increase in grain density that is caused by iron oxide cement.

The correlations of different parameters with permeability are of great interest for reservoir evaluation. The porosity – permeability relation shows the general trend of increasing permeability with increasing porosity. The large scatter in the relevant cross plot, especially for Abu Roash Formation, shows that a permeability prediction from porosity only is not significant. The correlations of magnetic susceptibility are great with grain density and specific internal surface S_{por} for all samples due to iron oxide filling the sample pore spaces.

The Susceptibility - Permeability cross plot for samples of both Bahariya and Abu Roash Formation shows increasing permeability with a decrease in magnetic susceptibility. The Porosity - Formation resistivity factor shows a good possibility to calculate the formation factor from porosity data. The well-known Archie's law between formation resistivity factor and porosity is confirmed by our data set and the resulting constant factor a = 3.96 and cementation factors m = 2.05 for the Bahariya Formation and resulting in constant factor a = 3.75 and cementation factors m = 1.83 for Abu Roash Formation from general Archie equation.

The determination of the form factor from the Börner equation has been determined. The interface conductivity has been determined from the imaginary part of conductivity. The relationship between the imaginary conductivity and the surface conductivity has been experimentally derived from the linear relationship $\sigma'' = l \times \sigma'_{surf.}$ Resulting l = 0.032 for samples of the Bahariya Formation and gradient l = 0.038 for the Abu Roash Formation. a similar relationship was found when the normalized chargeability determined the dependence of the IP response was used in place of the single-frequency imaginary conductivity. The determination of the form factor from the Börner equation is slightly lower than that of the resistivity ratio.

P-wave velocity decreases in general with increasing porosity in all studied samples. It was shown that the application of the Wyllie model equation fails to provide a reliable prediction of porosity for fluid-saturated samples from the compressional wave velocity data.

Acknowledgement

My appreciation is to the Egyptian Petroleum Authority to give us permission to work with the needed subsurface core sample data and publish the results. The authors would like to thank the Institute for Geophysics, Clausthal University of Technology, Germany, the Egyptian petroleum research institute, and Ain Shams University for supporting this study's findings.

References

Abuseda, H., Weller, A., Sattler, C.-D., Debschütz, W., (2016). Petrographical and petrophysical investigations of upper Cretaceous sandstones of the South West Sennan field, Western Desert, Egypt. Arabian Journal of Geosciences 9, 212.

Alsuwaidi, M., Mohamed, A. A., Mansurbeg, H., Morad, S., Alsuwaidi, A., Al-Shalabi, E. W., Gomes, J., Al-Ramadan, K., Mohammed, I.Q., Farouk, S., (2021). Depositional and diagenetic controls on reservoir quality of microporous basinal lime mudstones (Aptian), United Arab Emirates. Sedimentary Geology, 420, 105925.

Adler, P., Jacquin, C.G., Quiblier, J., (1990). Flow in simulated porous media. International Journal of Multiphase Flow 16, 691-712.

Athmer W. (2006). Petrologische und petrophysikalische Charakterisierung der stark anisotropen Bahariya Formation (Ägypten). - In: Müller R (ed.): Geoforschung 2006 - Beiträge aus Geologie, Paläontologie und Geophysik. – Clausthaler Geowissenschaften 5:19–33.

Archie, G.E., (1942). The electrical resistivity log is an aid in determining some reservoir characteristics. Trans AIME, Vol. 146, 45-62.

Börner, F., Schopper, J., Weller, A., (1996). Evaluation of transport and storage properties in the soil and groundwater zone from induced polarization measurements1. Geophysical prospecting 44, 583-601.

Carman, P.C., (1937). Fluid flow through granular beds. Trans. Inst. Chem. Eng. 15, 150-166.

Catuneanu, O., Khalifa, M.A., Wanas, H., (2006). Sequence stratigraphy of the lower Cenomanian bahariya formation, bahariya oasis, western desert, Egypt. Sedimentary Geology 190, 121-137.

Dominik, W., (1985). Stratigraphie und Sedimentologie (Geochemie, Schwermineralanalyse) der Oberkreide von Bahariya und ihre Korrelation zum Dakhla-Becken (Western Desert, Ägypten).

El Gezeery, M., Mohsen, S., Farid, M., (1972). Sedimentary basins of Egypt and their petroleum prospects. Proc 8th Arab Petrol Congr Algiers, 1-15.

El Sayed, A.M.A., (1981). Geological and petrophysical studies for the Algyo-2 reservoir evaluation, Algyo oil and gas field, Hungary. Ph. D. thesis, Hung. Acad. Sci., Budapest, 166.

Farouk, S., Al-Zubi, H., Abdelkader, T., Ahmad, F, (2018). Facies associations and chemostratigraphy of the Lower Cretaceous Kurnub Group and their boundaries, King Talal Dam section, northwestern Jordan. Environmental Geosciences, v. 25, no. 1, pp. 1–23.

Franks, GD., (1982). Stratigraphical modeling of Upper Cretaceous sediments of Bahariya Oasis. 6th EGPC Exp. Seminar, Cairo, 21 p.

Glover, P., (2009). What is the cementation exponent? A new interpretation. The Leading Edge 28, 82-85.

Halisch M, Weller A, Sattler C-D, Debschütz W, El-Sayed A.M.A., (2009). A complex core-log case study of an anisotropic sandstone, originating from Bahariya Formation, Abu Gharadig Basin, Egypt. Petrophysics 50:478–497

Herron, M., M., (1987). Estimating of intrinsic permeability of elastic sediments from geochemical data Trans., SPWLA. P. 6

Klinkenberg, L., (1941). The permeability of porous media to liquids and gases, Drilling and production practice, OnePetro.

Rink, M., and Schopper, J., (1974). Interface conductivity and its implications to electric logging, SPWLA 15th Annual Logging Symposium, Society of Petrophysicists and Well-Log Analysts.

Selim, S.S., Wafdy, R., Abu Khadrah, A.M., (2021). Sedimentological analysis and reservoir quality of the early Cenomanian transgressive sandstones, northern Western Desert, Egypt. Journal of Petroleum Science and Engineering, 197, 107948.

Scheidegger, A., (1974). The physics of flow through porous media. The University of Toronto, Toronto Press, 353p.

Schön, J.H., (1996). Handbook of Geophysical Exploration: Fundamentals and Principles of Petrophysics. Seismic Exploration. Physical Properties of Rocks. Pergamon.

Soliman, S., and Hassan, M., (1970). Petrology of the Middle Miocene rocks of Gebel El Rusas, Ranga and Abu Anz localities, Eastern Desert, Egypt. 7th Arab Petrol. Congr., Kuwait 60, 1-40.

Tiab, D., and Donaldson, E.C., (2015). Petrophysics: theory and practice of measuring reservoir rock and fluid transport properties. Gulf professional publishing.

Timur, A., (1968). An investigation of permeability, porosity, and residual water saturation relationships, SPWLA 9th annual logging symposium, Society of Petrophysicists and Well-Log Analysts.

Vinegar, H., and Waxman, M., (1984). Induced polarization of shaly sands: Geophysics, 49, 1267 – 1287, DOI: 10.1190/1.1441755.

Waxman, M. H., and Smits, L. J. M. (1968). Electrical conductivities in oil-bearing shaly sands: SPE Journal, 243, 107 – 122, DOI: 10.2118/1863-A.

Wyllie, M., and Gregory, A., (1953). Formation factors of unconsolidated porous media: Influence of particle shape and effect of cementation. Journal of petroleum technology 5, 103-110.

Wyllie, M., Gregory, A., Gardner, G., (1958). An experimental investigation of factors affecting elastic wave velocities in porous media. Geophysics 23, 459-493.

Wyllie, M., and Spangler, M., (1952). Application of electrical resistivity measurements to the problem of fluid flow in porous media. AAPG Bulletin 36, 359-403.

Wyllie, M.R.J., Gregory, A.R., Gardner, L.W., (1956). Elastic wave velocities in heterogeneous and porous media. Geophysics 21, 41-70.

JJEES

JJEES (2022) 13 (1): 48-53
ISSN 1995-6681

Jordan Journal of Earth and Environmental Sciences

Physicochemical Composition and Heavy Metals Tolerance of Bacterial Isolates in Leachate from Solid Waste Dumpsites in Delta North Senatorial District, Delta State

[1, 2*]Enerijiofi, K. E., [1]Okuguni, N. N. and [1]Ajayi, A. V.

[1]*Department of Biological Sciences, College of Basic and Applied Sciences, Samuel Adegboyega University, P.M.B. 001, Ogwa, Edo State, Nigeria.*
[2]*Applied Environmental Bioscience and Public Health Research Group, Department of Microbiology, University of Benin, Nigeria*

Received 12 May, 2021; Accepted 9 August 2021

Abstract

Leachates from solid waste dumpsites are a source of environmental contaminants which negatively affect the ecosystem and subsequently human health. The continuous bio magnification of heavy metals in the environment has remained as source of worry to public health experts. The aim of this study was to assess the physicochemical and heavy metals concentrations as well as heavy metals tolerance profile of bacteria isolated from leachate collected some towns; Isele-Uku (6^0 25' 0'N and 6^0 42' 0'E), Umunede (6^0 16' 0'N and 6^0 18' 0'E) and Agbor (6^0 7' 20'N and 6^0 5' 20'E) in Delta State, Nigeria. Standard laboratory procedures were used to analyse the samples. The mean concentrations of the physicochemical results ranged from 1060.00±3.15 to 2070.00±4.11µS/cm, 29.50±1.11 to 62.40±0.40mg/l, 78.9078.90±1.12 to 120.5078.90±0.22mg/l, 18.69±0.01 to 31.26±0.23mg/l, 0.05±0.11 to 0.90±0.01mg/l and 21.60 ± 0.49 to 32.80 ± 0.12 electrical conductivity, biological oxygen demand, chemical oxygen demand, Iron, Lead, nitrate respectively. Overall, Umunede had the highest bacterial load of 95%. Also, samples from Umunede had the most prevalent isolate, *Corynebacterium* sp. (26.87%) followed by *Pseudomonas aeruginosa* (25.76%) and least in *Bacillus cereus* (5.97%) at Isielu – uku. *Pseudomonas aeruginosa* displayed the highest resistance (70.59%) against chromium, *Bacillus subtilis* had the highest (83.33%) against cobalt. *Arthrobact*er sp. had the highest of 75.00% against lead and mercury. *Corynebacterium* sp. had the highest of 86.67% against and lead, *Alcaligenes* sp. displayed the highest resistance 81.82% against cobalt while *Acinetobacter* sp. had the highest (66.67%) against lead and mercury. The leachate contained electrical conductivity, chemical oxygen demand, biological oxygen demand, nitrate and iron and lead at concentrations beyond the acceptable limit for effluent discharge which makes it unfit for discharge without prior treatment.

Keywords: Heavy Metals, Leachate, Permissible Limit, *Pseudomonas Aeruginosa*, Public Health

1. Introduction

Leachates are solutions that results from leaching of soluble constituents in landfills which among other issues; disrupt environmental quality and by downward movement percolate into surrounding ground water (Enerijiofi and Ajuzie 2012; Bhalla et al., 2012;). Despite much stricter statutory controls, leachates from modern sites are known to contain range of contaminants; pathogenic microorganisms, antibiotics, heavy metals and lots more (Enerijiofi and Ekhaise, 2019a). These contaminants particularly heavy metals highly affect microorganisms in soil leading to alteration in diversity, population size and activity of the soil microbial community (Mgbemena et al., 2012). When plants grown on heavy metals laden soils, are consumed by man either as food for energy or medicine for treatment, the heavy metals gets into man's system which causes serious lethal effects including health and reproductive challenges (Oluseyi et al., 2014; Enerijiofi, 2021). In animals, induced micronuclei in mouse bone marrow cells in vivo by municipal landfill leachate was used to describe the biotoxicity of leachate, with the mouse been damaged when fed with leachate at low concentration of 5mg/L COD.

Biological and physicochemical techniques remain the most common methods of treating leachates because they possess the different removal potentials for varieties of pollutants. These discharged effluents must satisfy the discharge criteria (Bhalla et al., 2012). However, the characteristics of leachate depends on several factors such as waste composition and the age of waste, degree of decomposition, moisture content of waste, rate of water movement as well as temperature (Aluko et al., 2002, Fatubarin and Olojugba, 2014). The natural attenuation of assessing environmental risks of leachates that flow into the underground water determines the suitable corrective methods as well as monitoring regular mitigations (Yusof et al., 2009; Jelic et al., 2011).

Groundwater is a major source of potable water within the vicinity of this study area as well as Nigeria in general and its contamination leads to series of public health issues. The aim of this study was to assess the physicochemical composition and heavy metals tolerance of the isolated bacteria species from of leachate located within solid waste dumpsites in Delta North Senatorial District of Delta State, Nigeria.

* Corresponding author e-mail: kingsmore1luv@gmail.com

2 Materials and Method

2.1 characteristics of study area and collection of samples

The study area is along Agbor - Asaba Express way, a very busy road with different communities. It leads to the entire South East Geopolitical zones of Nigeria. The surface debris were removed and 200mls of leachate samples were aseptically collected from dumpsites located at Isele-Uku (6^0 25ˈ 0ˈˈ N and 6^0 42ˈ 0ˈˈ E), Umunede (6^0 16ˈ 0ˈˈ N and 6^0 18ˈ 0ˈˈE) and Agbor (6^0 7ˈ 20ˈˈ N and 6^0 5ˈ 20ˈˈ E) into sterile screw capped bottles. The samples were immediately transported to the microbiology laboratory for analyses.

2.2 Determination of physicochemical parameters

The method of APHA, (2011) was used to determine the physicochemical parameters which included pH, temperature, electrical conductivity, chloride, total dissolved solids, total soluble solid, chemical oxygen demand, biological oxygen demand, dissolved oxygen, turbidity, sulphate, nitrate and phosphate. The cations (sodium, potassium, calcium and magnesium) were determined with a flame photometer, model Jenway model PFP7 while the heavy metals (iron, copper, zinc, Aluminium, Manganese, Lead, Nickel and Cobalt) concentrations were analysed with the aid of atomic absorption spectrophotometer, model PG 550 (Enerijiofi et al., 2017a).

2.3 Inoculation and enumeration

The method of Holt et al. (1994) was used for isolation and enumeration of bacterial isolates. One mililitre of the leachate sample was homogenized in ten mililitres of distilled water to form the stock, followed by serial dilution of the leachate samples in ten -fold. Thereafter, 0.1ml aliquots from the third, sixth and ninth dilutions were pour - plated with freshly prepared nutrient agar plates in triplicate containing fushin, which prevents fungal growth The nutrient agar plates were incubated at 37°C for 48h and were observed for growth. The discrete colonies of bacteria were counted, calculated and expressed as colony-forming units per millilitre (CFU/ml)

2.4 Isolation, identification and characterization

The colonies were sub-cultured into Nutrient agar plates that were freshly prepared to obtain a pure colony. Isolation and Characterization of pure cultures of the various isolates were made and stored in the refrigerator at 4°C. They were identified by culturally and morphologically (Cheesbrough, 2005). The sub - cultured bacterial isolates were subjected to an array of relevant physiological and biochemical tests which included; catalase production, oxidase production, spore staining, sugar fermentation tests, Gram staining. The results were put together and the bacterial isolates were identified by comparison with the protocol of (Holt et al., 1994 and Cullimore, 2000).

2.5 Preparation of selected heavy metals solution

The stock solutions of the tested heavy metals were prepared separately by dissolving 500mg the respective metal salts; $HgCl_2$, $CdCl_2$, $CoCl_2$, $Pb(NO_3)_2$ and CrO_3 in 100ml of de ionized water which was followed by filtration. The mixture was thereafter filtered using 0.22µm membrane filters (Nucleopore Corp., Pleasanton, CA, USA). This was stored in sterilized flasks at 4°C in dark room for 24hrs before use for further studies (Enerijiofi and Ajuzie, 2012).

2.6 Heavy metals tolerance testing

Heavy metals resistance testing was carried out according to the method of (Mgbemena et al., 2012). Muller hinton agar was prepared with varying concentrations 0.00mg/ml, 0.50mg/ml, 1.00mg/ml, 1.50mg/ml, 2.00mg/ml, 2.50mg/ml, 3.00mg/ml, 3.50mg/ml, 4.00mg/ml, 4.50mg/ml and 5.00mg/ml respectively for the different heavy metals compounds of $HgCl_2$, $CdCl_2$, $CoCl_2$, $Pb(NO_3)_2$ and CrO_3. Zero point one mililitre of pure bacterial isolate was poured on the surface of heavy metal incorporated medium and spread evenly on the surface of the medium to allow for even distribution of the isolates. The medium without heavy metal served as control. The cultured plates were incubated at 37°C for 24hrs and thereafter observed for bacteria growth.

2.7 Statistical analysis of data

The means and standard errors were computed using conventional statistical method. The statistical package for social sciences (SPSS version 20) was used to generate analysis of variance (ANOVA), thereafter, Duncan's multiple range test was used to compare the means (Ogbeibu, 2005).

3 Results

The results of the concentrations of the physicochemical parameters of leachate samples are presented in Table 1.

Figure 1 records the frequency of occurrence of bacterial isolates. Overall, Umunede had the highest bacterial load of 95%. Also, samples from Umunede had the most prevalent isolate, *Corynebacterium* sp. (26.87%) followed by *Pseudomonas aeruginosa* (25.76%) and least with *Bacillus cereus* (5.97%) at Isielu – uku. In the overall, Umunede had the highest of 95% while Agbor had the least, 66%.Table 2 records the percentage of heavy metals tolerance in bacterial isolates. *Pseudomonas aeruginosa* displayed the highest resistance (70.59%) against chromium, *Bacillus subtilis* had the highest (83.33%) against cobalt. *Arthrobacter* sp. had the highest of 75.00% against lead and mercury. *Corynebacterium* sp. had the highest of 86.67% against lead, *Alcaligenes* sp. displayed the highest resistance (81.82%) against cobalt while *Acinetobacter* sp. had the highest (66.67%) against lead and mercury.

Table 1. physicochemical characteristics of leachates

PARAMETERS	A	B	C	FEPA (1991) limit
pH	7.80±0.21[a]	6.90±0.01[a]	7.10±2.01[a]	6 – 9
Temp. (0°C)	29.60±0.01[a]	29.50±0.20[a]	29.60±1.03[a]	30
EC (us/cm)	1060.00±3.15[a]	1780.00±3.01[a]	2070.00±4.11[b]	1000
Cl^-(mg/l)	142.00±0.46[a]	319.50±0.42[c]	284.00±0.23[b]	600
TSS (mg/l)	6.00±0.27[a]	4.00±0.21[a]	4.00±0.16[a]	30
TDS (mg/l)	51.00±0.31[a]	92.00±0.18[a]	1030.00±1.34[b]	2000
Turbidity (NTU)	740.00±2.45[b]	480.00±2.13[a]	420.00±1.99[a]	300
COD (mg/l)	120.50±0.22[b]	86.20±0.34[a]	78.90±1.12[a]	40
DO (mg/l)	4.00±0.18[a]	6.00±0.51[a]	5.00±1.01[a]	40
BOD (mg/l)	62.40±0.40[b]	30.80±0.11[a]	29.50±1.11[a]	10
Sulphate (mg/l)	5.24±1.11[a]	8.41±0.14[a]	6.20±0.23[a]	50
Nitrate (mg/l)	32.80±0.12[b]	24.00±0.19[a]	21.60±0.49[a]	1
Phosphate (mg/l)	13.51±0.44[a]	13.80±0.31[a]	12.42±0.02[a]	5
Calcium (mg/l)	42.40±0.23[a]	40.20±0.19[a]	38.80±0.61[a]	100
Potassium (mg/l)	16.80±0.12[a]	18.20±0.42[a]	16.40±0.42[a]	N/A
Magnesium (mg/l)	26.40±0.11[a]	25.80±0.16[a]	26.00±0.17[a]	100
Sodium (mg/l)	14.60±0.42[a]	12.80±0.27[a]	12.10±1.16[a]	200
Fe^{2+} (mg/l)	2.61±0.23[b]	1.69±0.22[a]	1.04±0.01[a]	20
Cu^{2+} (mg/l)	0.05±0.01[a]	0.06±0.14[a]	0.03±0.01[a]	1.5
Zn^{2+} (mg/l)	0.48±0.10[a]	0.61±0.11[a]	0.50±0.01[a]	1
Al^{3+} (mg/l)	0.68±0.10[a]	0.74±1.17[a]	0.72±0.12[a]	N/A
Mn^{2+} (mg/l)	0.35±0.10[a]	0.41±0.10[a]	0.48±0.01[a]	N/A
Pb^{2+} (mg/l)	0.90±0.11[b]	0.02±0.01[a]	0.03±0.01[b]	0.5
Ni^{2+} (mg/l)	0.09±0.32[a]	0.03±0.01[a]	0.05±0.01[a]	1
Co^{2+} (mg/l)	0.01±0.01[a]	0.01±0.01[a]	0.02±0.01[a]	0.5

Values represent the Means± Standard Deviation of twelve samples collected over a period of six months
Legend: Legend: A: Agbor (6^0 7ˡ 20ˡˡN and 6^0 5ˡ 20ˡˡE), **B: Umunede** (6^0 16ˡ 0ˡˡN and 6^0 18ˡ 0ˡˡE)**, C: Isielu –Uku** (6^0 25ˡ 0ˡˡN and 6^0 42ˡ 0ˡˡE)**, NI= Not indicated, TDS= total dissolved solid, TSS= total soluble solid, EC= electrical conductivity, COD= chemical oxygen demand, DO= dissolved oxygen, BOD= biological oxygen demand Fe = Iron, Cu = Copper, Zn = Zinc, Al = Aluminum, Mn = Manganese, Pb = Lead Ni = Nickel, Co = Cobalt, N/A= not available**

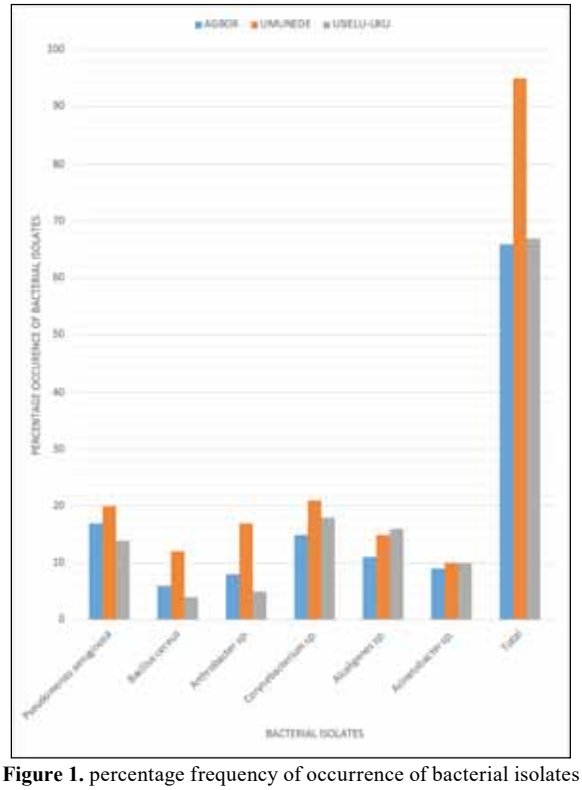

Figure 1. percentage frequency of occurrence of bacterial isolates

Table 2. percentage of heavy metals tolerance in bacterial isolates

Bacterial isolates	No. examined	Tolerance to Pb	Tolerance to Cd	Tolerance to Hg	Tolerance to Co	Tolerance to Cr
Pseudomonas aeruginosa	17	10 (58.82)	11 (64.71)	9 (52.94)	11 (64.71)	12 (70.59)
Bacillus subtilis	6	4 (66.67)	4 (66.67)	3 (50.00)	5 (83.33)	4 (66.67)
Athrobacter sp.	8	6 (75.00)	5 (62.50)	6 (75.00)	5 (62.50)	5 (62.50)
Corynebacterium sp.	15	13 (86.67)	10 (66.67)	12 (80.00)	9 (60.00)	11 (73.33)
Alcaligenes sp.	11	8 (72.72)	8 (72.72)	7 (63.64)	9 (81.82)	5 (45.45)
Acinetobacter sp.	9	6 (66.67)	5 (55.56)	6 (66.67)	5 (55.56)	5 (55.56)
Total	67					

4 Discussion

Leachates are liquid substances arising from municipal wastes. They are known to contain lots of biological and chemical contaminants which are hazardous to man and the environment. This study investigated the physicochemical composition and heavy metals tolerance of bacterial isolates in leachate from Delta State, Nigeria. The pH and temperature range reported support most biological functions in bacterial cells which are important in the natural treatment of leachate thereby reducing environmental contamination. The moderate acidic pH values obtained in the sites under study could be attributed to the removal of basic cations or nutrients from the surface of the soils in the dumpsites as a result of the effect of anthropogenic activities such as burning which resulted in the loss of nutrients. The results point to the obvious that certain reactions could be hastened by release of leachates and also, reduction in the oxygen solubility and intense odour due to anaerobic reaction. The turbidity values were higher than standard for discharge of waste water into stream (WHO, 2006; Oluseyi et al., 2014). This high value could have resulted from solubilisation of the organic component of the municipal solid waste. The electrical conductivity values reported indicates that the leachate samples have high concentration of soluble salts which is a good indicator of plant growth. There were significant difference in the electrical conductivity concentrations across the sites. The dissolved oxygen concentrations of the samples was within the stipulated limit FEPA (1991), which means that there was pollution by organic matter. Also, the high concentration of chemical oxygen demand and biological oxygen demand recorded showed high presence of organic contaminants which were actively decomposing due to their dissolved oxygen concentration and solubility in water. It is worthy to note that the result of this study showed that the chemical oxygen demand and biological oxygen demand were inversely proportional to dissolved oxygen which corroborated with earlier reports of Aluko et al. (2002) and Anyakora et al. (2011) from wastes dumpsites in Lagos. There were significant differences in the chemical oxygen demand and the biological oxygen demand across the sites. Nitrate recorded was above the limit. The high concentration could be responsible for the high number of bacterial diversity recorded. The presence of nitrate in the soil may be attributed to the mineralization of nitrogen as a result of organic matter in the soil. The phosphate concentration could be attributed to the presence of a high amount of organic matter and plant decomposition at the dumpsites (Ideriah et al., 2006). The high presence of lead could have been from incomplete combustion of hydrocarbons from automobiles and generating sets. It could also be due to the depositions of wastes from automobile mechanic workshops in these dumpsites. However, Michaela et al. (2018) reported that lead poisoning could lead to kidney failure, loss of appetite and brain damage as a result of prolong exposure. There were significant differences in iron and lead concentrations across the sites. Also, when plants are grown to maturity on such contaminated soils, there are possibilities that the heavy metals could get to man when they are taken in as drug or food (Momodu and Anyakora, 2010).

The leachate samples had highly bacterial load than the control indicating contamination. This may be attributed to high quantity of organic matter present in leachate samples which favoured bacterial growth compared to the control. The bacteria reported in this study were similar to ones previously identified *Citrobacter* sp. (4.35%), *Bacillus* sp. (26.08%), *Enterobacter* sp. (4.35%) *E. coli* sp. (4.35%), *Klebsiella* sp. (4.35%), *Neisseria* sp. (4.35%), *Pseudomonas* sp. (4.35%), *Shigella* sp. (4.35%), *Staphylococcus* sp. (13.04%), *Streptococcus* sp. (26.08%), and *Vibrio* sp. (4.35%) (Obire et al. 2002; Michaela et al. 2018). The indiscriminate release of leachate from these municipal waste dumpsites could pose public health risks to the citizens whose food and water supplies may, perhaps, become contaminated as a result of leakage from dumpsites during rains (Eghomwanre et al. 2020). The bacteria identified could cause lots of diseases such as gastro-intestinal infections, shock, dysentery, typhoid fever and diarrhoea. *Citrobacter*, *Klebsiella*, *Enterobacter* and *Escherichia* are members of the coliforms group. They are gram negative rods that inhabit the human intestinal tract, with its main reserviour being the sewage system (Enerijiofi and Ajuzie, 2012). *Pseudomonas aeruginosa* is considered an opportunistic pathogen that can cause wound infections leading to sepsis and mortality from chronic septicaemia. The high organic matter recorded in leachate may have accounted for their high numbers in the samples studied. Other isolates; *Bacillus Arthrobacter*, *Alcaligenes, Corynebacterium* and *Acinetobacter* species have been described as human opportunistic pathogens which could lead to food poisoning upon ingesting contaminated food or water (Eja et al., 2010). All the bacterial and fungi isolates identified from leachate samples have been reported to be associated with wastes and waste biodegradation (Obire *et al*., 2002).

The heavy metals resistance was generally high for all metals especially lead and cobalt which were above 80%. This high values points to the obvious that the rate of discharge of heavy metals into the environment is on the increase which

could lead to public health epidemic. The finding in this study in agreed with earlier reports Jelic et al. (2011) in Nigeria and Abdelately et al. (2011) in Egypt where they recorded a corresponding high bacterial resistance rate in effluent samples. These heavy metals have been reported to prevent ossification of bones in man by taking the place of Calcium in bones. They have also been implicated in reproductive disorders like inhibition of libido as well as prevent ovulation in males and females respectively (Enerijiofi and Ekhaise, 2019a). The implication is that resistance to heavy metals is a worldwide issue and worst off in developing countries where regulations are lacking and open disposal is fast becoming a culture.

5 Conclusion

This study revealed a significant difference in the concentrations recorded for electrical conductivity, chemical oxygen demand, biological oxygen demand, nitrate, iron and lead. The aforementioned physicochemical parameters were also beyond the acceptable limit and do not meet the standard for effluent discharge. The high microbial load reported could be linked to the increased nitrate and phosphate in the examined leachate. Also, the high heavy metals resistance recoded is worrisome. Education as well as the construction of well - lined landfills can reduce the level of contamination by leachate. However, the heavy metals resistance isolates could be used in remediating the soil of its heavy metals content.

Acknowledgement

The authors are grateful to the Department of Biological Sciences, College of Basic and Applied Sciences, Samuel Adegboyega University, Ogwa, Edo State, Nigeria for providing a conducive environment for this research.

Authors' contributions

The first author conceived the research idea, designed the experiment and prepared the manuscript. The second and third authors did the literature search, generated results from the laboratory and performed data analysis. All authors did sampling, read and accepted the final version of the manuscript.

Competing interests

No competing interests exist between the authors weather financial or otherwise.

References

Abdelately, L. M., Khalil, W. K. B., Ali, T. H., Mahrous, K. F. (2011). Heavy metal resistance and gene expression analysis of metal resistance genes in gram positive and gram negative bacteria present in Egyptian soil. Journal of Applied Sciences in Environmental Sanitation 6 (2): 201 -211

Aluko, O.O., Sridhar, M. K. C., Oluwande, P. A. (2002). Characterization of leachates from municipal solid waste landfill site in Ibadan Nigeria. Journal of Environmental Health Research 2(1) 32-37.

Anyakora, C., Nwaeze, K., Awodele, O., Nwadike, C., Arbabi, M., Coker, H. (2011). Concentrations of heavy metals in some pharmaceutical effluents in Lagos, Nigeria. Journal of Environmental Chemistry and Ecotoxicology3 (2): 25 – 31

Association of Official Analytical Chemists (2005). Method of Analysis, Washington D.C. 225pp. Bhalla, B., Saini, M. S. and Jha, M. K. (2012). Characterization of leachate from municipal solid waste landfilling sites of Ludhiana, India: A comparative study Concurrent Engineering Research and Applications 2 (6): 732 - 745

Cheesbrough, M. (2005). District Laboratory Practice in Tropical Countries Cambridge University Press, United Kingdom. P.30 - 41.

Cullimore, D.R. (2000). Practical Atlas for Bacterial Identification. CRC Press P. 209.

Eghomwanre, A.., Obayagbona, N. and Ilontumhan, C. (2020). A Microbiological and Physicochemical Assessment of Top Soils from Makeshift Open Waste Dumpsites in the Premises of some Schools in Benin City. Jordan Journal of Earth and Environmental Sciences 11 (1): 71-76

Eja, M. E., Alobi, N. O., Ikpeme, E. M., Ogri, O. R. Inyang, A. O. (2010). Environmental and public health – related assessment of solid waste management in Uyo, Akwa Ibom State, Nigeria. World Journal of Applied Science and Technology 2: 110 - 123.

Enerijiofi, K. E. and Ajuzie, C. U. (2012). Health impact of some heavy metals resistance in microbes isolated from Ikhueniro refuse dumpsite, Benin City. Nigerian Journal of Microbiology 26: 2593 – 2599.

Enerijiofi, K. E., Ekhaise, F. O. and Ekomabasi, I. E. (2017a). Biodegradation Potentials of Cassava Mill Effluent (CME) by Indigenous Microorganisms. *Journal of Applied Sciences and Environmental Management* 21 (6): 1029 – 1034. https://dx.doi.org/10.4314/jasem.v21i6.5.

Enerijiofi K. E. and Ekhaise, F. O. (2019a).Physicochemical and Microbiological Qualities of Government Approved Solid Waste Dumpsites in Benin City. Dutse Journal of Pure and Applied Sciences 5 (2a): 12 - 22

Enerijiofi, K. E. (2021). Bioremediation of environmental contaminants: a sustainable alternative to environmental management, In: Bioremediation for Environmental Sustainability: toxicity, mechanisms of contaminants degradation, detoxification and challenges edited by Saxena, G., Kumar, V., Shah, M. P.Elsevier, USA. 2**:** 461 – 480.

Fatubarin, A. and Olojugba, M. R. (2014). Effect of rainfall season on the chemical properties of the soil of a southern Guinea savanna ecosystem in Nigeria. Journal of Ecology and the Natural Environment 6(4): 182-189.

FEPA (1991). Federal Environmental Protection Agency. National Guidelines and Standards for Industrial Effluents and Water Quality Tests. FEPA (Nigeria) Official Gazette, Nigeria.

Holt, J. G., Krieg, N. R., Sneath, P. H. A. (1989). Bergey's Manual of Determinative Bacteriology 4. London: Cambridge University Press P. 2493.

Ideriah, T. J. K., Omuaru, V. O. T. and Adiukwu, P. U. (2006). Soil quality around a solid waste dumpsite in Port Harcourt. African Journal of Ecology 44(3):388-394.

Jelic, A., Gros, M., Ginebreda, A., Cespedes-Sanchez, R., Ventura, F., Barcelo, D. (2011). Occurrence, partition and removal of pharmaceuticals in sewage water and sludge during Wastewater treatment. Water Research 45(3): 1165 -1176

Mgbemena, I. C., Nnokwe, J. C., Adjeroh, L. A., Onyemekara, N. N. (2012). Resistance of bacteria isolated from Otamiri River to heavy metals and some selected antibiotics. Current Research Journal of Biological Sciences 4(5): 551 – 556

Michaela, E., Odohb, A. O., Chukwurac, E., Bend, M. G. (2018). Heavy metal and microbial load properties of dumpsite leachates: case study of Onitsha dumpsite, South – East, Nigeria. Journal of Toxicological Analysis 1(1): 1-6

Momodu, M. and Anyakora, C. (2010). Heavy metal contamination of ground water: The Surulere case study. Research Journal of Environmental Earth Science 2(1): 39 -43

Obire, O., Nwallbeta, O., Adue, S. B. N. (2002). Microbial community of a waste-Dumpsite. Journal of Applied Sciences and Environmental Management 6(11):78 - 83.

Ogbeibu, A. E. (2005). Biostatistics: A Practical Approach to Research and Data Handling. Mindex Publishing Company

Limited, Benin City. 264pp.

Oluseyi, T., Adetunde, O., Amadi, E. (2014). Impact assessment of dumpsites on quality of near - by soil and underground water: a case study of an abandoned and a functional dumpsite in Lagos, Nigeria. International Journal of Science, Environment and Technology 3(3):1004 – 1015.

WHO, (2006). World Health Organisation guidelines for drinking water quality 3rd Edition. Vol 1.

Yusof, N., Haraguchi, A., Hassan, M. A., Othman, M. R., Wakisaka, M., Shirai, Y. (2009). Measuring organic carbon, nutrients and heavy metals in rivers receiving leachate from controlled and uncontrolled municipal solid waste (MSW) landfills. Waste Management 29: 2666–2680.

JJEES

JJEES (2022) 13 (1): 54-59
ISSN 1995-6681

Jordan Journal of Earth and Environmental Sciences

Water Audits of Academic Institutions in Water Stressed Countries; the Case of the Jordan University

Ola Al-Qawasmi[1] and Munjed Al Sharif[2]

[1]Department of Land, Water, and Environment, University of Jordan, Researcher at National Agricultural Research Center, Baqa'a-Jordan
[2]Civil and Environmental Engineering Department, German Jordanian University, Amman, Jordan

Received 26 June 2021; Accepted 14 August 2021

Abstract

Water use efficiency is considered as a step forward towards water auditing for assessing the financial, social, and environmental benefits. The diversity of activities and water end-use in the university can be considered as significant as in a small city where residential, commercial, and industrial uses are present. The end-use analysis is important for understanding the reduction in water demand due to retrofit fixtures to a more efficient one. A mixed-methods study used qualitative methods such as the questionnaire's distribution, and quantitative methods such as physical flow rate measurement for the sanitary fixtures and the laboratory equipment. Sanitary installation-plumbing supply fittings standard JS 1945:2011 was used as a benchmark. In addition to the feasibility study. Eighty percent of the volume of water consumption went to the schools and the administrative offices. The main internal use of water was the toilet with percent reached 64%. Adopting water use efficiency would reduce the water demand to 13.7%, and this would be reflected in money savings that would be 19911 ($/quarter). Retrofitting fixtures indoors on the university campus is not enough and should concern changing behaviors in the university community by incorporating water conservation in the academic curriculum.

Keywords: Water Audit, Water end-use Analysis, Water Flow Rate, Water-saving Devices, Water Scarcity, Water use Efficiency.

1. Introduction

The world is facing an increasing water deficit that is intensified by the impacts of climate change. This is especially true in arid and semi-arid regions. For that, many countries are adopting the concept of sustainability, water demand management, water use efficiency, and water audit or (Water End-use Analysis) towards managing and sustaining this precious source. The main source for water in Jordan is groundwater with about 59% of all sources (MWI, 2017). Groundwater depends mainly on annual rainfall, besides the type and distribution of the rainfall storms in the whole year, but rainfall fluctuates from year to year and even is suffering from declining trends due to climate change. The management of water resources in Jordan has serious challenges. The most viable short-term option available to the Government of Jordan is to manage its water demand. Decreasing the waste of water will decrease the depletion and pollution of water resources Velazquez et al., 2013). Water efficiency is considered one of the key futures available to water sector administrators to address water scarcity issues (El-Nwsany et al., 2019), also water audits can help by keeping a check on the losses and finding out ways to minimize them (Irene et al., 2019). In addition, social responsibility is a key component of sustainable development (El-Nwsany et al., 2019). The behavior patterns of water users will also need to be adjusted toward greater water conservation practices and more efficient water use. A water audit or water end-use analysis is necessary for managing water demand that can provide yield financial and environmental benefits. It presents the potential for water conservation and reducing the annual water demand by 30.85% through adopting and retrofitting water-saving devices in sanitary places (Oduro-Kwarteng et al., 2009). The water end-use analysis was defined that the ways customers use water daily by different sanitary fixtures with frequency use (Oduro-Kwarteng et al., 2009). Universities may be considered as small cities in terms of population, size, and daily activities that generate direct and indirect impacts on the environment (Alshuwaikhat and Abubakar, 2008). Besides, institutions of education in Jordan are among the large consumers of water representing about 14% of the commercial water consumption (MWI, 2012 a). This is since there are 32 public and private universities and academies housing about 350 thousand students, about 20 thousand administrative employees, and 11.5 thousand faculty members (MoHE, 2020). In general, water audit studies are very few, even though they are a very important tool to be a reference for managing water at any institution. This study aimed to characterize the water consumption pattern at the University of Jordan and evaluate to address the water deficit and high consumption and cost in the university.

2 Materials and Method

2.1 Study area

The University of Jordan is located in the residential and commercial districts of Amman, and its coordinates are (E: 35.869952 and N: 32.015621) as shown in Figure 1. Some of its facilities provide services to local communities and surrounding areas. The University of Jordan is characterized by a large number of utilities including research centers

* Corresponding author e-mail: ola7279@yahoo.com

and faculties. The Water, Energy, and Environment Center helped in achieving this study by providing the main information about the total area of all buildings in the University of Jordan campus around 120,000 m^2. In 2019, the number of employees and all students at the University of Jordan was 50 thousand people containing schools of science, arts, and humanities. The University of Jordan has three major research centers, a printing house, a sports club, a mosque, and many restaurants. The irrigated green area of the university is about 550,000 m^2. There are four female residences (two international residences that enjoy high standards in terms of facilities furniture and services, and two other standard residences), the number of workers and female students in those residences is around 964 people. The main source of water is from the municipality network. According to the billing data by the Amman water utility (Miyahuna company), the average quarterly (three months) consumption in 2018 was 47,427 m^3.

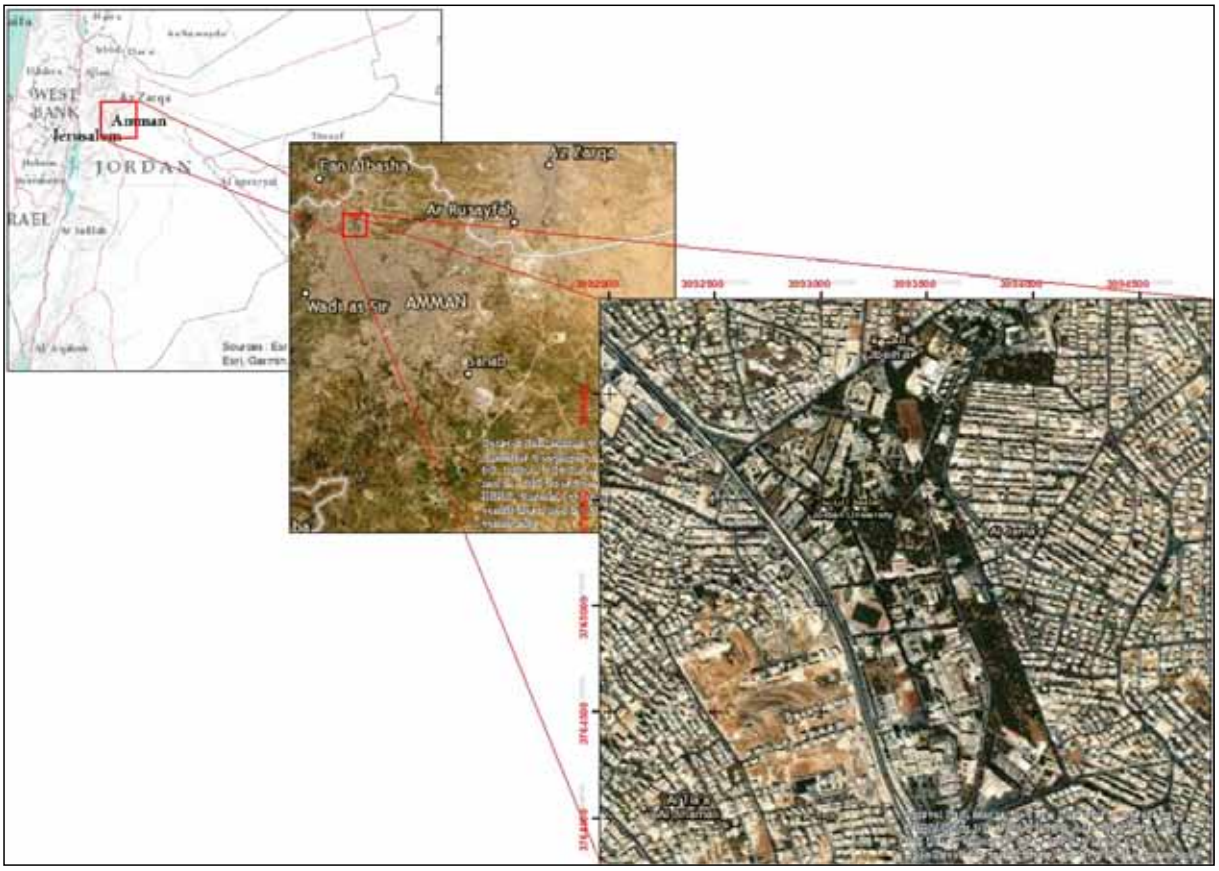

Figure 1. The University of Jordan Location

2.2 Methodology

The Water Audit for the University of Jordan was carried out between 3/31- 9/4/2019. A mixed-methods study used such as qualitative and quantitative tools. The qualitative study was included the distribution of questionnaires for female students in the residences, and interviews with employees. Two questionnaires were developed and provided to the university before doing a water audit. One questionnaire was for all facilities of the university, with information related to the number of people (students, academics, and employees) using the facilities and the number of occupancy days. The other questionnaire was for the female students in the residences.

There are two types of female residences inside of the Jordan university campus, the international residence where each room has its utility of a small kitchen and bathroom, while the female students of the residents shared the utilities for each floor. One hundred seventy-seven students filled out questionnaires from both types of residences. Recorded data about the amount of water leakage and the number of leakage incidents were obtained from the maintenance department in the university and were included in the calculations. The data from local female residences has been directly measured.

The quantitative method used was the physical flow rate which was measured manually by using the beaker and the timer for the sanitary fixtures and some equipment in the laboratories except for those that had fixed volume for each use such as the equipment in the dental clinic.

Quarterly billing water data was used as a reference during calculations of the water audits for all utilities that got water from the same meter, such as the residences, printing house, mosque, nursery, etc. Sanitary fixtures rate measurement was done in each building on the campus randomly, and the average flow rate of each sanitary fixture was accredited for each utility in the calculation. In addition, the number of people that occupy those buildings daily was estimated. The assumed behavior used in the calculations in the water audit depended on the data obtained from the previous two questionnaires. Equation (1) explain the volume of consumed water in each fixture

$$V = f \times oc \times t \times su \times 60 \quad \text{..... (1)}$$

Where,

V is the volume of consumed water in each fixture (m3/quarter)
f is the measured flow rate (l/min)
oc is the number of people who occupied the utilities
t is the number of times used
su is the assumption of the rate of fixture use each time
The number (60) is the assumed occupancy days in each quarter

The water consumption in the residences and the utilities inside the university campus could not be validated since the university does not have sub-meters in its building to monitor the water consumption and the leakage.

On the other hand, the water consumption for green areas was estimated after interviewing the agricultural engineers of the university and based on the water landscape guide for the Ministry of Water and Irrigation (MWI, 2012b), the source of irrigated water, times, and period for irrigating. These estimates were then compared with water irrigation amount information provided by the Water, Energy and Environment Center - The University of Jordan.

Sanitary installation-plumbing supply fittings standard JS 1945:2011 was used as a benchmark to assess water flow rate by fittings after measuring it, and the potential of water-saving. Data analysis included the corresponding statistics used to analyze the data generated and collected. An excel spreadsheet was used in the calculation. The potential percent savings are calculated as the difference between baseline average water use for fixtures and the benchmarks water use for fixtures. Each potential percent saving for fixture type was multiplied with the water used in the fixture to get the potential water saving as explained in equation (2).

$$PWS = \left(\frac{A-B}{A} \times 100\right) \times V \quad \text{..... (2)}$$

Where;

PWS is the potential of water-saving (m^3/quarter)
A is baseline average water use for fixtures (l/min)
B is the benchmarks water use for fixtures (l/min)
V is the volume of consumed water in each fixture (m^3/quarter) in equation (1)

The feasibility study was done depending on its water resource, cost of water cubic meter, and the number of fittings that should need water-saving devices as explained in equation (3).

$$PMS = PWS \times C \quad \text{..... (3)}$$

PMS is the potential of money-saving ($/quarter)
PWS is the potential of water-saving (m^3/quarter) in equation (2)
C is the cost of one cubic meter

3. Results

The results were built through information obtained as open files from the water, energy, and environment center, the questionnaire analysis which was distributed to the female students' residents that the percentages of female students in the international and the local residences that responded were 48%, 13% respectively, and the flow rate measuring for fixtures and equipment in whole the Jordan university campus.

3.1 Sanitary fixtures flow rates for the university buildings

The water flow rate per each type of sanitary fixture was measured manually by using a beaker and timer. There were variations in the flow rate of the same type of fixture within the schools and administrative offices of the university. Table (1) shows the average water flow rate per type of fixture for the faculties in the university and the female students' residence.

Table 1. Average flow rate of different sanitary fixtures

	Kitchen sink (l/min)	Lavatory (l/min)	Toilet (l/flush)	Bidet (l/min)	Shower (l/min)
Faculties	9	8	5	6	*16.5
Female students residence	10.5	8.8	5	7	7.5

*For swimming pool

Table (2) shows the benchmarks water flow rate for each fixture in the Jordan standard (JS 1945:2011), while Figure 2 shows the comparison of actual fixtures flow rates with the Jordan Standard. Table (3) shows the deviation of the flow rate of fixtures from the benchmark.

Table 2. Sanitary installation-plumbing supply fittings Jordan standard (JS 1945:2011)

Fixture	Toilet	Urinal	Bidet	Lavatory	Showerhead	Sink
Jordan Standard	6	1.9	4	4.5	7.6	8.3

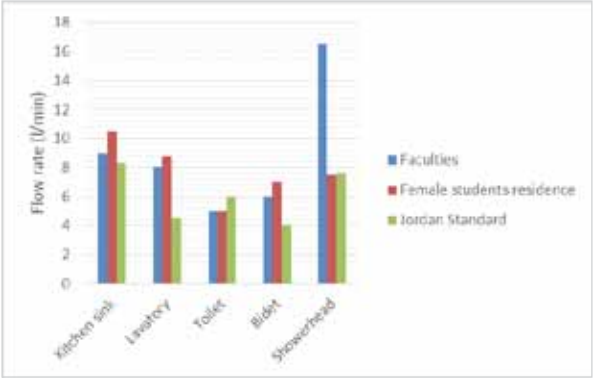

Figure 2. Comparison between the actual fixtures flow rates and the Jordan Standard (JS 1945:2011)

Table 3. The deviation of actual flow rate from the Jordan standard (JS 1945:2011)

Fixture	Toilet	Lavatory	Bidet	Sink	Showerhead
Faculties	-	44%	33%	8%	54%
Female students residence	-	49%	43%	21%	-

3.2 Potential of water-saving

Depending on water end-use analysis and reference of sanitary installation-plumbing supply fittings standard JS 1945:2011, the percentage of potential saving from the installation of water-saving devices is 13.7% as shown in Figure 3.

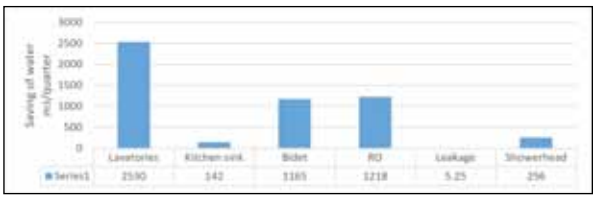

Figure 3. The amount of savings in cubic meters per quarter if the Jordanian standards are applied

3.3 Water end-use analysis

The amount of water consumption depends on many factors. The main factors are the volume of the occupied area, number of employees and students, type of irrigation for landscapes, type of fixtures, and flow rates. By analyzing the collected data, the percentage of water consumption for the schools and the administrative offices was 80% of the total volume of water consumption, and for other utilities was 20%. The 20% of total water consumption was distributed between the utilities of the University as shown in Figure 4.

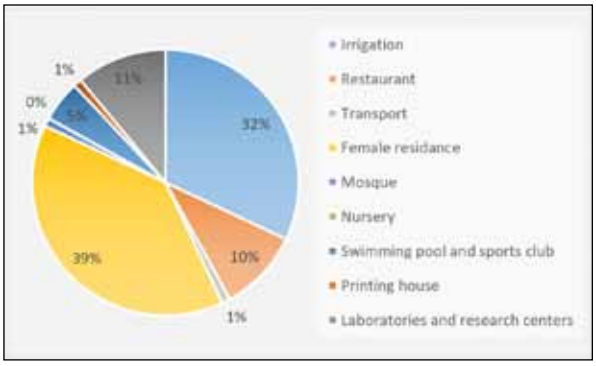

Figure 4. Water consumption percentages in the utilities of the University of Jordan

The distribution of water use within the academic and administrative buildings of the university and within the female students' residences is shown in Figure 5 and Figure 6 respectively. Toilets were shown to be the most important internal use of water with 64% in the schools' buildings and 29% in the female residences.

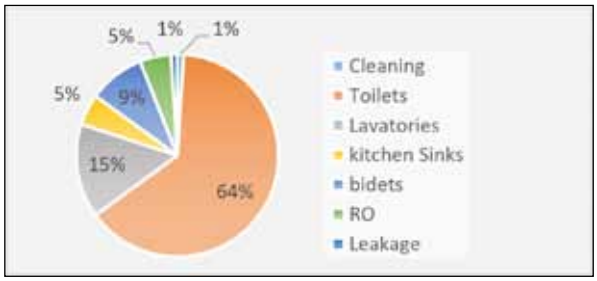

Figure 5. Percentage distribution of water consumption per each type of sanitary fixture in schools buildings

3.4 Feasibility study for water-saving devices

The goal of the study was to recognize the consumption characteristics of the different utilities within the University of Jordan campus, evaluate the water consumption per each type of sanitary fixture for the university using water end-use analysis, estimate the potential of water-saving and assess the cost-effectiveness of using water-saving devices after adopting water demand management approach to decrease the volume of water used for different sanitary fixtures.

The high consumption of some sanitary fixtures was a result of their high flow rate. Therefore, implementing the standard flow rates will lead to saving in both water and money. Tables (4), and (5) are examples of the feasibility study.

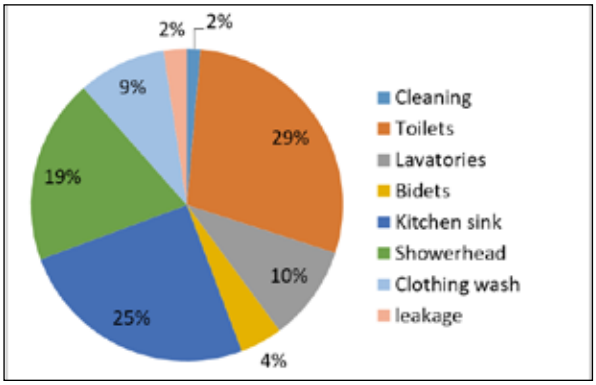

Figure 6. Percentage distribution of water consumption per each type of sanitary fixture in the female residences

Table 4. Feasibility study for Lavatories faucets of schools and administrative buildings

Average lavatories flow rate (l/min)	8
The volume of consumed water by lavatories (m^3/quarter)	5783
Potential of water-saving after installing water-saving devices (m^3/quarter)	2530
Price of one cubic meter ($)	3.056
Potential of money-saving after installing water-saving devices ($/quarter)	7732.394
Number of water-saving devices that needed to install on the lavatories	386
Cost of one water-saving device ($)	2.816
The total cost of water-saving devices for all lavatories ($)	1086.976
Payback period (months)	1

Table 5. Feasibility study for showerheads for the swimming pools of the sports club

Average Showerheads flow rate (l/min)	16.5
The volume of consumed water by showerheads (m3/quarter)	475
Potential of water-saving after installing water-saving devices (m3/quarter)	256
Price of one cubic meter ($)	3.056
Potential of money-saving after installing water-saving devices ($/quarter)	783.098
Number of water-saving devices that needed to install on the lavatories	15
Cost of one water-saving device ($)	2.816
The total cost of water-saving devices for all showerheads ($)	42.24
Payback period (months)	1

The price of water depended on the source of the supplied water, the water tariff of one cubic meter by the network was around $3.056. Table (6) shows the summary of the potential amount of water-saving and the potential of money-saving in the university as a whole.

Table 6. Summary of potential water and money-saving

Utilities	The volume of water consumption (m^3)	Potential water saving (m^3)
Schools and administrative offices	37700	5118
Female students' residences	3824	559
Mosque	63.7	19.4
Restaurant	939	57.8
Transport	72	-
Irrigation	3118	-
Nursery	51.7	-
Swimming pools-sport club	474.7	256
Printing house	117.8	-
Laboratories and research centers	1046.7	504.5
Total	47407.6	6514.7
Potential money-saving ($/quarter)	19911	

4. Discussion

Increasing water use efficiency remains the key strategy to conserve water without deteriorating the lifestyle of people or service level (Oduro-Kwarteng et al., 2009). Efficient sanitary fixtures can reduce water demand from 30-50% (EC, 2006). In the USA too, the water-saving devices program was implemented for 10 years from 1985-1996, the results of the program showed that reducing water demand reached 25% (Kanakoudis, 2002). When the University of Jordan implemented water use efficiency in its campus, the water demand would be reduced to 13.7%.

On the other hand, Toilets are considered the most important internal use of water with 64% in the schools' buildings at the University of Jordan. For validation of the University of Jordan study, Australia has significantly decreased the volume of water used for flushing water closets from an average of 11-13 liters per flush to less than 4 liter per flush, due to the development of the dual flush WCs (White, 1999; Day and White, 2003). And in 1996, the Australian authorities made standards for reducing the dual flush to 3/6 liters (Sharma, 2004). Jordan standards and metrology organization made Sanitary installation-plumbing supply fittings standard JS 1945:2011 in 2011. Accordingly, the study has used this standard as a benchmark to assess water flow rate by fittings after measuring it, the volume of flush in the toilet of the University of Jordan was 5 (l/flush). Besides, Oduro-Kwarteng et al. 2009 (Oduro-Kwarteng et al., 2009) explained the average daily number of bathes and WC flushing per respondent was 1.72 and 2.12 respectively. The average daily number of WC flushing was 2.53 for females and 2.01 for males. The frequency fixture used was estimated, duration was determined by the female student residence questionnaire especially, then they were used in the simple equation after multiplying them with the number of students and employees. For leakage; Velazquez et al., (2013) showed that 89% of leakage resulted from human behavior and just 11% of leakage was resulted due to technological failures. The leakage in Jordan University is controlled. Quantifying leakage is important to understand the level of awareness of the university community (Velazquez et al., 2013). Otherwise, wasting water by bathing could be attributed to the fact that some of the showerheads have high flow rates and students spend a lot of time bathing. Hence, the questionnaire results for 177 girls in four in campus female students' residences of the Jordan university showed that 34.5% of those females bathe daily, the average time for bathing was around 26 minutes. 44.1% of them do not close the showerhead during bathing. It is recommended to increase awareness and create educational programs to address water scarcity issues for all students in all stages are important. EL-Nwsany et al. (2019) explained that involving university students in water conservation will help in focusing on social responsibility, where social responsibility is a key component of sustainable

development. Retrofitting with water-saving devices has been practiced in several countries to conserve water. In the USA, a residential water end-use study explained the potential water conservation due to showerheads and toilets alone was estimated to be up to 32% (Dickinson et al., 2003). Moreover, the water management indoor the university campus plays the main role in saving water. Water tariffs and the price of efficient fixtures play a main role in the financial benefits. For that, Velazquez et al., (2013) found in his study that the payback period of the retrofit inefficient fixture is very long and the cost-effectiveness is not feasible, but depending on water end-use analysis results for the University of Jordan that was shown in the tables (4 and 5), it was proven that the outcome is the opposite and the cost-effectiveness is reachable and payback period usually takes few months or less. In general and regardless of benefit-cost analysis of fixtures retrofitting, water value, and saving that summarized in table (6) have financial benefit more than the costs of implementing a comprehensive demand management program (UK Environmental Agency, 2006).

5. Conclusions

The end-use analysis for water consumption for large consumers including universities and academic institutions is important for understanding the reduction in water demand due to retrofit fixtures to a more efficient one. The high rates of water consumption of some sanitary fixtures are due to the high flow rate of water in some of these fixtures. Therefore, adopting the recommended flow rate in the JS1945:2011 will result in both water and money savings. A comprehensive assessment of the water supply and financial costs and benefits are important to the successful adaptation of water demand management. Water-saving translates into cost savings. Retrofitting of fixtures indoor the university campus is not enough and should be accompanied by changing behaviors in the university community. Measures that could be used to promote water conservation on the campus are retrofitting with water-efficient fixtures, awareness campaigns on water conservation practices on campus, and incorporation of water conservation in the academic curriculum (RPI, (2006); PU, (2006); UoM, (2006). In addition, installing water sub-meters for every building or green area on the campus to monitor the volume of water consumption and to control the leakage that recognizes the actual water consumption and to estimate an exact water demand (Avishek et al., 2020).

Acknowledgments

I would like to acknowledge the Water, Energy, and Environment Center at the University of Jordan which played a role in providing facilities to achieve this work.

References

Alshuwaikhat, H. M., & Abubakar, I (2008). An integrated approach to achieving campus sustainability: assessment of the current campus environmental management practices. Journal of cleaner production, 16(16), 1777-1785.

Avishek, K., Kumari, M., Singh, P. D., & Lakra, K. (2020). Water Audit: Sustainable Strategy for Water Resource Assessment and Gap Analysis. Sustainable Development Practices Using Geoinformatics, 169-183.

Day, D., & White, S (2003). Minimum performance standards for showerheads in Australia: the benefits and the barriers. Water Science and Technology: Water Supply, 3(3), 239-245.

Dickinson MA, Maddaus LA, Maddaus WO (2003). Benefits of the United States nationwide plumbing efficiency standards. Water Science and Technology: Water Supply, 3(3), 231-237.

EC (2006). Water conservation, Environment Canada

EL-Nwsany, R. I., Maarouf, I., and El-Aal, W. A (2019). Water management as a vital factor for a sustainable school. Alexandria Engineering Journal, 58(1), 303-313.

Irene, C., Deepthi, S. N., Garg, P., Jasmin, S., & Varughese, A. (2019). Water Audit of the campus of Kelappaji College of Agricultural Engineering and Technology (Doctoral dissertation, Department of Irrigation and Drainage Engineering).

JSMO (2011). Sanitary installation-plumbing supply fittings standard JS 1945:2011: Jordan Standards and Metrology Organization.

Kanakoudis, V. K (2002). Urban water use conservation measures. Journal of Water Supply: Research and Technology—AQUA, 51(3), 153-163.

MoHE (2020). Statistical report for the year 2019/2020. Ministry of High Education and Scientific Research

MWI (2012a). Best Management Practices for High Rise High Density. Ministry of Water and Irrigation. Accessed 14/4/2019 http://www.mwi.gov.jo/sites/en-us/Best%20Managment%20Practices/water%20High%20Rise%20English.pdf

MWI (2012b). Landscape water efficiency guide. Ministry of Water and Irrigation. Accessed 14/4/2019 http://www.mwi.gov.jo/sites/en-us/Best%20Managment%20Practices/Landscape%20Water%20Efficiency%20Guide.pdf

MWI (2017). Facts and figures- water sector of Jordan: Ministry of Water and Irrigation.

Oduro-Kwarteng, S., Nyarko, K. B., Odai, S. N., & Aboagye-Sarfo, P (2009). Water conservation potential in educational institutions in developing countries: case study of a university campus in Ghana. Urban water journal, 6(6), 449-455.

PU (2006). "Environmental audit of Princeton University", Princeton University. Available online at: www.princeton.edu [Accessed 20 April 2019]

RPI (2006). "Water conservation initiative: eco-logic", Rensselaer Polytechnic Institute. Available online at: www.nwf.org [Accessed 20 April 2019]

Sharma, S (2004). UNESCO-IHE Lecture Notes on Water Demand Management, Delft.

UK Environmental Agency (2006). Save water, Environmental Agency, UK.

UoM (2006). Sustainable water conservation. University of Manitoba

Velazquez, L., Munguia, N., & Ojeda, M (2013). Optimizing water use in the University of Sonora, Mexico. Journal of cleaner production, 46, 83-88.

White, S (1999). Integrated resource planning in the Australian water industry. Proceedings of CONSERV99, American Water Works Association, Monterey, California, February.

JJEES

JJEES (2022) 13 (1): 60-63
ISSN 1995-6681

Jordan Journal of Earth and Environmental Sciences

Evaluation of Aquifer Characteristics within Birnin Kebbi Metropolis, Northwestern Nigeria Using Geoelectric Survey

Ologe Oluwatoyin[1*] and Ola-Buraimo A.Olatunji[2]

[1]Department of Applied Geophysics, Federal University Birnin Kebbi, Nigeria.
[2]Department of Geology, Federal University Birnin Kebbi, Nigeria

Received 1 April 2021; Accepted 10 July 2021

Abstract

Birnin Kebbi metropolis is located in northwestern Nigeria, characterized by extensive Gwandu Formation of the Sokoto Basin. There are few or no published records of subsurface information. The study is geared towards characterizing different aquifers that inhabit groundwater in the area. The geophysical method employed is Schlumberger soundings at 51 points with half-current electrode separation (AB/2) varying from 1m to 100m.

The interpreted resistivity data reveals four lithologic units across the study area: the topsoil, fine-medium sandstone, coarse sandstone and the bedrock. The fine-medium sandstone and coarse sandstone layers serve as the major aquifer units within the area of study. The fine-medium sandstone layer is the best aquifer because of its textural and associated structural features. The aquifer unit has an average resistivity value of 220Ω-m and thickness ranges from <5m to 15 m. In this study, the aquifer layers tend to decrease in thickness westward, thereby making the coarse sandstone layer as alternative aquifer unit within the area. The resistivity data has provided information on the hydrogeologic framework and subsurface geological characteristics of major aquifer units in the study area. This will assist borehole abstraction in the area with a view towards drilling productive boreholes.

Keywords: Schlumberger Sounding, Aquifer Units, Delineation, Sokoto Basin

1. Introduction

It is a known fact that water is essential for the survival of life and the need for water is constantly increasing due to growth in population and urbanization (Ola-Burimo et al, 2018). The increase in demands for drinking water, agriculture and industrial purposes are not commensurate with availability (Ola-Buraimo et al, 2018), this prompted the need to investigate the geological properties responsible for the aquifers in the study area. The search for better living made it very difficult to control the influx of both skilled and unskilled people in and out of Birnin Kebbi metropolis. This has brought about stress on the groundwater resources in the capital city coupled with the fact that the Kebbi State Water Board no long produce water for the populace. Geoelectric method was adopted for this research in order to avoid drilling of dry boreholes which is commonly experienced in the area. It should be noted that the present study is a continuation of earlier part carried out by Ologe et al, (2018) using the same methodology in the same study area but dealt with assessment of groundwater distribution while this present study is considering the characteristics of aquifers in same study area. This approach is important in order to evaluate the aquifers geoelectrical characteristic in terms of their similarities or differences in their geological properties.

1.1 Study Location and Geology

The study area, Birnin Kebbi has coordinates of Longitude 12˚ 16' and 12˚ 42' N and Latitude 4˚ 00' and 4˚ 34' E Figure 1. The geology of the study area is well articulated in the work of Ola-Buraimo et al, (2018). The outcrop at different parts of the study area were described to be massive claystone characterized by the alternation of reddish and purple coloured clays of various thicknesses(Ola-Buraimo et al, 2018). The top of the intercalated clays is capped by ironstone which forms screes and boulders at the foot of the hills as a result of weathering while the topmost head of the hill is flat and extensive with steep sides Ola-Buraimo et al, 2018). The outcrops are said to be intensively fractured and associated with other structures such as loadcasts within the claystone (Ola-Buraimo et al, 2018). Birnin Kebbi is predominantly a gentle undulating plain with an average elevation varying from 250m to 400m above sea level; the plain is occasionally interrupted by low mesas and other escarpment feature (Kogbe, 1979, Obaje 2009). the sedimentary structures present in the study area was described to be two types, sedimentary and tectonic types. Sedimentary structures are contemporaneously formed structures that were formed during deposition of a sedimentary rock and these structures result from combined factors of environment of deposition and nature of the transporting medium (Ola-Buraimo et al, 2018). Tectonic structures were described to have formed after deposition of the rock and indurations of the facies due to stress and strain from earth movements. Tectonic structures could be in micro and mega scale, formed as a result of tectonic impact on the deposits (Ola-Buraimo et al, 2018; Ologe et al, 2018). Sedimentary structures identified in the field were described to be bedding, cross lamination, channel fill, clinoform,

* Corresponding author e-mail: toyin.ologe@gmail.com

loadcast, bioturbation and ichnofossil (organic structure), while types of tectonic structures encountered are faults, fracture and joints in the study area (Ola-Buraimo et al, 2018).

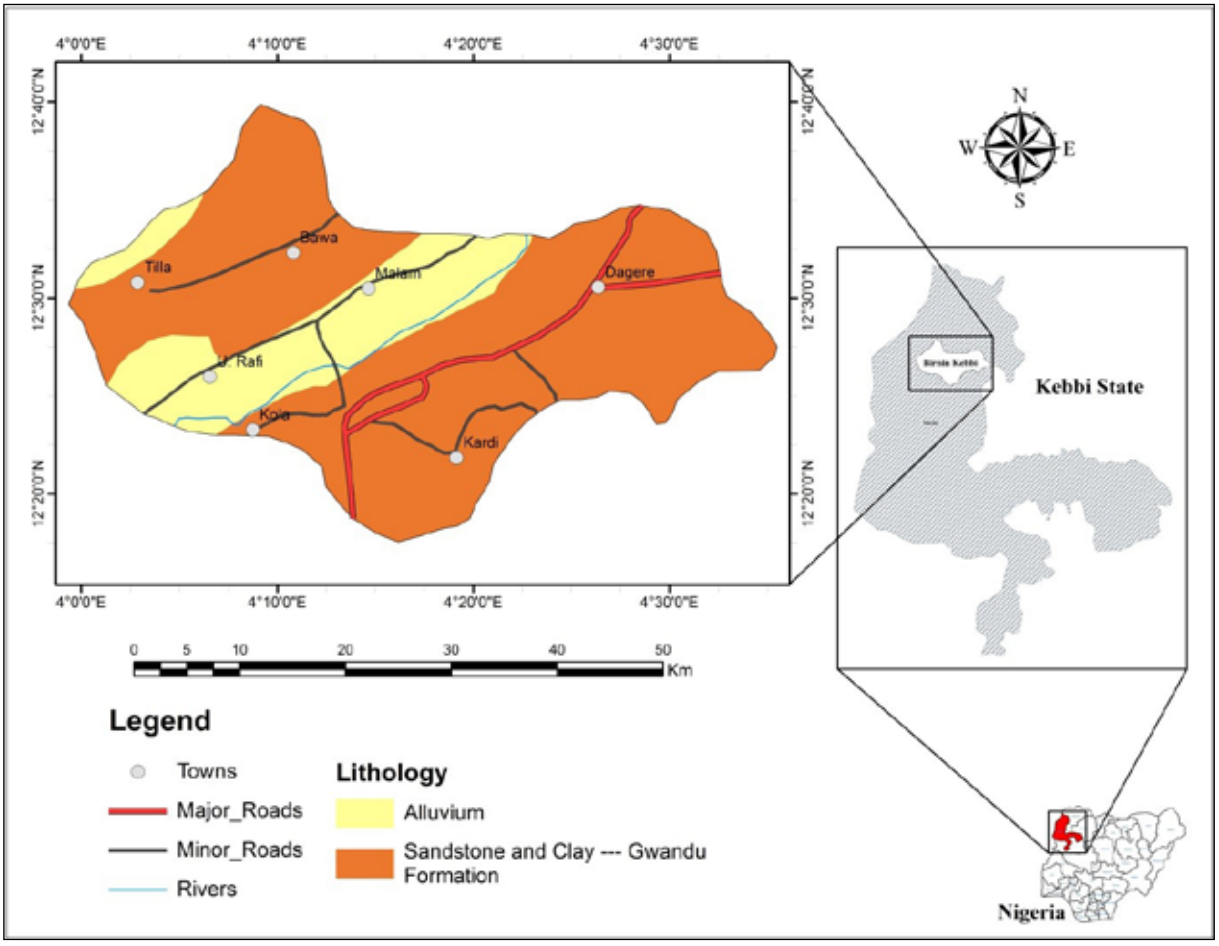

Figure 1. Location and Geological map of Birnin Kebbi area Northwestern Nigeria.

2. Materials and Methods

The R50 d. c. resistivity meter equipment was used for the VES survey. The vertical electrical resistivity sounding utilized schlumbeger configurations. In Schlumbeger array Figure 2, the separation between the current electrodes (AB) is successively expanded while the two potential electrodes (MN) have a short separation and remain partially stationary at the depth sounding position (Ologe et al, 2018). The geoelectric survey is such that the minimum electrode spacing "AB/2" = 1 m and gradually increase to a maximum spread length "AB/2" of 100 m (Ako and Osondu, 1986; Olorunfemi and Fashuyi, 1993). A total of 51 VES points were occupied to cover the study area (Ologe et al, 2018). The measured unit is the apparent resistivity, ρa, which is the product of a geometrical factor, K, and the quotient of the measured potential, ΔU, and the source current, I. The apparent resistivity is plotted versus AB/2 in meters on bilogarithmic paper resulting in a VES curve. The VES curve showed the change of resistivity with depth, since the effective penetration increases with increasing electrode spacing.

From the resistance values (R) obtained from the resistivity meter, apparent resistivity values were calculated by multiplying the corresponding geometric factors, K with the resistance values. The apparent resistivity values were plotted against the electrode spread (AB/2). This was subsequently interpreted. The interpretation of VES curves (DCINV software program by Markku Pirttijärvi, 2005) involves segment-by-segment of sounding curves with rms values not >0.1. This exercise yields geo-electric parameters and layer resistivity; thickness values were calculated.

The field data and the obtained data were input into the system for computer iteration as a starting model in an iterative forward modelling technique 1-D inversion pro- gram (Pirttijarvi, 2005) which in turn displayed the resultant theoretical curves. Therefore, the parameters were subsequently varied until what was considered the best possible fit between the field and the theoretical curve was obtained for each VES station. The parameters for the final model give the layer resistivity and thickness for the VES points. The resultant geo- electric parameters obtained from the iteration were used to establish the geoelectric sections. The quantitatively interpreted sounding curves gave interpreted results as geoelectric parameters in layer resistivity and layer thickness (see Figures 3a to d).

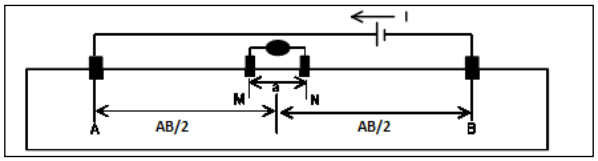

Figure 2. Schlumbeger Configurations Array

Q –Curve Type

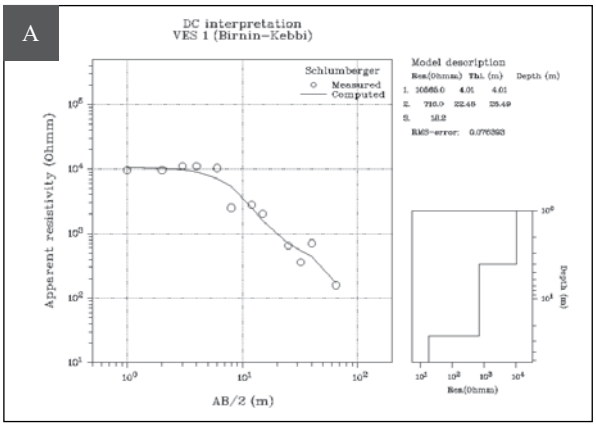

A –Curve Type

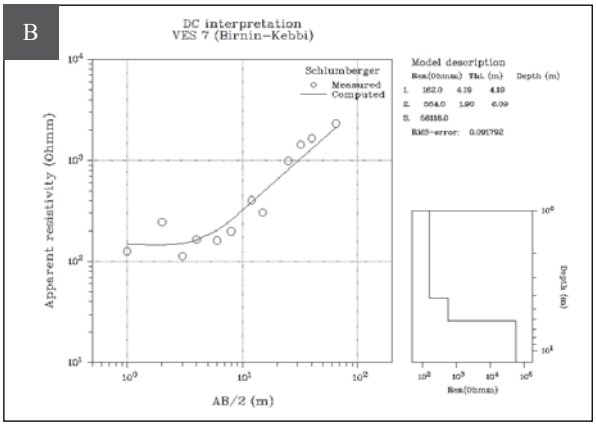

H–Curve Type

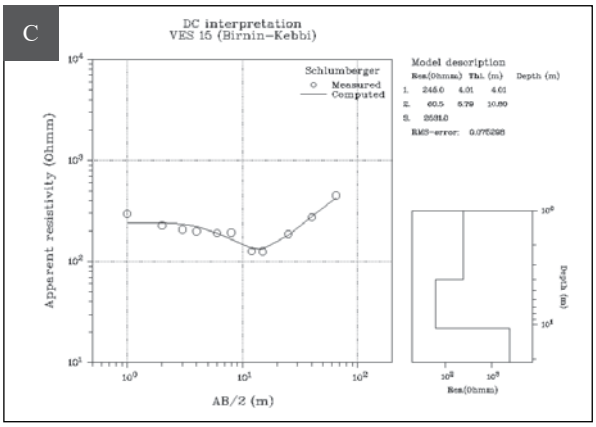

QH-Curve Type

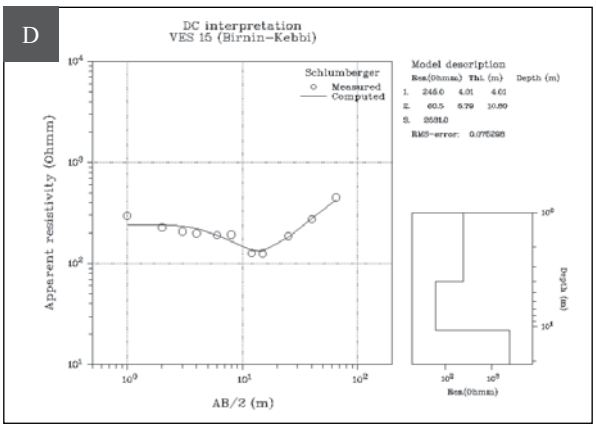

Figure 3a-d: Typical Sounding Curves from the Study Area

3. Results and Discussion

3.1 Aquifer types

The curves obtained from the sedimentary terrain of the study area vary from simple curve A, H, K, Q, KH, HA, HK types to complex curve KHA and KHK types. They are similar to those obtained by Omosuyi et al., (2008); Faleye and Olorunfemi (2015) and Ologe et al., (2018) on aquifer characterization and groundwater potential assessment of the sedimentary basin of Ondo State and Kebbi State respectively. The resistivity data interpretation reveals four lithologic units across the study area vis-à-vis topsoil, fine-medium sandstone, coarse sand and the bedrock. The predominant curve type is the K curve type having percentage frequency of 17.7%, the pictorial statistical analysis of the result is presented in Figure 4. The high percentage recorded by the K curve type within this study area has relationship to predominantly high groundwater potential and rock type associated with it. The least percentage of (5.9%) corresponds to KHA curve type. The curve types were grouped on the basis of the aquifer types. The curve types were grouped into

i) Group One: H, Q, K, A

ii) Group Two: HA, KH, HK, KHK, KHA

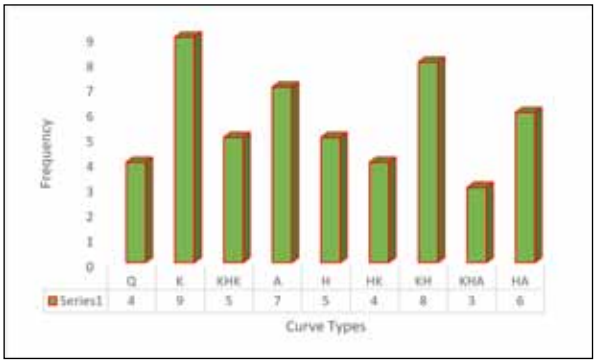

Figure 4. Frequency of Curve Types across the Study Area

Group One: Aquifers in this group correspond to layer 2 in A, H, Q, K curve types. The aquifer type is that of fine-medium sand layer.

Group Two: The aquifer in this group consist of layer 3 of HA, KH, HK, and layer 4 of KHK and KHA which correspond to coarse sandstone. Thus, from the study area, two major aquifer types were mapped which were coarse sandstone and fine-medium sandstone. However, areas underlain by the fine-medium sandstone aquifer are more promising in terms of groundwater development than the coarse sandstone aquifer.

3.2 Aquifers Identification

The resistivity parameter of a geoelectric layer is an important factor to adjudge an aquifer or otherwise (Omosuyi, 2010). To delineate or identify aquiferous or non-aquiferous layers, resistivity contrasts must exist across the subsurface lithologies (Ologe and Abdulsalam, 2018, Omosuyi, 2010). Figures 5 and 6 show four interpretive geoelectric sections taken in the W-E and SW-NE directions. These sections show variation in the subsurface lithofacies and electrical resistivity contrasts both vertically depicting the thickness of the aquifer and laterally showing lateral

decrease in lithofacies thickness and pinchout structure of the subsurface lithologies.

Figure 5 is a geoelectric section which shows an interpreted resistivity data of four lithologic units; topsoil, fine-medium sandstone, coarse sandstone and the bedrock. The topsoil which is relatively thin is characterized by resistivity values which vary between 39.3 to 2050 Ohm-m and thickness values between 1.1m to 2.1m. The high resistivity anomaly in VES 41 may be due to textural characteristics in terms of grain size, grain roundness and sorting which are controlling factors of porosity and permeability. This may also be related to structures such as fractures, joints and faults associated with the study area (Ola-Buraimo et al., 2018 and Ologe et al., 2018). Underlying the overburden layer is the identified aquifer unit of different locations characterized by sand unit of 8.1m thickness towards the east and thin layer in the western part.

Figure 6 also shows the geoelectric section drawn in the southwest – northeast direction across vertical sounding points 31, 13, 49 and 44. The top soil along the section has resistivity values ranging from 397 Ohm-m to 781 Ohm-m characteristic of lateritic soil. Beneath the top soil layer there is a relatively high resistivity value of 723 Ohm-m to 2389 Ohm-m, characterized by fine-medium sandstone unit which does not extend to VES 44 location, suggestive of pinchout structure. In some other cases, areas associated with relatively thin fine-medium sandstone compared to relatively thick (15m) underlying coarse sandstone is associated with resistivity values between 107 Ohm-m to 212 Ohm-m; characterizing prolific coarse sandstone aquifer units.

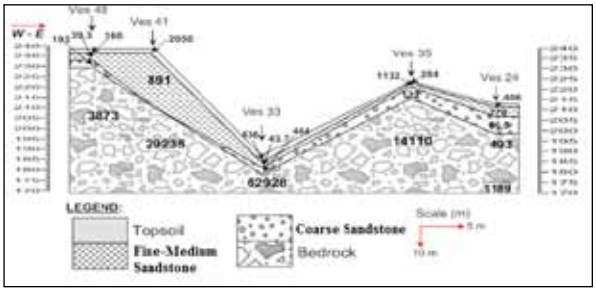

Figure 5. A W-E Geoelectric Section Embracing VES 48, 41, 33, 35 and 24

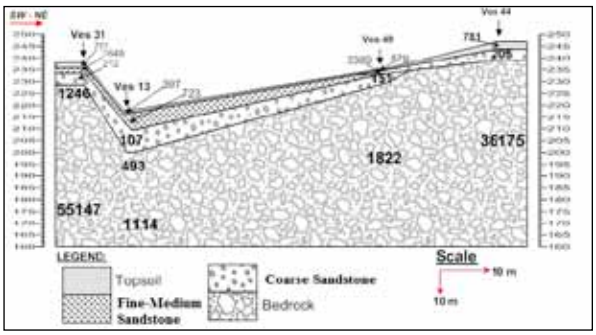

Figure 6. An SW-NE Geoelectric Section Embracing VES 31, 13, 49 and 44

4. Conclusion

The application of surface geophysics using VES technique has greatly helped in delineating the area of study aquifers characteristics with good prospect for groundwater development programme. The aquifer in the area comprises of coarse sand-sandstone layer. The aquifer thickness is variable and ranges from <5m to 15 m. In this study, the resistivity data has provided information on the hydrogeologic framework and subsurface characteristics of major aquifer units in the study area. This will no doubt guide borehole abstraction in the area with a view to drilling productive boreholes.

Acknowledgement

The authors show gratitude to the sponsor-Tertiary Education Truth Fund (TETFUND) an Internal Based Research (IBR) through Federal University Birnin Kebbi area (FUBK), Nigeria for providing grants in carrying out this second part of the research study. We also appreciate those that assisted us during the VES data acquisition.

References

Ako, B.D., and Osondu, U.C (1986). Electrical Resistivity survey of Keri-Keri Formation Darazo, Niger. J. Afr. Earth Sci. 5(5):527-534.

Ayuk, M.A., Adelusi, A.O., Adiat, K.A.N (2013): Evaluation of groundwater potential and aquifer protective capacity assessment at Tutugbua-Olugboyega area, off Ondo road, Akure Southwestern Nigeria. International Journal of Physical Sciences Vol. 8(1), pp. 37-50,

Faleye, E.T., and Olorunfemi, M.O. (2015). Aquifer Characterization and Groundwater Potential Assessment of the Sedimentary Basin of Ondo State Ife Journal of Science,17(2): 429-439.

KOGBE, C.A. (1979). Geology of the southeastern (Sokoto) sector of the Iullmemeden Basin. Bulletin, Department of Geology. Ahmadu Bello University, Zaria. 2(1), XV + 420pp.

Obaje, N.G. (2009). Geology and Mineral Resources of Nigeria. Springer Dordrecht Heidelberg London New York, 221p

Ola-Buraimo, A.O., Ologe, O., Benemaikwu. D.O (2018). Field Geology and Microbiological Investigation of Borehole, Public Tap water and Hand-dug Wells in some Parts, Kebbi State Northwestern Nigeria. Nigeria Journal of Scientific Research, ABU,Zaria. (in press).

Ologe, O., Ola-Buraimo, A.O., Bakari, A.M., Adamu, A (2018). Groundwater Distribution Assessment of Birnin Keppi Using Linear Schlumberger Configuration, Kebb State, Northwestern Nigeria, Nigerian Journal of Scientific Research, 17 (3).266-272.

Ologe, O. and Abdulsalam, N. N. (2018). Delineation of Potential Groundwater Aquifer Zones around Offa, Southwestern Nigeria using Surface Geophysics, Kada Journal of Physics, Vol. 2 (1), 23-31.

Ologe, O., Mallam, A., Abdulsalam, N. N. (2018). Application of Aeromagnetic Data in Delineating Structural Patterns in Kebbi State, Northwestern, Nigeria. Minna Journal of Geosciences. Vol. 2 (2), 82-94.

Omosuyi, G. O., Ojo, J. S. and Olorunfemi, M. O. (2008). Geoelectric Sounding to Delineate

Shallow Aquifers in the Coastal Plain Sands of Okitipupa Area, Southwestern Nigeria. Pacific Journal of Science and Technology. 9(2):562-577.

Olorunfemi, M.O., and Fasuyi, S.A (1993). Aquifer types and the geoelctric/hydrogeologic characteristics of part of central basement terrain of Nigeria (Niger State). J. Afr. Earth Sci. 16(3):309-317.

Pirttijarvi, M. (2005). DCINV: 1-D Interpretation of Electrical (DC) Soundings Software. Oulu, 2005.

JJEES

JJEES (2022) 13 (1): 64-73
ISSN 1995-6681

Jordan Journal of Earth and Environmental Sciences

Geological, Mineralogical and Physical Properties of Aswan Kaolinitic Clays, Egypt: Implications for Industrial Applications

Hossam K. Sharaka[1*], Hatem M. El-Desoky[2],
Mohamed W. Abd El-Moghny[2], Nabil A. Abdel Hafez[2], Sayed A. Abuelleban[1]

[1] Egyptian Mineral Resources Authority, 3 Salah Salem Rd., Abbassiya, P.O. Box 11517, Cairo, Egypt
[2] Al-Azhar University, Faculty of Science, Geology Department, Nasser City, P.O. Box 11884, Cairo, Egypt

Received 14 June 2021; Accepted 16 July 2021

Abstract

The upper Cretaceous succession from Northeast Aswan-Egypt consists of the Nubia group (Abu Aggag, Timsah, and Umm Barmil formations). This work is aimed at characterization and evaluation of refractory properties of some selected clay deposits in Northeast Aswan, Egypt to ascertain whether its suitability as a refractory material and for relevant application in Egyptian manufacturing industries. The ceramic properties depend on the clay mineral contents and the degree of crystallinity. The chemical and mineralogical composition have indicated that iron and titanium oxides (hematite and anatase) are considered accessory (coloring) minerals. No emissions of HCl and SO_2 to the atmosphere were noticed through the treatment process of these clays that indicates it is environmentally safe. The primary physical properties (e.g. apparent porosity, water absorption, apparent specific gravity, and bulk density) were used to evaluate the product quality and to determine the industrial applications of the different refractory products.

Keywords: Kaolinite; Plastic Clay; Ceramic; Fired Clay; Physical Properties; Aswan; Egypt.

1. Introduction

The exposed sedimentary succession in the studied area belongs to upper-cretaceous sediments and can be subdivided into three rock units depending on the stratigraphic position. These units are related to the Nubian Sandstone (Group) Facies, namely Abu Aggag, Timsah, and Um Barmil formations. The three formations are separated by major unconformities (Fawwaz et al., 2017). Attia (1955) classified the Nubian Sandstone Succession into three groups, from base to top as follows: Group (I), Group (II), and Group (III). El-Naggar (1970) followed the classification of Attia (1955) and gives the group's formal names, Abu Aggag, Timsah, and Um Barmil formations, respectively.

The area is occupied generally by a clastic sequence underlain by the basement complex. Klitzsch (1986) subdivided the upper Cretaceous sedimentary sequence in the study area into three units: the basal Abu Aggag Formation, the Timsah Formation, and the uppermost Umm Barmil Formation. The first group (Abu Aggag Formation) is uncomfortably overlain the Precambrian basement rocks. The second group (Timsah Formation), uncomfortably overlies the Abu Aggag Formation and underlies the Um Barmil Formation. This Formation contains a considerable amount of economic clays and oolitic-iron ore oxides. The last group (Um Barmil Formation), uncomfortably overlain the Timsah Formation and is composed mainly of sandstone of continental origin and covered partially by Quaternary deposits. The structural pattern of the studied area is dominated by normal faulting that is related to the extensional forces affecting the studied area.

Kaolinitic clays are considered to be the most important raw materials for ceramics, refractories, paper, paints, pharmacy, etc. (Grim, 1962; Jepson, 1984; Murray 1999, 2000; Harvay and Lagaly, 2006; Christidis, 2011). Refractory materials are those that are physically and chemically capable of resisting high temperatures. High-quality refractory materials resist high-temperature fluctuations between 1000 ^{0}C and 1500 ^{0}C and are also good as thermal and electrical insulators (Ameh and Obasi, 2009; Umaru et al., 2012). Ball clay has a temperature of deformation (melting) at 1670 °C, whereas after firing became denser and vitreous (Hosterman, 1984; Wilson, 1998). The primary raw materials (e.g. kaolinite, chromite, and magnesite) are used for the production of various refractory products (Umaru et al., 2012). Aluminosilicate sources (e.g. kaolinite mineral) and magnesite refractory products are the main types used in the Nigerian manufacturing industries (Omowumi, 2001).

El-Desoky et al. (2019) studied the Cretaceous and Oligocene clay materials of the Bahariya Oasis for the first time to use in the ceramic industry, especially vitrified clay pipes for sewers. They assigned that these raw materials are more appropriate for manufacturing the clay pipes because their clay materials are mainly kaolinite that needs the lowest water content during formation and this means low thermal energy in the drying process. Baioumy and Ismail (2014) assumed the suitability of the Aswan ball clays as good quality and environmentally friendly raw materials for ceramic and refractory industries. Farouk et al. (2020) study the rock units which contain high amounts of kaolinitic materials of the Cretaceous age in the application for sewage

* Corresponding author e-mail: hossam.sharaka_2014@yahoo.com

clay pipes. They reported that the technological properties of the processed samples showed positive results for all requirements with the Naqb El Sillim Formation; meanwhile, the Malha and Abu Aggag formations showed some negative results in water absorption and chemical resistance.

The present paper aims to study the geology of an area extending around Wadi Abu Aggag and Wadi Abu Subeira (Figure 1) Northeast Aswan, and located between latitudes 24° 05`- 24° 15` N and longitudes 32° 50` to 33° 00` E. Also, the occurrence, refractory properties, and suitability of Aswan ball clay to be used in industry will be presented in this work.

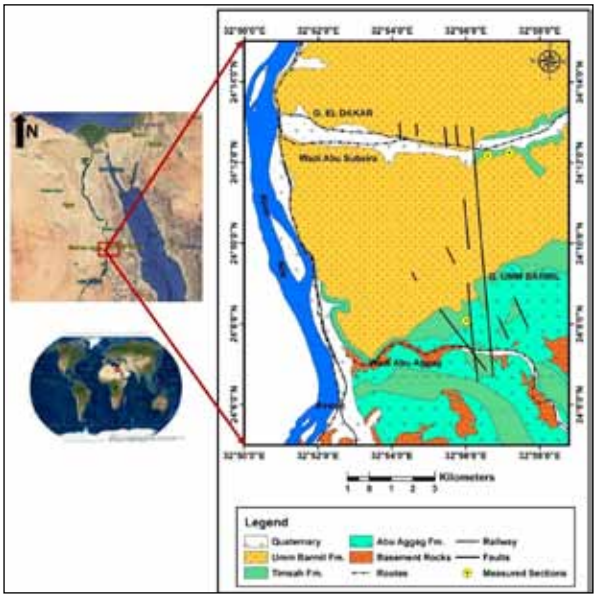

Figure 1. Landsat image and Geological map showing the studied sections at Wadi Abu Aggag (AG) and Wadi Abu Sobeira (AS) Northeast Aswan, Egypt (modified after Attia, 1955)

2. Geologic Setting

The area of study is mainly built up of Precambrian (igneous and metamorphic) rocks at the base and sandstones and clays of the Nubian Sandstones Series (Upper Cretaceous) in the upper part. The igneous rocks are composed of diorites, granodiorites, and red granites (Aswan granite), while the metamorphic rocks are mainly schists with subordinate gneisses. Nevertheless, the sedimentary sequence in the studied areas is represented by three units: the basal Abu Aggag, the Timsah, and the uppermost Um Barmil formations.

The clay-bearing formation is made up of clayey sandstone alternating with clay, siltstone, and iron-rich beds. The clastic beds are related to the Timsah Formation. Clays are varicolored (pale to dark grey, light grey, reddish grey, brownish grey, and yellowish-grey), massive to laminated, moderately hard, fragmented with some detrital quartz, and iron oxide minerals (Figures 2 and 3). Abundant and/or minor amounts of carbonaceous materials, with some gypsum veinlets, increase upwards. The sandstone is greenish-white, grey, reddish grey, brownish yellow, fine to coarse-grained, cross-bedded, ripple-marked, and indurated very hard. The total thickness of the middle group ranges between 20 meters to 45 meters.

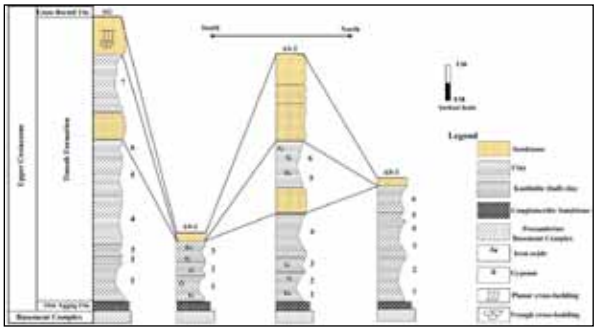

Figure 2. General lithostratigraphic columnar sections of Abu Aggag (AG), and Abu Subeira (AS-1, 2, and 3) at Northeast Aswan, Egypt.

Figure 3. Field photographs showing Aswan kaolinitic clays; A) varicolored kaolinitic clays at Wadi Abu Aggag; B) room and pillar method for raw material extraction; C) the passage for underground mining; D) pale to dark grey bed with plant remains; E) sandstone cap-rock of the upper part of the Timsah Formation at Wadi Abu Subeira; and F) operating interface at Wadi Abu Subeira.

2.1. Abu Aggag Formation:

The Abu Aggag Formation was first introduced by El-Nagger (1971) to describe the sedimentary rocks unit that overlies the basement rocks and underlies the Timsah Formation at Wadi Abu Aggag northeast Aswan. It is distributed underneath the Timsah Formation and occasionally without overburden, especially in the areas close to the basement complex. The most characteristic features are conglomerate, pebble-bands, and kaolinitic sandstone with paleosol in the lower part. Abu Aggag Formation is composed of basal conglomerate, kaolinitic beds, clays, sandstones, sandy clay to clayey sandstone. The thickness of this unit ranges from a few meters to about 50 meters. The total thickness depends on the elevation of the Precambrian rocks upon which the deposition of the sandstone series has taken place. Attia (1955) gave a Cenomanian age to this Formation, while El-Naggar (1970) gave a Turonian age.

2.2. Timsah Formation

The Timsah Formation was named firstly by Attia (1955) for the siltstone and fine-grained sandstone with thick claystone intercalations exposed at Gebel Timsah, Northeast Aswan. It uncomfortably overlies the Abu Aggag Formation and uncomfortably underlies Um Barmil Formation. Stratigraphically, Timsah Formation lies between the fluvial cycles of the Abu Aggag Formation at the base and the Umm Barmil Formation at the top (Fawwaz et al., 2017). Attia (1955) assigned a Senonian age to this rock unit, while El-Naggar (1970) assigned a Coniacian-Santonian age. The total thickness ranges between 15 to 45 meters. The Timsah Formation has a relatively large reserve (~ 10 million metric tons) and the production rate is approximately 5000 metric tons per month.

The Timsah Formation at Wadi Abu Aggag (AG) and Wadi Abu Subeira (AS) (Figures 1-3) is composed of sandstone in the upper part and pale to dark grey, brownish to yellowish-grey, massive to laminated, and moderately hard clays at the base. The sandstone is greyish to greenish-white, grey, reddish-grey, brownish-yellow, and yellowish to pale-grey, fine to coarse-grained, trough and cross-bedded, and very hard to indurate. Clays characterized by varicolored ranges from (brownish to yellowish-grey, reddish-brown, violet, and whitish to pale-grey), massive, compacted, jointed, with some gypsum veinlets and iron oxide patches at Wadi Abu Aggag (Figures 2 and 3A). On the other hand, clays in Wadi Abu Subeira are light to dark grey, massive, compacted, soft soap, with gypsum veinlets which increased upward, and some planets remain (Figures 2 and 3B, D).

2.3. Um Barmil (Nubia) Formation

Russegger (1837) introduced the term "Nubia Sandstone" for these un-fossiliferous sandstones underlying the Cretaceous beds of southern Egypt and northern Nubia. Youssef (1949) was the first to describe the claystone and shales in the upper part of the Nubia Sandstone, but he did not separate these rocks as a formation. Nubia (Um Barmil) Formation uncomfortably overlies Timsah Formation and conformably underlies the Quseir Formation to the north of the study area. It is composed of sandstone, clayey sandstone, and gritty sandstone, clay, and kaolinitic beds alternated with sandstone and grey clay (Fawwaz et al., 2017). It attains a thickness of about 60 meters. El Naggar (1971) gave Santonian-Campanian age to this Formation.

3. Materials and Methods

3.1. Materials

Four litho-stratigraphic sections exposed at the studied area, one from Wadi Abu Aggag (AG) and three from Wadi Abu Subeira (AS1, 2, and 3) were fields described, measured, and sampled (Twenty-two samples). The mineralogical & chemical composition and thermal behavior of the studied clay samples were accomplished.

3.2. Methods of investigation

The four selected representative claystone samples were examined using an X-ray Diffraction analysis (XRD) automated powder diffractometer system of Philips type PanALytica equipment model X-Pert-PRO with Ni-filter, Cu-K alpha radiation (λ=1.542Å) at 45 kV, 35 mA, and normal scanning speed 0.03o/sec. The chemical composition of the major oxides (Twenty-two samples) was determined by using the X-ray Fluorescence (XRF) technique using a Philips model Pw/2404 at 30 Kwt. Both XRD and XRF analyses were carried out at the central laboratory sector of the Egyptian Geological Survey.

Four composite samples were examined by Differential Thermal (DTA) and Thermo-gravimetric (TGA) analyses at Housing and Building National Research Center (HBRC) Cairo, Egypt, using a computerized DT.50 thermal analyzer (Shimadzu Co., Kyoto, Japan). The heating rate was 20°C/min.; the heating temperature was up to 1000°C under a nitrogen atmosphere (30 ml/min).

The primary physical properties (e.g. apparent porosity, water absorption, apparent specific gravity, and bulk density) for four composite claystone samples were examined according to (ASTM-C20). The shrinkage test was carried out according to (ASTM-C326). The mechanical properties of these samples were determined by using a modulus of rupture test (MOR) according to (ASTM-C99 and C120). These properties are widely used in the evaluation of product quality and the determining of industrial applications of the different refractory products. The mechanical properties were carried out at the Sweillem Vitrified Clay Pipes Com., Egypt.

4. Results

4.1. Mineralogical and chemical results

The XRD results have revealed that the studied samples are mineralogically composed of quartz, kaolinite, and dolomite as well as iron oxide and anatase as accessory (coloring) minerals (Figure 4). The studied samples were plotted on a ternary diagram of [SiO_2/Al_2O_3/(Fe+Ti+Mg+Ca+K+Na)] can be classified as silico–aluminous clays (Figure 5).

The results of the chemical analysis have revealed high concentration values of SiO_2 and Al_2O_3 (with average values of 59.17% and 23.35%, respectively). TiO_2 and Fe_2O_3 average values are 1.97% and 5.67%, respectively (Table 1). Loss on ignition values ranges from 3.92% to 13.38% (with an average value of 7.99 wt. %). Aswan ball clay contains a low concentration of Cl and SO_3 (0.01 and 0.08, respectively). The SiO_2/Al_2O_3 ratios range from 1.72 to 4.09, whereas the Al_2O_3/SiO_2 ratios range from 0.24 to 0.58. Besides, Al_2O_3/Fe_2O_3 ratios range from 1.22 to 15.98 (Table 1).

4.2. DTA and TGA results

The rate of firing curve changes according to the points of decomposition and loss on ignition (Földvári, 2011). These can be noted by using differential thermal (DTA) and thermogravimetric (TGA) analyses that are very important techniques to study the thermal behavior of clays for the refractory industry. The studied samples are characterized by the initial endothermic peak at around 100°C that appears as a small peak in all the studied samples. A second endothermic reaction peak appears at a range between 120 to 150 °C as a weak peak only in the samples of Wadi Abu Subeira (Figure 6).

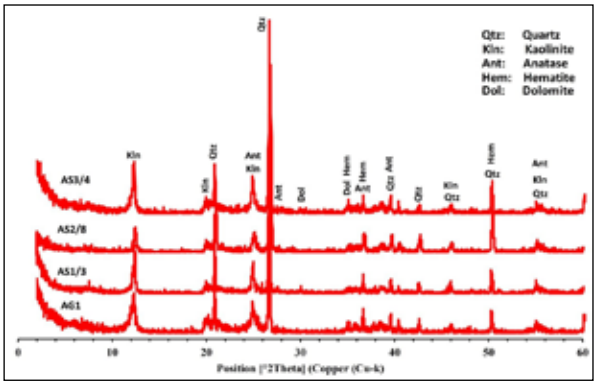

Figure 4. Representative XRD patterns of clay raw materials at Abu Aggag (AG) and Abu Subeira (AS1, 2, and 3) sections of the Upper Cretaceous kaolinitic clay at Northeast Aswan, Egypt. Note the mineral abbreviations of rock-forming minerals taken from (Kretz, 1983; Whitney and Evan, 2010).

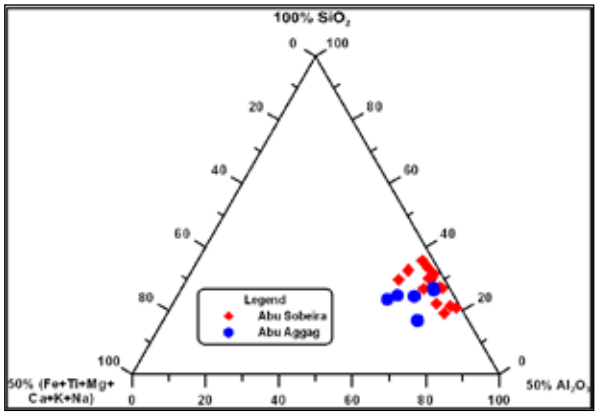

Figure 5. Ternary diagram of [SiO_2/Al_2O_3/(Fe+Ti+Mn+K+Ca+Na)] illustrated the chemical composition for the studied samples at Abu Aggag (AG) and Abu Subeira (AS) sections at Northeast Aswan, Egypt (after Garcia-Valles et al., 2020).

Furthermore, another endothermic reaction peak appears at 340 °C and appears small in the Abu Aggag sample. The second large symmetric major endothermic reaction peaks appear at around 520-580 °C in all the studied samples. An exothermic reaction peak appears at about 1000 °C. The dehydration curve indicates weight (humidity) loss below 300°C with an average loss value of 0.28%, while the lost weight as a result of the dehydroxylation reaction between 500 to 600°C of kaolinite gives an average value of 3.69%.

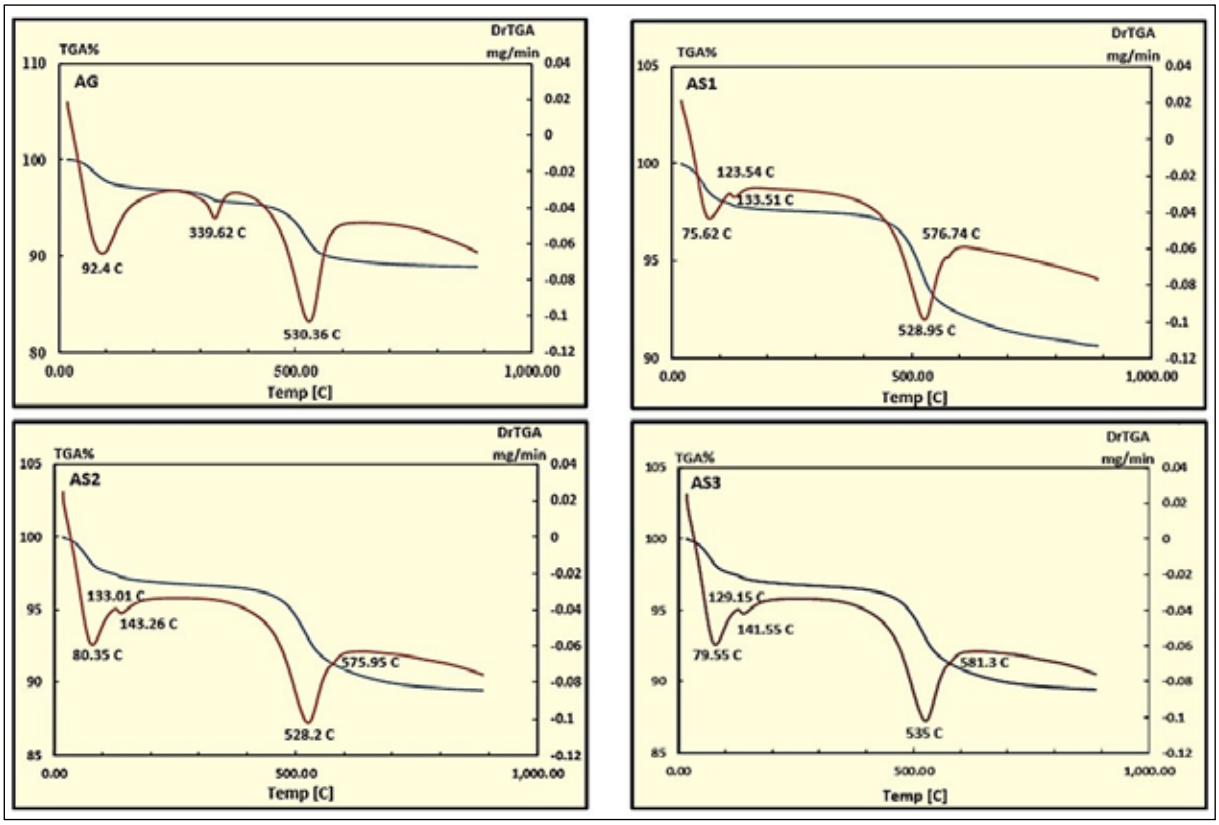

Figure 6. Differential thermal (DTA) and thermogravimetric (TG) for kaolinitic clay (Composite) samples at Wadi Abu Aggag (AG) and Wadi Abu Subeira (AS1, 2, and 3), northeast Aswan, Egypt.

Table 1. Chemical composition of the studied clays compared with other studied clay samples

Sections	S. No.	SiO_2	TiO_2	Al_2O_3	Fe_2O_3	MnO	MgO	CaO	Na_2O	K_2O	P_2O_5	Cl	SO_3	LOI	Sum	Kaolinite content	Si/Al ratio	Al/Si ratio	Al/Fe ratio
Abu Subeira	AS1-1	62.36	1.49	24.27	2.36	0.01	0.69	0.11	0.01	0.93	0.01	0.01	0.21	7.52	99.98	52.84	2.57	0.39	10.28
	AS1-2	65.61	1.90	25.05	1.89	0.01	0.54	0.05	0.01	0.67	0.01	0.01	0.17	3.92	99.84	54.54	2.62	0.38	13.25
	AS1-3	54.02	2.61	28.71	2.34	0.01	0.27	0.53	0.01	0.03	0.10	0.01	0.30	10.50	99.44	62.51	1.88	0.53	12.27
	AS2-1	68.67	1.76	17.36	4.95	0.01	1.05	0.06	0.01	0.76	0.03	0.01	0.02	5.05	99.74	37.80	3.96	0.25	3.51
	AS2-2	64.65	1.81	19.93	5.41	0.01	0.95	0.06	0.01	0.73	0.03	0.01	0.06	6.07	99.73	43.39	3.24	0.31	3.68
	AS2-3	71.35	1.44	19.02	1.19	0.01	1.15	0.03	0.01	0.65	0.03	0.01	0.36	4.55	99.8	41.41	3.75	0.27	15.98
	AS2-4	70.12	1.68	19.75	2.35	0.01	0.68	0.08	0.01	0.65	0.03	0.01	0.04	4.47	99.88	43.00	3.55	0.28	8.40
	AS2-5	55.25	1.49	22.56	5.98	0.01	2.42	1.48	0.36	0.88	0.01	0.01	0.04	9.25	99.74	49.12	2.45	0.41	3.77
	AS2-6	51.00	1.49	23.22	2.91	0.01	2.68	4.30	0.01	0.67	0.01	0.01	0.04	13.38	99.73	50.56	2.20	0.46	7.98
	AS3-1	51.33	1.46	28.48	7.27	0.01	0.19	0.02	0.01	0.11	0.01	0.01	0.03	10.81	99.74	62.01	1.80	0.55	3.92
	AS3-2	58.53	1.68	26.65	2.88	0.01	0.42	0.10	0.01	0.61	0.01	0.01	0.11	8.72	99.74	58.02	2.20	0.46	9.25
	AS3-3	58.04	1.69	26.73	3.67	0.01	0.29	0.07	0.01	0.36	0.01	0.01	0.04	8.80	99.73	58.20	2.17	0.46	7.28
	AS3-4	53.12	1.63	30.96	2.70	0.01	0.06	0.04	0.01	0.08	0.01	0.01	0.03	11.18	99.84	67.41	1.72	0.58	11.47
	AS3-5	58.75	2.03	28.01	1.82	0.01	0.05	0.13	0.01	0.35	0.01	0.01	0.02	8.70	99.9	60.98	2.10	0.48	15.39
	AS3-6	51.74	1.94	26.70	11.19	0.01	0.05	0.01	0.01	0.27	0.01	0.01	0.02	7.77	99.73	58.13	1.94	0.52	2.39
Abu Aggag	AG1	60.22	2.12	23.87	3.92	0.01	0.45	0.16	0.01	0.10	0.02	0.01	0.04	8.79	99.72	51.97	2.52	0.40	6.09
	AG2	61.19	1.93	23.46	4.14	0.01	0.62	0.06	0.01	0.24	0.31	0.01	0.05	7.70	99.73	51.08	2.61	0.38	5.67
	AG3	52.06	2.47	21.54	13.33	0.01	0.90	0.13	0.01	0.54	0.01	0.01	0.01	8.73	99.75	46.90	2.42	0.41	1.62
	AG4	50.26	2.43	20.49	16.35	0.01	0.83	0.13	0.01	0.41	0.01	0.01	0.01	8.80	99.75	44.61	2.45	0.41	1.25
	AG5	62.83	1.88	15.35	12.55	0.01	2.11	0.04	0.01	0.12	0.01	0.01	0.08	4.73	99.73	33.42	4.09	0.24	1.22
	AG6	55.87	2.56	21.22	9.50	0.01	1.12	0.30	0.01	0.92	0.07	0.01	0.02	8.12	99.73	46.20	2.63	0.38	2.23
	AG7	55.76	3.40	21.15	9.30	0.01	0.75	0.47	0.01	0.26	0.18	0.01	0.04	8.38	99.72	46.05	2.64	0.38	2.27
Average		58.76	1.94	23.39	5.82	0.01	0.83	0.38	0.03	0.47	0.04	0.01	0.08	7.99	99.76	50.93	2.61	0.41	6.78
Farouk et al., 2020		52.88	1.96	24.04	7.82	0.22	0.64	0.68	0.3	1.4	0.14	0.01	0.2	9.74	99.39	52.34	2.2	0.46	3.08
Brazil (São Simão) ball clay		54.42	0.68	27.87	2.6	0.01	1.22	1.1	0.01	2.2	0.01	0.01	0.01	9.85	99.99	60.68	1.95	0.51	10.72

4.3. Physical properties results after thermal treatment

The water absorption, bulk density, apparent porosity, linear shrinkage, and modulus of rupture are considered as the main physical properties were determined after the thermal treatment of the studied samples as follows:

4.3.1. Bulk density

The bulk density gave values ranging from 1.72 to 1.91 gm/cm^3 (with an average value of 1.82 gm/cm^3). This value lies within the range of the standard Fireclay (Table 2; and Figure 7a).

4.3.2. Shrinkage

The firing shrinkage results range from 0.00 to 3.6% (with an average value of 1.8%). This value is less than the recommended range of the standard samples of 7% - 10% for fired clays (Table 2; and Figure 7a).

Smectite effects

The smectite content strongly affects the rheological behavior of the clay dispersion. Smectite has particle sizes lower than kaolinitic minerals, and when added, it increases the surface area of the solid material. Therefore, the presence of smectite minerals significantly increases viscosity. Besides, in the absence of good quality ball clay, small smectite contents may even contribute to stabilizing the system. However, the amount of smectite cannot be too high or it can compromise the productive process (Laursen et al., 2019).

4.3.3. Water absorption

The water absorption values range from 8.28 to 14.75% (with an average of 11.52%). This value is slightly near the range of the standard Fireclay (Table 2; and Figure 7b).

4.3.4. Apparent porosity

The obtained results gave an apparent porosity value that ranges from 13.33 to 22.86% (with an average value of 18.09%) as indicated in (Table 2; and Figure 7b). This value is also less than the required value (20% - 30 for calcined clay (Gilchrist 1977).

4.3.5. Modulus of rupture

The average values of the modulus of rupture (MOR) range from 2.56 to 9.54 MN/m^2 (with an average value of 6.05 MN/m^2). These values are less than the obtained value of the standard fireclay values of MOR range from 2 - 4 MN/m^2 and (Table 2; and Figure 7a-b).

Table 2. Comparison of the determined properties of investigated clay with some established refractory standards

Physical properties of fire clay	Calcined Temperature	The current study (Northeast Aswan)	Nigerian Ozanagogo clay	Standard Fireclay
Firing Shrinkage (%)	800 – 1200 C°	0.00 – 3.60	1.01	7 - 10
Bulk density (gm/cm3)		1.72 – 1.91	2.14	1.71 - 2.1
Apparent porosity (%)		13.33 – 22.86	20.4	20 - 30
Water absorption (%)		8.28 – 14.75	------	12 - 20
Modulus of rupture (MN/m2)		2.56 – 9.54	8.28	2 - 4

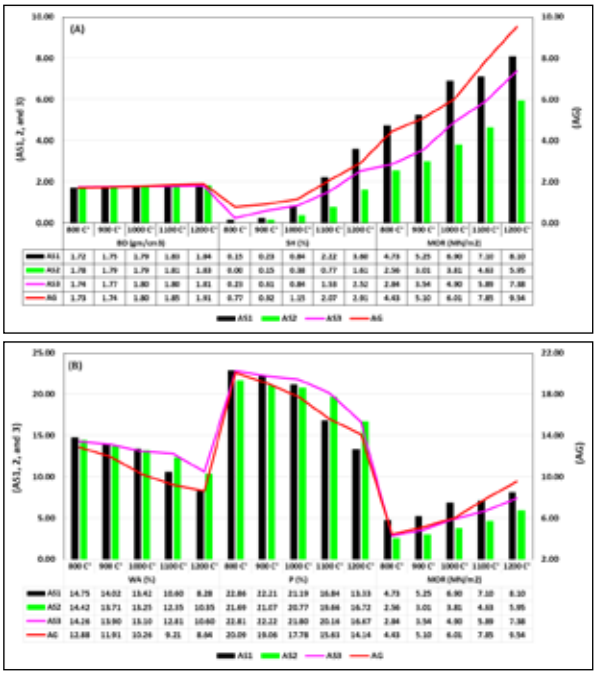

Figure 7. Illustrated the primary physical properties: A) Bulk density (BD) and Shrinkage (SH) against modulus of rupture (MOR); B) Porosity (P) and water absorption (WA) versus MOR.

5. Discussions

Plastic (Ball) clay is a term used to describe light to dark grey, fine-grained, high plasticity sedimentary kaolinitic clays. The name “ball clay” is related to an early method of mining, when traditional hand tools were used to extract the clay in rough cube shapes. Ball clay in the study area is extracted by the room and pillar method (Figure 3b) using mechanical equipment, of which the most popular are hydraulic excavators.

It was cut into 15 to 17 kg cubes and during transport, the corners of the cubes were knocked through handling and storage these cubes became rounded off leaving “balls”. It is also, sometimes referred to as plastic clay (Andreola et al., 2009). Ball clay is formed by chemical weathering of parent rocks (aluminosilicate feldspars-rich source rocks), to give kaolinite. After that, paleo-rivers and streams transport and deposit kaolinite mixed with other minerals and the carbonaceous matter (plant remains (Phlebopteris sp) Masoud et al. (2013).

The presence of iron oxides indicates a surficial oxidation process. The variation in thickness of the studied kaolinitic clays may be related to their sedimentary supply, the nature of the sedimentary basin, and the relief of the Precambrian basement rocks (Figure 2). SiO_2 and Al_2O_3 are the main

oxides in the studied samples (Table 1) that reflect their mineralogical composition. The XRD results have revealed that the high silica content is related to the high amount of quartz of terrigenous origin. Nevertheless, the silica content (50.26−71.35 wt. %) falls within the standard range of 46-62 % that is required for the production of good refractory materials as reported by Yami and Umaru (2007) from the Nigerian clays.

Furthermore, these values lie within the range of the German requirements (55−70 wt. %) and slightly near to the Belgian requirements (60−81 wt. %) (European Commission Ceramic Manufacturing Industry 2007). The degree of kaolinization and the amount of Al_2O_3 content depends upon the intensity of the chemical weathering. Meanwhile, the Al_2O_3 content of the studied samples (15.35–30.96 wt. %) is very close to the Belgian (15–27 wt. %) requirements, and less than the German requirements (20-35 wt. %) (European Commission Ceramic Manufacturing Industry 2007). The chemical composition of analyzed samples revealed that these samples belong to silico–aluminous clays (Figure 5) and are similar to Kaolinitic Clays from Terra Alta (Catalonia, Spain).

The Si/Al ratio (Table 1) is higher than the pure kaolinite (1.17) (Felix, 1977) and is attributed to the presence of high quartz content in the argillaceous sandstone. Plummer and Romary (1967); Ogbukagu (1980) suggested that the Si/Al geochemical ratio ranges from (1.6 to 2.6) for plastic fireclay, (2.4 to 4.0) for ball clay, and (3.5 to 6.7) for siliceous fireclay. This indicates the studied clay samples are close to Brazil (São Simão) ball clay. On the other hand, Al/Si ratio is lower than the value of 0.85 assigned for the ideal kaolin introduced by Schroeder et al., 2004; Ga´miz et al., 2005.

Al_2O_3/Fe_2O_3 ratio defines the possible uses for clays in ceramic technology. If it > 5.5, it is considered alumina-rich, if it < 5.5, they are iron-rich and can be used in the manufacture of building materials (e.g. bricks, tiles, etc.) Garcia-Valles et al. (2020). In the present study, the Al/Fe ratio (Table 1) ranges from 1.22 to 15.98 (with an average value of 6.78). The majority of the Abu Sobeira (AS) samples have an Al/Fe ratio > 5.5, whereas, all samples of Abu Aggag (AG) have an Al/Fe ratio < 5.5, except two samples (AG1 and 2) consists of Al/Fe ratios > 5.5. This indicates that the studied samples of Abu Sobeira are useful for manufacturing refractory ceramics and are considered alumina rich than Abu Aggag samples.

Titanium oxides (e.g. Anatase) have an average value of 1.94% (Table 1). It is higher than Brazil (São Simão) ball clay of (0.68 wt. %) and average shale (0.82 wt. %) reported by Condie (1993). Also, it matches with data published by (Baioumy and Ismail, 2014) and Farouk et al. (2020). Ti occurred as disseminated or colloidal within the clays as discrete minerals (Degens, 1965). Anatase is the main titanium mineral identified by XRD (Figure 4). Furthermore, during the weathering and deposition process of kaolinite, Ti oxides are detrital but can be adsorbed within the kaolinite structure (Murray and Keller, 1993). In the present work, it is present as adsorbed colloidal of TiO_2 and Fe_2O_3.

Fe_2O_3 (higher than 3%) is a direct measure of the iron mineral contents such as hematite as revealed by XRD (Figure 4); the iron content is responsible for generating the reddish color of samples after the firing process. The iron oxide contents range from (1.19 to 16.35 wt. %) is similar to the German requirements (1.0–10 wt. %) and higher than the maximum limit values of the Belgian requirements (1.0–7.4 wt. %) (European Commission ceramic manufacturing industry 2007). Clays used in the production of porcelain tile must have Fe_2O_3 <1%, while ball clays used for the production of light-firing bodies such as sanitary ware is overall accepted at a limit of 3% of Fe_2O_3 (Table 3) Laursen et al. (2019). The dark-coloring after the firing process and the decrease of firing temperature are related to the presence of an iron oxide higher than 3% (Tables 1 and 3). The decreasing firing temperature is related to the development of a large amount of liquid phase during firing. Besides, a great number of coating compounds are required when iron oxides are present in the ceramic industrial technology by high concentration (Laursen et al., 2019).

A high amount of iron oxide leads to deformation of the ceramic structure, incorporation of iron ions in the glassy phase and/or in the crystalline phases, and the development of dark-firing bodies (Jiang et al., 2017). Furthermore, the temperature required for alteration of soft clay body into a long-lasting refractory body depends on the presence of alkali elements (e.g. K, Na, and Ca) in the raw materials. The depletion and low flow agents of these elements as indicated in (Table 1) reflect that these clays require high temperatures for densification and the formation of glassy phases for the ceramification process.

Small amounts added as fluxing agents (alkaline elements) are adequate to greatly reduce the firing temperature without causing high pyro-plastic deformation of the bodies (Melchiades et al., 2011). The low content of CaO and MgO oxides is related to the low content of carbonate minerals such as dolomite (Tables 1; Figure 4). Nevertheless, neither calcite nor gypsum was detected in the XRD pattern, which suggests a micro-environmental heterogeneity of the kaolinitic clay (Masoud et al., 2013).

The contained Magnesium oxide ranges from 0.05 to 2.68 % in some selected clay samples. MgO is usually used as insulators in industrial cables and as primary refractory materials for laboratory crucibles and as a principal fireproofing ingredient in construction materials (Umaru et al., 2012). LOI reflects the mass loss during firing due to dehydroxylation of clay minerals and the elimination of organic matter. Ball clays usually have a high percentage of organic matter that can be colloidal, non-colloidal, or both (Laursen et al., 2019). The LOI of the studied clay (Table 1) was close to that of the traditional ball clay from Brazil, São Simão clay, which may indicate a lower amount of clay material or organic matter in these clays. The studied clays have mineralogical compositions close to the data of ball clays (Murray, 2007).

Thermal analysis of the studied samples (Figure 6) has a very low content of carbonaceous materials as revealed by XRF analysis where the samples have a low content of calcium and magnesium oxides that makes these samples safe in the thermal treatment during drying and firing

processes. The thermal behavior results (DTA and TGA) match the results of Grim, 1968; Todor, 1976; Smykatz-Kloss, 1974a; Kulp and Trites, 1951; Bray et al., 1998; Kallai, 2013; Laursen et al., 2019).

Bulk Density (BD) of calcined clay depends upon the specific gravity of the raw material, method of manufacturing, and degree of burning (Gilchrist, 1977). With increasing temperature, the density and strength of the calcined clay increase, while its water absorption and apparent porosity decrease. This indicates that the BD has a positive relationship with the firing temperature (Figure 7a) and is due to the increased consolidation between particles in the body (Alexander et al., 2013). The BD values of the studied samples are slightly similar to the typical bulk density for fireclay (Table 2), which ranges from 1.71 to 2.1 gm/cm^3 as suggested by Gilchrist (1977).

Generally, a fireclay must have a firing shrinkage (FS) lower than 8% to retain good mechanical performance (Weng et al., 2003; Abdeen and Shihada, 2017). The firing shrinkage increases with increasing firing temperature and the formation of a glassy phase (Figure 7a). However, the low value obtained in this study (Table 2) could be attributed to thermal stability that serves as an anti-shrinkage agent (Misra, 1975).

The water absorption (WA) indicates the amount of moisture that may be absorbed and could be subjected to destructive freezing in outdoor structures. Furthermore, the apparent porosity (AP) is a measure of the amount of open pore space in the fired samples, relative to its bulk volume, and is expressed as a percent. Less than 22% of water absorption and apparent porosity is considered promising for slow-calcined materials. This should be within the limit of 12 to 20% (Table 2) according to the BS-5628: Part 1:2005 and Indonesian Standard SNI 15-2094-2000 (O'Neill and Barnes 1979; Abdeen and Shihada, 2017; Fernando, 2017).

The WA and AP have a negative relationship with firing temperature, while there is a reverse relationship between water absorption and shrinkage (Figure 7a-b); there is also a positive relationship between water absorption and porosity (Figure 7b). These results could be an indication of the relative resistance to damage during freezing and thawing. The modulus of rupture (MOR) is a measure of the fracture strength of materials against the forces of breakage or crack due to the application of a certain amount of pressure, the distance over which the force was applied, and the width and thickness of the sample (Alexander et al. 2013; Abdeen and Shihada, 2017).

The MOR values are considered slightly similar to the standard values as the calcined clay (strength ranges from 2 to 4 MN/m^2) is believed to have performed well (ASTM Part 17/2005) (Table 2; and Figure 7a-b). This is related to the combined effect of both clay and organic matter content that allowed them to achieve higher strength values. The maximum means of dry density of 1.91 Mg.m^3 was recorded and approximately satisfies the requirements of the minimum density of 2.0 Mg.m^3 of the British Standard No. 3921 (1985) for calcined clay which stated the results of all the fired clay samples satisfy the recommended apparent porosity and water absorption values of 22.86% according to the Indonesian Standard (SNI) 15-2094-2000 (20%) and 14.75% according to the British Standard No. 5628: Part 1 (2005) (12%). The maximum compressive and flexural strength of calcined clay (9.54 MN.m^2) were recorded and are higher than the British Standard No. 3921-1985 (5 MN.m^2).

The ceramic properties depend on the clay mineral content and the crystallinity of kaolinite (Leonelli et al., 2001; Andreola et al., 2002). Based on the thermal analyses (thermogravimetric peaks), it is possible to determine the crystallinity degree of kaolinite (e.g. extremely disordered <530 °C, strongly disordered 530-555 °C, slightly disordered 555-575 °C, and well-ordered >575 °C) which introduced by Smykatz-Kloss (1974b).

In the present study, the raw material is characterized by a low-ordered kaolinite structure which can be noted by DTA analyses from the large endothermic peak around 530 °C. Also, it's characterized by high plasticity and an abundance of clay fractions (less than 2 µm) reported by Baioumy and Ismael (2014) and matches the international standard for the ceramic industry. Also, Fe and Ti oxides are considered as the main impurities elements in the raw materials. These oxides affect the whiteness of the raw materials and adversely affect their quality that limited their applications. The beneficiation method to remove these impurities depends on the type, content, and distribution of the Ti and Fe oxides. However, the white-firing properties of the ceramics industry can be determined by the amounts of coloring/fluxing oxides within the clay. The quality parameters depend on Al_2O_3/SiO_2 ratio, Fe_2O_3, and TiO_2 contents.

For enhancing the whiteness and hence upgrading the quality of the deposit, the contaminated oxides could be removed by bleaching, magnetic separation, or flotation for use in paper coating and filling, and in higher-grade ceramics (Abdel-Khalek et al., 1998; Abdel-Khalek, 1999; Murray, 2007). Tableware and Sanitary ware typically include 30% ball clay to provide high plasticity, workability, bonding properties, and good white-fired color. Raw materials and processing conditions are the main controlling quality factors for the ceramics industry. The studied "Ball clays" are used in many different industries and have a wide range of colors related to their sedimentary origin and are considered as a vital material in the ceramic and refractory industry. The nature of the aluminosilicate resources (e.g. Kaolinite) gives a very high whiteness after firing, but it is brittle and weak when it is used alone and must be mixed with ball clay to produce a workable, malleable, and more plasticity raw material.

Table 3. Standard properties of the potential use for the kaolinitic clays in ceramics technology (after Laursen et al., 2019).

Ceramic Properties	Standard
Iron oxide content (w/w)	<3.0%
Loss on ignition (w/w)	>8%
Mass loss 200-400 °C (organic matter, w/w)	<2.0%
Amount of smectite type mineral (w/w)	<5%
Particle equivalent diameter <2 µm	>40%
Plasticity index	>12%
Modulus of rupture of the green body (MPa)	>1.5

6. Conclusions

In the present study, the selected clay materials from northeast Aswan to realize their suitability for the ceramic and refractories industry:

1) The upper Cretaceous kaolinitic clay of the Timsah Formation consists mainly of kaolinite, and quartz, while anatase, dolomite, and hematite are considered accessory minerals. The source rocks of these clays are considered to be the weathering products of the parent's Precambrian basement rocks.

2) The thermal (DTA and TGA) results indicate a very low content of carbonaceous materials, which makes the deposits safe in the thermal treatment during drying and firing processes.

3) The Abu Sobeira clay samples are more suitable for application in ceramic and refractory industries as a result of high kaolinite content that needs low thermal energy in the firing process.

4) Aswan ball clay indicated no emissions of HCl and SO_2 gases through the firing process and is considered friendly to the environment.

5) Primary physical properties of the processed samples fall within the range of the standard requirements; while, the shrinkage showed some negative results and was less than the standard requirements.

6) The application of Aswan deposit is restricted to the fabrication of tiles, bricks, and Sanitary ware. It could be used in the ceramic industry, which plays a primary role to impart plasticity or aiding rheological stability during the shaping processes.

Acknowledgments

We greatly thank the Chief-Editor Prof. Fayez Ahmad and the reviewers for improving the manuscript. Special thanks are given to Dr/Abdeen El Naggar, Housing and Building National Research Center, for DTA and TGA analyses, interpretations, and problem-solving. The authors gratefully acknowledge Dr. Ahmed Wahid, Sweillem Vitrified Clay Pipes Company, for his effort to determine the primary physical and mechanical properties of clay samples.

References

Abdeen, H.H. and Shihada, S.M. (2017). Properties of Fired Clay Bricks Mixed with Waste Glass. Journal of Scientific Research and Reports 13(4): 1-9.

Abdel-Khalek N.A. (1999). The Egyptian kaolin: an outlook in the view of the new climate of investment. Applied Clay Science 15: 325-336.

Abdel-Khalek N.A., Hassan F., Arafa M.A. (1998). Froth flotation of ultrafine Egyptian kaolin. Fizykochemiczne Problemy Mineralurgii 32: 265-273.

Alexander, A.J., Fatai, A.A., Abdulkarin, S.A., Umar, A.S. (2013). Evaluation of the Refractory Properties of Nigerian Ozanagogo Clay Deposit. Journal of Minerals and Materials Characterization and Engineering 1: 321-325.

Ameh, E.M. and Obasi, N.L. (2009). Effect of rice husk on insulating bricks produced with Nafuta and Nsu clays. Global Journal of Engineering & Technology 661-668.

Andreola, F., Barbieri, L., Corradi, A., Lancelotti, I., Manfredini, T. (2002). Utilization of municipal incinerator stage slag for manufacturing porcelainized stoneware tiles. Journal of European Ceramic Society 22: 1457-1462.

Andreola, F., Siligardi, C., Manfredini, T., Carobonchi, C. (2009). Rheological behavior and mechanical properties of porcelain stoneware bodies containing Italian clay added with bentonites. Ceramic International 35 (3): 1159-1164.

ASTM C-120 (2000). Standard Test Method Specification for Modulus of Rupture of Flexure Testing of Slate (Modulus of Rupture, Modulus of Elasticity), 3p.

ASTM C-20 (2010). Standard Test Method Specification for Apparent Porosity, Water Absorption, Apparent Specific Gravity, and Bulk Density of Burned Refractory Brick and Shapes by Boiling Water, 3p. www.astm.org

ASTM C-326 (2014). Standard Test Method Specification for drying and firing shrinkages of ceramic whiteware clays. ASTM Book of Standards, USA. www.astm.org

ASTM C-99 (1993). Standard Test Method Specification for Modulus of Rupture of Dimension Stone, 3p. www.astm.org

ASTM Part-17 (2005). Refractories, Glass, Ceramic Materials, Carbon, and Graphite Products. Philadelphia 7-9, 51-61.

Attia, M.I. (1955). Topography, geology, and iron ore deposits of the district east of Aswan. Geol. Surv. Egypt. Special Publication, Cairo, Egypt, 262p.

Baioumy, H.M. and Ismael, I.S. (2014). Composition, origin, and industry suitable of the Aswan ball clays, Egypt. Applied Clay Science 102: 202-212.

Bray, H.J., Redfern, S.A.T., Clark, S.M. (1998). Time-temperature-dependent dehydration of Ca-montmorillonite: an in-situ XRD study. Mineralogical Magazine 62: 647-656.

British Standard No. 3921 (1985). Specification for fired clay (AMD 8946).

British Standard No. 5628: Part 1 (2005). Code of practice for the use of masonry. Structural use of unreinforced masonry.

Christidis, E.G. (2011). Industrial clays. EMU Notes in Mineralogy, Mineralogical Society 9: 341-414.

Condie, K.C. (1993). Chemical composition and evolution of the upper continental crust: contrasting results from surface samples and shales. Chemical Geology 104(1-4): 1-37. https://doi.org/10.1016/0009-2541(93)90140-E

Degens, E.T. (1965). Geochemistry of sediments: A Brief Survey. First Ed., Prentice-Hall, 342p.

El-Desoky, H., Farouk, S., Heikal M., El-Mahallawy, M., Wahid, A. (2019). Geochemical and technical investigation of some clay materials in the Bahariya Oasis, Western Desert, Egypt: Implication in the vitrified clay pipes Industry. Journal of African Earth Sciences 160: 103612, 17p. https://doi.org/10.1016/j.jafrearsci.2019.103612

El-Naggar, Z.R. (1970). On a proposed lithostratigraphic subdivision for the late Cretaceous-early Paleogene succession in the Nile Valley, Egypt, UAE. 7th Arab Petroleum Congress, Kuwait: 64p.

European Commission (2007). Ceramic Manufacturing Industry: Reference document on best available techniques in the ceramic manufacturing industry 260p. https://eippcb.jrc.ec.europa.eu/sites/default/files/2019-11/cer_bref_0807.pdf

Farouk, S., El-Desoky, H., Heikal M., El-Mahallawy, M., Wahid, A. (2020). Egyptian Cretaceous clay deposits: Insights on Mineralogy, Geochemistry, and Industrial uses. Arabian Journal of Geosciences, 13: 556, 22p.

Fawwaz, S., Sheliby, A. Salem, Y., Sharaka, H.K., Yousef, A., Fathi, M., Hamdy, A., Abdelraof, A., Herazy, S. (2017). Geology of sedimentary rocks, northeast Aswan area, southeastern Desert, Egypt. Geological Survey of Egypt. Final Report

(unpublished-internal report), expedition G5/2016: 56p.

Felix, N.S. (1977). Physico-chemical studies on bentonites with special reference to Fayoum Deposits: Ph.D. Thesis, Faculty of Science, and Cairo University. Egypt.

Fernando, P.R. (2017). Mechanical and Physical Properties of Fired Clay Brick Partial Doped with Coconut Shell Ash. Journal of Energy and Natural Resources 6(5): 58-63.

Földvári, M. (2011). Handbook of the thermogravimetric system of minerals and its use in geological practice. Geological Institute of Hungary, Budapest 213: 180p.

Ga´miz, E., Melgosa, M., Sa´nchez-Maran˜o´n, M., Martı´n-Garcı´a, J.M., Delgado, R. (2005). Relationships between chemico-mineralogical composition and color properties in selected natural and calcined Spanish kaolins. Applied Clay Science 28: 269-282.

Garcia-Valles, M., Alfonso, P., Martínez, S., Roca, N. (2020). Mineralogical and Thermal Characterization of Kaolinitic Clays from Terra Alta (Catalonia, Spain). Minerals (MDPI) 10(142), 15p. Doi:10.3390/min10020142.

Gilchrist, J.P. (1977). Fuel, furnaces, and refractories. Pergamon Press, Oxford: 35-70.

Grim, R.E. (1962). Applied clay mineralogy. McGraw-Hill, New York: 442p.

Grim, R.E. (1968). Clay mineralogy. Mc Graw-Hill Book Co., New York: 596p.

Harvay, C.C. and Lagaly, G. (2006). Handbook of clay science. Developments in Clay Science 1: 1245, Elsevier.

Hosterman, J.W. (1984). Ball clay and bentonite deposits of the Central and Western Gulf of Mexico Coastal plain, United States. United States Government printing office, Washington. Geological Survey Bulletin 1558-C, 28p.

https://pubs.usgs.gov/bul/1558c/report.pdf

Indonesian Standard (SNI) 15-2094 (2000). Massive red bricks for masonry works, National Standardization Agency of Indonesia.

https://www.scirp.org/(S(vtj3fa45qm1ean45%20vvffcz55))/reference/referencespapers.aspx?referenceid=2938332.

Jepson, W.B. (1984). Kaolins: their properties and uses. Philosophical Transactions of the Royal Society of London 311: 411-432.

Jiang, F., Li, Y., Zhao, L., Cang, D. (2017). Novel ceramics prepared from inferior clay rich in CaO and Fe2O3: Properties, crystalline phases evolution, and densification process. Applied Clay Science 143: 199-204.

Kallai, L.H. (2013). Thermally modified clay minerals. Dev. Clay Science 1: 289-308.

Klitzsch, E. (1986). Plate tectonics and cratonal geology in Northeast Africa (Egypt-Sudan). Geologische Rundschau 75: 755-768.

Kretz, R. (1983). Symbols for rock-forming minerals. American Mineralogist 68: 277-279.

Kulp, J.L. and Trites, A.F. (1951). Differential thermal analysis of natural hydrous ferric oxides. American Mineralogist 36: 23-44.

Laursen, A., Santana, L.N.L., Menezes, R.R. (2019). Characterization of Brazilian Northeastern plastic clays. Cerâmica 65 (376): 578-584.

Leonelli, C., Bondioli, F., Veronesi, P., Romagnoli, M., Manfredini, T., Pellacani, G.C., Canillo, V. (2001). Enhancing the mechanical properties of porcelain stoneware tiles: a microstructural approach. Journal of European Ceramic Society 21: 785-793.

Masoud, A.A., Christidis, G., Koike, K. (2013). Characterization of El-Tih kaolin quality using mineralogical, geochemical, and geostatistical analyses. Clay Minerals 48: 1-20.

Melchiades, F.G., Dos Santos, L.R., Nastri, S., Boschi, A.O. (2011). Fluxing agents for porcelain tiles produced by the dry route. CASTELLÓN (SPAIN) Conference Paper: 11p.

Misra, M. I. (1975). Refractories: Their manufacture, properties, and uses. 4th Ed., SMT, Lakshmi Misra, Krishna Colony, and Ghamapur 8(13): 22-42.

Murray H.H. (2007). Applied Clay Mineralogy: Occurrences, Processing and Application of Kaolins, Bentonites, Palygorskite-Sepiolite, and Common Clays. Elsevier, Developments in Clay Science 2: 180p.

Murray, H.H. (1999). Applied clay mineralogy today and tomorrow. Journal of Clay Minerals 34: 39-49.

Murray, H.H. (2000). Traditional and new applications for kaolin, smectite, and palygorskite: a general overview. Journal of Applied Clay Science 17: 207-221.

Murray, H.H. and Keller, W.D. (1993). Kaolin Genesis and Utilization. Clay Minerals Society 1: 1-24.

Ogbukagu, I.N. (1980). Refractory clays from the Ogwashi-Asaba Formation, Southeast Nigeria. Nigeria Field 5: 76-82.

Omowumi, O. J. (2001). Characterization of some Nigerian clays as refractory materials for furnace lining. Nigerian Journal of Engineering Management 2(3): 1-4.

O'Neill, B.J. and Barnes, J.H. (1979). Properties and uses of shales and clays, Southwestern Pennsylvania: Pennsylvania Geological Survey, Mineral Research Report 77: 689p.

Plummer, N. and Romary, J.F. (1967). Kansas clays, Dakota Formation. State Geological Survey Kansas, Bulletin 67.

Russegger, J. R. (1837). Kreide und Sandstein. Einflub von Granit auf letzteren. N. Jb. Mineralogie: 665-669.

Schroeder, P.A., Pruett, R.J., Mealear, N.D. (2004). Crystal-chemical changes in an oxidative weathering front in a Georgia kaolin deposit. Clays and Clay Minerals 52: 211-220.

Smykatz-Kloss, W. (1974a). Differential Thermal Analysis. Application and Results in Mineralogy. Springer Verlag, Berlin-Heidelberg-New York, 185 p.

Smykatz-Kloss, W. (1974b). The determination of the degree of (dis)order of kaolinite by means of DTA. Chemie der Erde 33 (4): 358–364.

Todor, D.N. (1976). Thermal analysis of minerals. Clay Mineral 13: 1-132.

Umaru, M., Aliyu, A.M., Aris, M.I., Munir, S.M. (2012). A Comparative study on the refractory properties of selected clays in north-central Nigeria. Academic Research International 2(1): 6p.

Weng, C.H., Lin, D.F., Chiang, P.C. (2003). Utilization of sludge as brick materials. Advanced. Environmental Research 7(1): 679-685.

Whitney, D. and Evans, B.W. (2010). Abbreviation for names of rock-forming minerals. American Mineralogist 95: 185-187.

Wilson, I.R. (1998). The constitution, evaluation, and ceramic properties of ball clays. Ceramica 44: 88-117.

Yami, A. M., and Umaru, S. (2007). Characterization of some Nigerian clays as refractory materials for furnace lining. Continental Journal of Engineering Sciences 2: 30-35.

Youssef, M.I. (1949). Stratigraphical studies in Quseir area. Bulletin Institute Desert Egypt 7(2): 35-54.

المملكة الأردنية الهاشمية

صندوق دعم البحث العلمي

الجامعة الهاشمية

المجلة الأردنية لعلوم الأرض والبيئة

JJEES

مجلة علمية عالمية محكمة

المجلد (١٣) العدد (١)

http:// jjees.hu.edu.jo/

ISSN 1995-6681

المجلة الأردنية لعلوم الأرض والبيئة

مجلة علمية عالمية محكمة

المجلة الأردنية لعلوم الأرض والبيئة: مجلة علمية عالمية محكمة ومفهرسة ومصنفة، تصدر عن عمادة البحث العلمي في الجامعة الهاشمية وبدعم من صندوق البحث العلمي - وزارة التعليم العالي والبحث العلمي، الأردن.

ترسل البحوث إلكترونيا إلى البريد الإلكتروني التالي:

رئيس تحرير المجلة الأردنية لعلوم الأرض والبيئة

jjees@hu.edu.jo

لمزيد من المعلومات والأعداد السابقة يرجى زيارة موقع المجلة على شبكة الانترنت على الرابط التالي:

www.jjees.hu.edu.jo

المملكة الأردنية الهاشمية صندوق دعم البحث العلمي الجامعة الهاشمية

JJEES

المجلة الأردنية لعلوم الأرض والبيئة

المجلد (13) العدد (1)

مجلة علمية عالمية محكمة تصدر بدعم من صندوق دعم البحث العلمي

ISSN 1995-6681 jjees.hu.edu.jo آذار 2022